



SSI Rapport

99:13 D. BARTLETT, P. DRAKE, L. LINDBORG, H. KLEIN,
TH. SCHMITZ AND M. TICHY

*Determination of the Neutron and Photon
Dose Equivalent at Work Places in Nuclear
Facilities of Sweden*

An SSI – EURADOS comparison exercise. Part 2: Evaluation



Statens strålskyddsinstitut
Swedish Radiation Protection Institute

AUTHOR/FÖRFATTARE: D. Bartlett, P. Drake, L. Lindborg, H. Klein, Th. Schmitz and M. Tichy

DIVISION/AVDELNING: Environmental Measurements and Dosimetry/Avdelningen för miljöövervakning och mätning.

TITLE/TITEL: Determination of the Neutron and Photon Dose Equivalent at Work Places in Nuclear Facilities of Sweden. An SSI – EURADOS comparison exercise. Part 2: Evaluation.

SUMMARY: Various mixed neutron-photon fields at workplaces in the containment of pressurised water reactors and in the vicinity of transport containers with spent fuel elements were investigated with spectrometers and dosimeters. The spectral neutron fluences evaluated from measurements with multisphere systems were recommended to be used for the calculation of dosimetric reference values for comparison with the readings of the dosimeters applied simultaneously.

It turned out that most of the moderator based area dosimeters overestimated, while the TEPC systems generally underestimated the ambient dose equivalent (DE) values of the rather soft neutron fields encountered at these workplaces. The discrepancies can, however, be explained on the basis of energy dependent responses of the instruments used. The ambient DE values obtained with recently developed area dosimeters based on superheated drop detectors and with track etch based personal dosimeters on phantoms, however, were in satisfying agreement with the reference data.

Sets of personal dosimeters simultaneously irradiated on a phantom allowed to roughly estimate the directional dependence of the neutron fluence. Hence, personal and limiting dose equivalent quantities could also be calculated. The personal and ambient DE values were always conservative estimates of the limiting quantities.

Unexpectedly, discrepancies were observed for photon DE data measured with GM counters and TEPC systems. The up to 50 % higher readings of the GM counters may be explained by a considerable contribution of high energy photons to the total photon dose equivalent, but photon spectrometry is necessary for final clarification.

SAMMANFATTNING: Dosekvivalenten har studerats på några olika arbetsplatser där såväl foton- som neutronstrålning förekommer. De platser som utretts har varit belägna innanför inneslutningen till en tryckvattenreaktor samt nära en behållare med använt kärnbränsle. Strålfälten har studerats såväl med spektrometriska som med dosimetriska metoder.

Efter noggrann analys rekommenderades att neutronfluens-spektrerna bestämda med multisfärspektrometrar skulle användas för beräkning av de dosimetriska referensvärden, d.v.s de värden som de olika dosmätarnas resultat skulle jämföras med.

Det visade sig att handburna instrument baserade på moderering av neutronfluensen överskattade referensvärdena, medan vävnadsekvivalenta proportionalräknare underskattade dem. Detta kan förklaras med ledning av instrumentens energiberodande för neutroner.

Ett nytt instrument baserat på principen för "bubbel"-detektorn, liksom persondosmätare baserade på "track etch" tekniken, bestämde miljö- respektive persondosekvivalenten med tillfredsställande noggrannhet.

Persondosmätare placerade på olika sidor av ett fantom bestämde neutronfluensens olika riktningsskomponenter. Med den kunskapen kunde sedan persondosekvivalenten och skyddsstorheterna beräknas. Såväl person- som miljödosekvivalenten utgjorde konservativa uppskattningar av skyddsstorheterna.

Oväntat stora skillnader upptäcktes mellan miljödosekvivalentvärden uppmätta med GM-rörs baserade handburna instrument och vävnadsekvivalenta proportionalräknare vad gäller doskomponenten från gammastrålning. De upp till 50% högre GM-rörsvärdena kan sannolikt förklaras av ett väsentligt dosbidrag från höga fotonenergier, men foton-spektrometriska resultat är nödvändiga för ett slutligt klarläggande.

SSI rapport : 99:13

Juni 1999

ISSN 0282-4434



Statens strålskyddsinstitut
Swedish Radiation Protection Institute

Determination of the Neutron and Photon Dose Equivalent at Work Places in Nuclear Facilities of Sweden

An SSI-EURADOS comparison exercise

Part 2: Evaluation

D. Bartlett^{a)}, P. Drake^{b)}, L. Lindborg^{c)}, H. Klein^{d)}, Th. Schmitz^{e)} and M. Tichy^{f)}

- a) National Radiological Protection Board, Chilton, Didcot, Oxon, OX11 0RQ, UK
- b) Vattenfall AB, Ringhals, S-430 22 Väröbacka, Sweden
- c) Swedish Radiation Protection Institute, S-17116 Stockholm, Sweden
- d) Physikalisch-Technische Bundesanstalt, Bundesallee 100,
D-38116 Braunschweig, Germany
- e) Forschungszentrum Jülich GmbH, KFA, D-52425 Jülich, Germany
- f) Tristolicina 5, 1500 Prague, Czech Republic

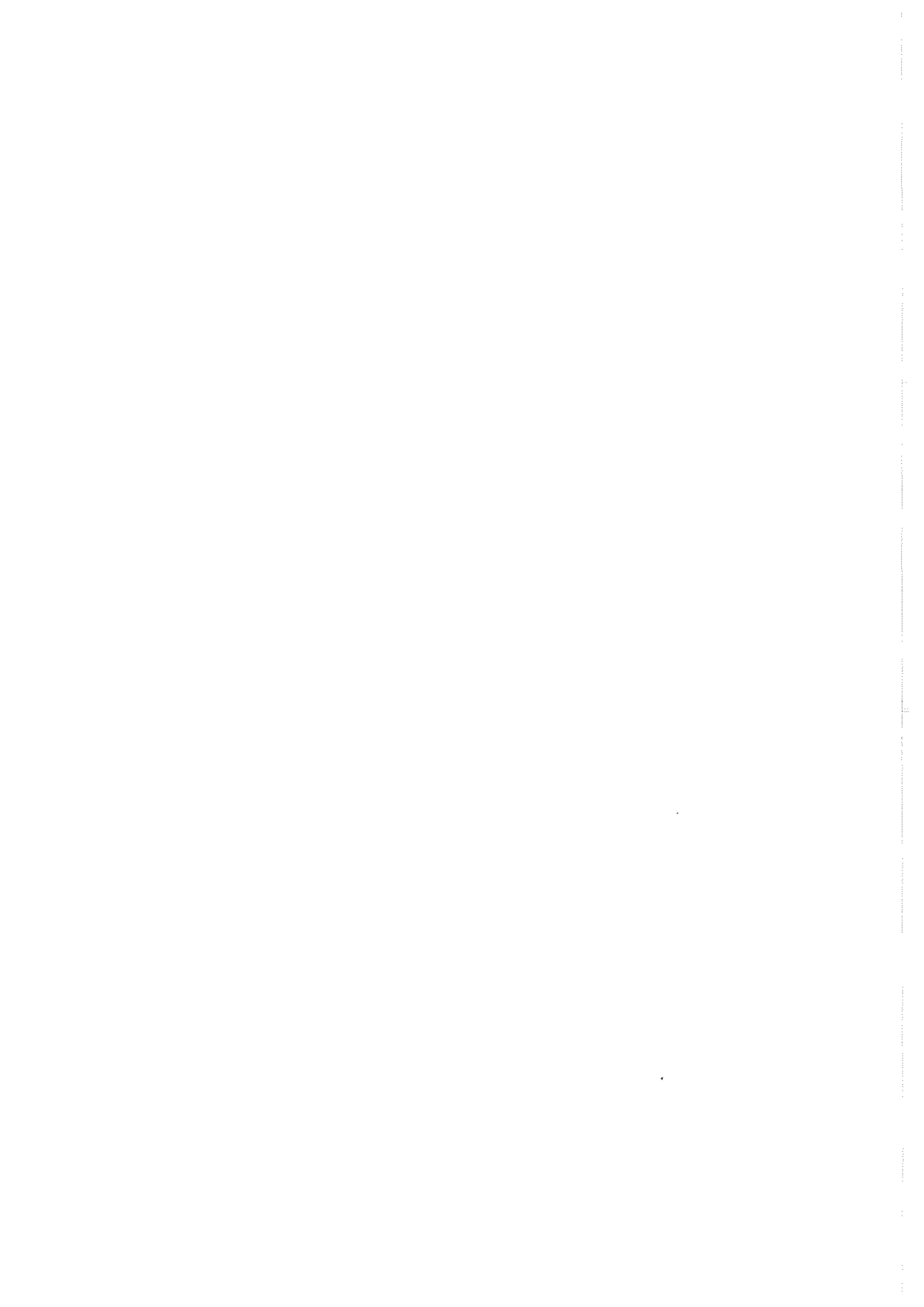


Table of Contents

	Page
1. Introduction.....	2
2. Evaluation of the Spectral Neutron Fluence	4
2.1 Comparison of the Data Submitted.....	5
2.2 Additional Unfolding.....	12
2.3 Selection of the Recommended Solution.....	39
3. Measurements with Tissue Equivalent Proportional Counters (TEPC)	48
4. Personal Dosimeters on Phantoms.....	60
4.1 Estimation of the Directional Characteristics of the Radiation Fields.....	60
4.2 Calculated Dosimetric Quantities	62
4.2.1 Calculation for Neutrons.....	62
4.2.2 Calculation for Photons	65
4.3 Comparison of Dosimeter Readings with Calculated Quantities.....	68
4.3.1 Comparison for Neutron Measurements.....	68
4.3.2 Comparison for Photon Measurements	70
5. Comparison of all Dosimetric Data	74
6. Conclusions.....	88
7. References.....	91

1. Introduction

In collaboration of EURADOS working groups #7 and #10 with the Swedish Radiation Protection Institute (SSI) the mixed neutron-photon radiation fields have been characterized at various places in the containment of pressurized water reactors in Ringhals and in the environment of a transport cask with spent fuel elements at the intermediate storage facility (CLAB) in Oskarshamn using spectrometers and dosimeters. Taking advantage of this unique occasion the results of various instruments of the same kind and those of different systems employed could be intercompared.

The results were submitted by the participants to the various evaluators according to the questionnaires distributed. The final reports of all participants were compiled in an external SSI-report [1].

Comparison of the spectral neutron fluences obtained from Bonner sphere spectrometer^{a)} measurements already exhibited systematic differences. The integral fluence values deviated not more than $\pm 5\%$ from the mean, but for the corresponding integral dose equivalent values one data set systematically deviated by about 40 - 50% from a well defined mean of the other data (see section 7 of Ref. 1). These discrepancies were therefore the reason for a very detailed evaluation (see section 2).

Also the dose and dose equivalent data derived from the measurements with six different tissue equivalent proportional counters (one of them using the variance-covariance method) showed an unexpected large scatter of the results, in particular for the neutron dose equivalent values (see section 4 of Ref. 1). A detailed analysis was necessary taking also into consideration the evaluated spectral fluence for a consistency check (see section 3).

The spectral fluence was also required when the directional dependence of the neutron fields was derived from the measurement with six personal dosimeters on phantoms assuming a superposition of an isotropic and directional component with the same shape. In the case of personal dosimeters with spectrometric properties even different shapes could be used (see section 4).

Last, but not least, the dose equivalent reference values evaluated from the spectrometric measurements are compared with the TEPC^{b)} results and the readings of various (ambient) dose equivalent instruments employed. Also the various photon dose rates are compared in section 5.

^{a)} The abbreviations BSS and BS are used in this report for Bonner spheres spectrometer and Bonner spheres, respectively.

^{b)} The abbreviation TEPC is used for tissue equivalent proportional counter.

2. Evaluation of the Spectral Neutron Fluence

Five groups participated with neutron spectrometers, four of them using Bonner spheres (BS) with active or passive thermal neutron detectors and one group employing proportional counters and a stilben scintillator for recoil proton spectrometry (RPS).

Table 1, however, shows that at maximum three different BSS's were used at five (of seven) positions while for the remaining two positions at least two different data sets could be compared for the entire neutron energy range from thermal to some MeV. The BS results were complemented by high resolution measurements performed at four (of seven) positions for neutron energies higher than 70 keV.

Table 1: Neutron spectrometers employed in the containment of pressurized water reactors in Ringhals and in the environment of a transport cask with spent fuel elements, located in the Intermediate Storage Facility (CLAB) at Oskarshamn.

Laboratory	Spectrometer	Ringhals				CLAB		
		A	F	G	L	D	E	P
GSF/Neuherberg	BS (LiI-scint.)	x	x	x	x	x	x	x
IAR/Lausanne	BS (cyl. ^3He -PC)	-	x	x	x	x	x	x
NPL/Teddington	BS (Au-act. foil)	x	-	-	-	-	-	-
PTB/Braunschweig	BS (spher. ^3He -PC)	-	-	x	x	x	x	x
KAI/Rosendorf	recoil proton det.	x	-	-	x	x	x	x

The evaluation was performed in three steps, first comparing the results as submitted, then applying a common energy binning for the spectral fluence, the response matrices and the fluence-to-dose-equivalent conversion functions before comparing and finally performing an independent unfolding of those data sets regarded as reliable. (The original idea to construct a weighted average of all spectra measured had to be abandoned because the number of reliable results remaining was too low.)

2.1 Comparison of the Data Submitted

The neutron spectra and integral quantities are shown in Figure 1 (CLAB and Ringhals) and Table 2 as submitted by the participants.

Up to nine integral quantities are compared:

- 4 (5) supergroup fluences (the energy interval 10 keV - 1 MeV was later subdivided in two supergroups),
- the total fluence and
- the total dose equivalent for three different conversion functions according to ICRP21 (H21, [2]), ICRU39 (H39, [3]) and ICRP60 (H60, [4])

These values slightly changed (Table 3) if a common data binning (49 bins for SAND 2 instead of 53, 44 or 47 groups used by PTB, GSF or IAR resp.) and the same conversion functions were applied (with the largest changes for H21, possibly due to different interpolation procedures used by the participants). The integral quantities were calculated by means of the TRESPE code provided by A.V. Alevra [5]. For the purpose of comparison with the high resolution data of KAI the group fluence was also calculated for the energy interval from 0.07 MeV to 2 MeV. Only these data will be used in the further discussion.

The measured spectra can be divided in two groups (Table 4):

- a. The spectra measured at CLAB pos. P,D and E and at Ringhals in the lock to the containment building (pos. L) are characterized by comparable fluence fractions in the thermal, the 1/E and the fission part, but the major fraction of the DE is due to neutrons with energies above 100 keV.
- b. The spectra measured in the containment building belong to rather soft fields with less than 10% and 50% in fluence and DE, respectively above 100 keV. The thermal and epithermal fractions are prevailing.

The integral results of the three BSSs used at five positions are compared in Fig. 2. While the integral fluence never deviates by more than 10% from the mean value for all data sets, one set of DE data is systematically 40-50% lower than the mean of the two other data sets which are close together.

Table 2: Comparison of supergroup and total fluence rates [$\text{cm}^{-2} \text{s}^{-1}$] as submitted by the participants for the measurements in the containment of pressurized water reactors in Ringhals (L, G, F, A) and in the environment of a transport cask with spent fuel element at the Intermediate Storage Facility CLAB in Oskarshamn (D, E, P). The total dose equivalent rates [nSv/s] were calculated with fluence-to-dose equivalent functions H_{MADE} , $H^*(10)$ and H_{60} according to ICRU 21 [2], ICRU 39 [3] and ICRP 60 [4].

Comparison of integral values as submitted by participants											
	PTB	IAR	(IAR/PTB)-1	GSF	(GSF/PTB)-1	PTB	IAR	(IAR/PTB)-1	GSF	(GSF/PTB)-1	
						Ringhals-L					
< 0.4 eV	44.59	50.53	13.3%	33.63	-24.6%	239.12	318.32	33.1%	215.50	-9.9%	
0.4eV-10keV	188.26	188.86	0.3%	175.20	-6.9%	1270.20	1403.61	10.5%	1226.00	-3.5%	
10-100 keV	36.82			36.42	-1.1%	273.16			205.80	-24.7%	
0.1-1. MeV	38.99			40.41	3.6%	252.04			280.30	11.2%	
0.01-1. MeV	75.81	67.86	-10.5%			525.2	404.35	-23.0%			
> 1. MeV	4.37	1.67	-61.8%	5.66	29.5%	3.04	0.66	-78.4%	2.79	-8.2%	
total fluence	313.00	308.92	-1.3%	291.30	-6.9%	2038.00	2126.94	4.4%	1930.00	-5.3%	
H _{made}	10.97	7.69	-29.9%	11.33	-3.7%	56.86	38.74	-31.9%	57.28	0.7%	
H*(10)	11.73	7.40	-36.9%	12.19	-1.1%	61.85	34.55	-44.1%	63.33	2.4%	
H ₆₀	17.43	10.88	-37.6%	18.08	3.7%	94.31	49.83	-47.2%	98.60	4.5%	
						Ringhals-G					
< 0.4 eV	39.91	43.33	8.6%	34.30	-14.1%	1367.10	1668.27	22.0%	1129.00	-17.4%	
0.4eV-10keV	152.81	150.81	-1.3%	142.70	-6.6%	1269.90	1092.29	-14.0%	1239.00	-2.4%	
10-100 keV	33.37			24.87	-25.5%	170.21			170.30	0.1%	
0.1-1. MeV	36.12			43.43	20.2%	112.84			105.10	-6.9%	
0.01-1. MeV	69.49	61.38	-11.7%			283.05	130.20	-54.0%			
> 1. MeV	2.01	1.18	-41.4%	3.50	73.9%	1.61	0.11	-93.4%	0.02	-98.7%	
total fluence	264.20	256.70	-2.8%	248.80	-5.8%	2922.00	2890.86	-1.1%	2643.00	-9.5%	
H _{made}	8.93	6.75	-24.4%	10.56	18.3%	48.43	34.29	-29.2%	41.61	-14.1%	
H*(10)	9.74	6.60	-32.2%	11.60	19.2%	45.76	29.33	-35.9%	39.50	-13.7%	
H ₆₀	14.69	9.81	-33.2%	17.38	18.3%	66.24	40.29	-39.2%	62.09	-6.3%	
						Ringhals-A					
						GSF	IAR	(IAR/GSF)-1	GSF	NPL	(NPL/GSF)-1
						Ringhals-F			Ringhals-A		
< 0.4 eV	2260.00	3365.23	48.9%			4987.00					
0.4eV-10keV	4080.00	4668.40	14.4%			9221.00	7999.00	-13.3%			
10-100 keV	853.10					1417.00	1696.00	19.7%			
0.1-1. MeV	1170.00					1492.00	1377.00	-7.7%			
0.01-1. MeV		1281.21									
> 1. MeV	0.79	4.73	499.6%			109.50	39.81	-63.6%			
total fluence	8364.00	9319.57	11.4%			17220.00	11110.00				
H _{made}	225.60	154.4	-31.6%			448.90	325.90	-27.4%			
H*(10)	251.80	139.51	-44.6%			465.50	351.10	-24.6%			
H ₆₀	396.70	200.79	-49.4%			705.30	347.90	-50.7%			

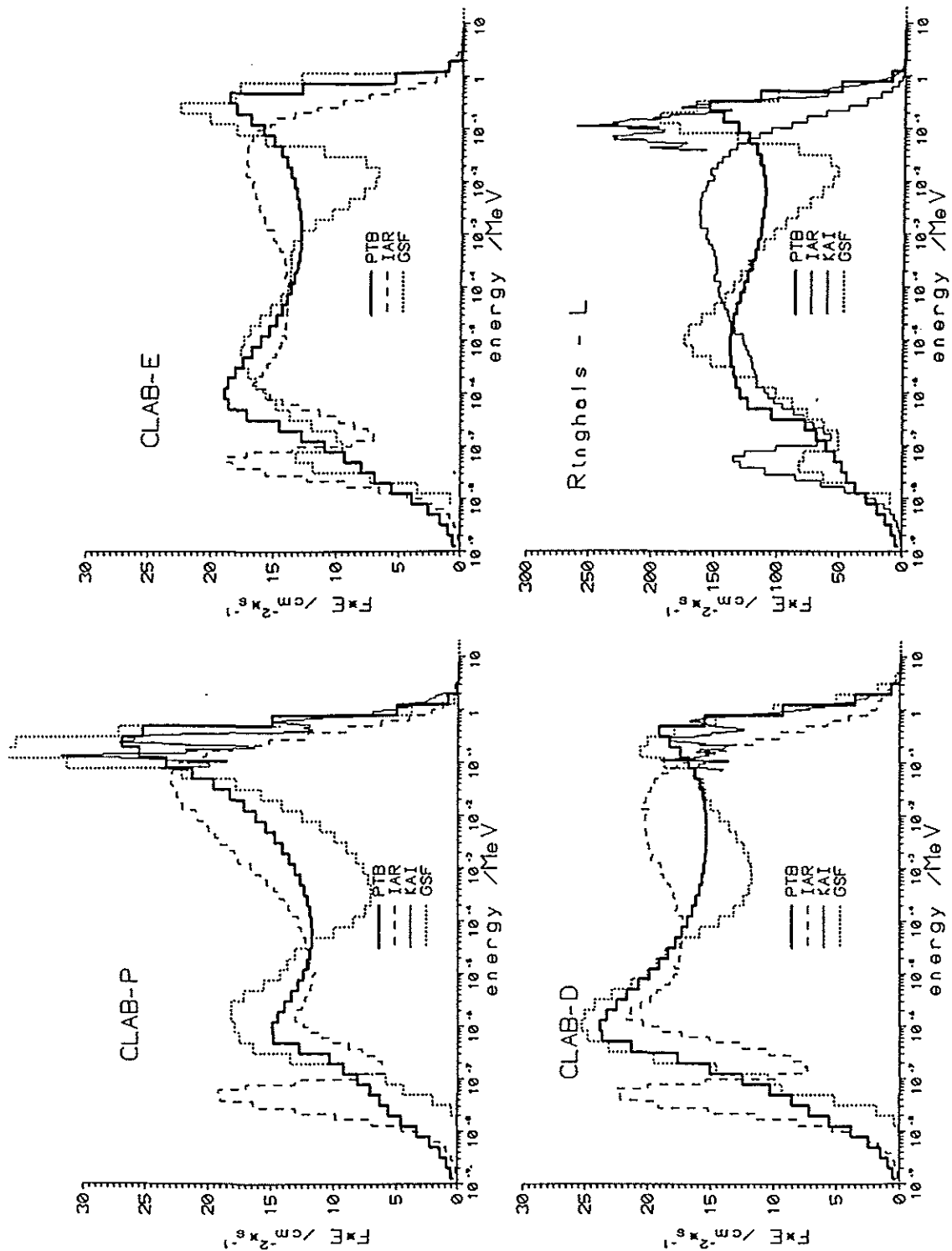


Figure 1: Spectral neutron fluence rate F (in a lethargy representation) measured with Bonner sphere spectrometers (GSF, IAR, NPL, PTB) and recoil proton detectors (KAI) in the containment of pressurized water reactors in Ringhals (L, G, F, A) and in the environment of a transport cask with spent fuel elements at the Intermediate Storage Facility CLAB in Oskarshamn (D, E, P) as submitted by the participants of the comparison exercise.

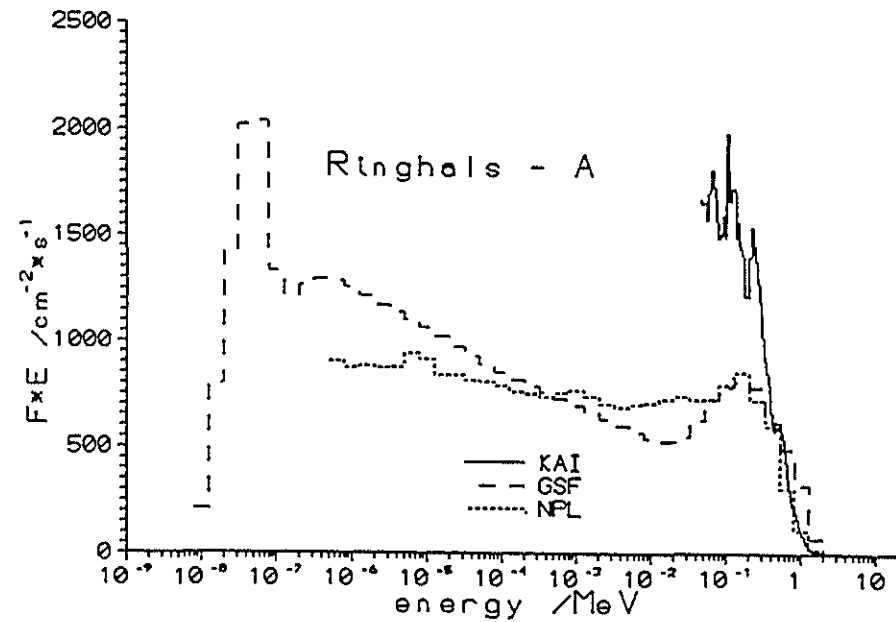
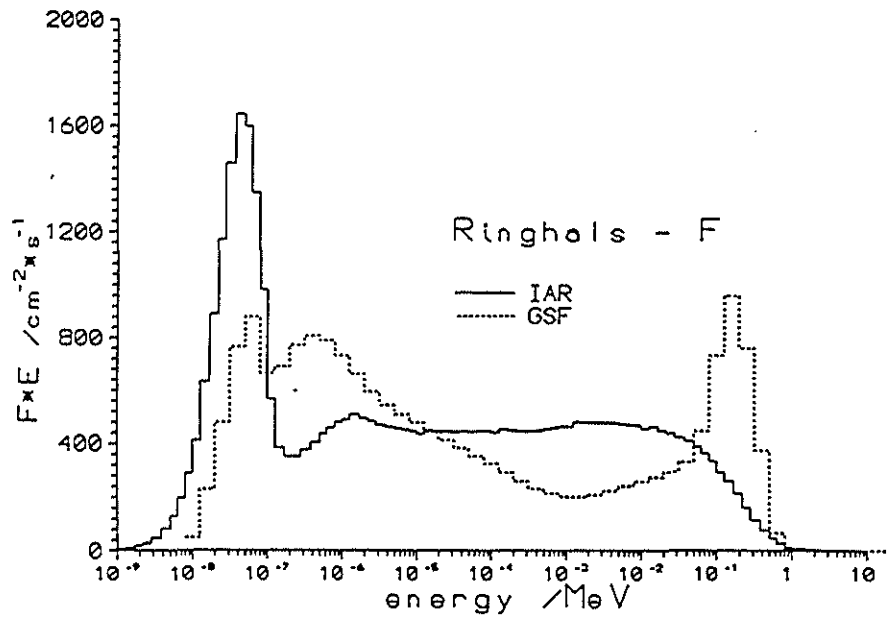
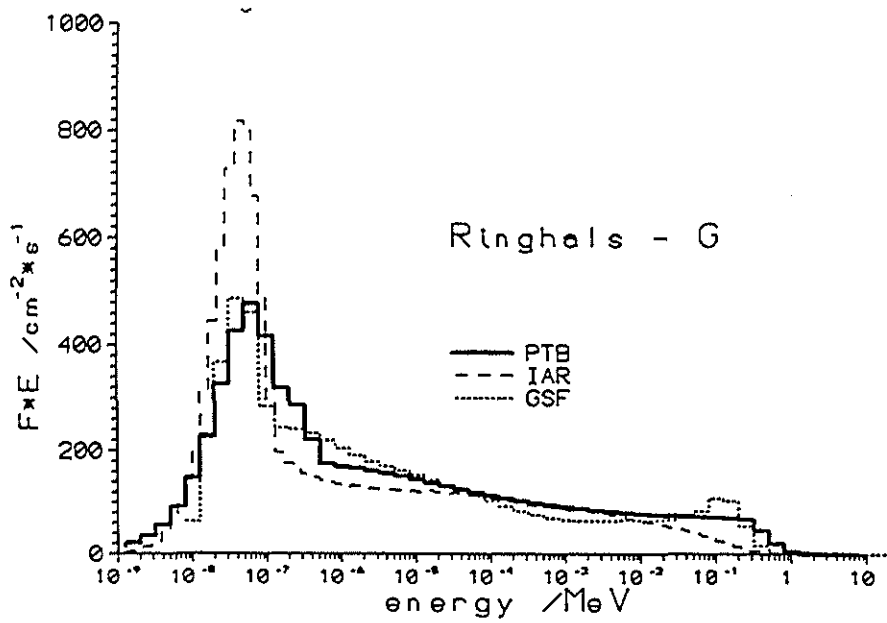


Figure 1: (continued)

Table 3: Same as Table 2, but fluence and DE rates ($[\text{cm}^{-2} \text{s}^{-1}]$ and $[\text{nSv/s}]$ resp.) are calculated for a common binning of neutron spectra and conversion functions. In addition, integral fluence values were also calculated in the energy range from 70 keV to 2 MeV for comparison with the KAI high-resolution measurements

Comparison of intergal values calculated from submitted spectra

	PTB	IAR	(IAR/PTB)-1	GSF	(GSF/PTB)-1	PTB	IAR*	(IAR*/PTB)-1	GSF	(GSF/PTB)-1
		CLAB-D					Ringhals-L			
< 0.4 eV	44.59	50.45	13.1%	33.44	-25.0%	239.12	318.09	33.0%	218.15	-8.8%
0.4eV-10keV	188.26	188.80	0.3%	176.89	-6.0%	1270.20	1404.40	10.6%	1236.8	-2.6%
10-100 keV	36.82	45.10	22.5%	36.62	-0.5%	273.16	314.60	15.2%	204.43	-25.2%
0.1-1. MeV	38.99	22.77	-41.6%	41.00	5.2%	252.04	90.11	-64.2%	287.17	13.9%
0.01-1. MeV	75.81	67.87	-10.5%	77.62	2.4%	525.2	404.705	-22.9%	491.6	-6.4%
> 1. MeV	4.37	1.67	-61.7%	5.98	36.8%	3.04	0.66	-78.4%	3.1295	2.9%
total fluence	313.00	308.80	-1.3%	293.93	-6.1%	2038.00	2127.89	4.4%	1949.7	-4.3%
Hmade	10.97	7.29	-33.5%	11.49	4.7%	56.86	36.59	-35.6%	58.116	2.2%
H*(10)	11.73	7.41	-36.9%	12.35	5.3%	61.85	34.58	-44.1%	64.067	3.6%
H60	17.43	10.89	-37.5%	18.30	5.0%	94.31	49.88	-47.1%	98.712	4.7%
		CLAB-E					Ringhals-G			
< 0.4 eV	39.91	43.29	8.5%	34.51	-13.5%	1367.10	1667.80	22.0%	1149.10	-15.9%
0.4eV-10keV	152.81	150.85	-1.3%	144.07	-5.7%	1269.90	1094.60	-13.8%	1253.00	-1.3%
10-100 keV	33.37	39.30	17.8%	24.79	-25.7%	170.21	109.65	-35.6%	170.72	0.3%
0.1-1. MeV	36.12	22.07	-38.9%	43.95	21.7%	112.84	20.44	-81.9%	108.90	-3.5%
0.01-1. MeV	69.49	61.365	-11.7%	68.74	-1.1%	283.05	130.0905	-54.0%	279.62	-1.2%
> 1. MeV	2.01	1.18	-41.4%	3.87	92.7%	1.61	0.11	-93.4%	0.02	-98.5%
total fluence	264.20	256.68	-2.8%	251.19	-4.9%	2922.00	2892.60	-1.0%	2681.80	-8.2%
Hmade	8.93	6.37	-28.7%	10.70	19.8%	48.43	35.64	-26.4%	42.52	-12.2%
H*(10)	9.74	6.60	-32.2%	11.77	20.9%	45.76	29.34	-35.9%	39.94	-12.7%
H60	14.69	9.81	-33.2%	17.79	21.1%	66.24	40.30	-39.2%	57.69	-12.9%
		CLAB-P								
< 0.4 eV	30.71	42.25	37.6%	20.06	-34.7%					
0.4eV-10keV	134.85	143.25	6.2%	123.36	-8.5%					
10-100 keV	44.47	51.79	16.5%	42.20	-5.1%					
0.1-1. MeV	50.12	28.36	-43.4%	62.76	25.2%					
0.01-1. MeV	94.59	80.15	-15.3%	104.96	11.0%					
> 1. MeV	1.70	0.97	-43.0%	1.14	-33.0%					
total fluence	261.80	266.87	1.9%	249.52	-4.7%					
Hmade	10.47	7.16	-31.6%	11.22	7.2%					
H*(10)	11.88	7.63	-35.7%	13.14	10.6%					
H60	18.28	11.53	-36.9%	20.53	12.3%					
	GSF	IAR	(IAR/GSF)-1			GSF	NPL	(NPL/GSF)-1		
		Ringhals-F					Ringhals-A			
< 0.4 eV	2274.90	3363.50	47.9%			5052.70				
0.4eV-10keV	4127.40	4675.30	13.3%			9316.60	8000.30	-14.1%		
10-100 keV	848.35	962.30	13.4%			1423.40	1696.1	19.2%		
0.1-1. MeV	1199.70	319.02	-73.4%			1516.80	1377.00	-9.2%		
0.01-1. MeV	2048.05	1281.32	-37.4%			2940.20	3073.10	4.5%		
> 1. MeV	0.89	4.74	434.4%			119.09	39.82	-66.6%		
total fluence	8451.20	9324.80	10.3%			total >0.4 eV	12375.89	11113.00		-10.2%
Hmade	228.80	154.40	-32.5%			455.95	322.20	-29.3%		
H*(10)	254.57	139.51	-45.2%			471.58	347.48	-26.3%		
H60	394.40	200.91	-49.1%			697.99	525.68	-24.7%		
	KAI	IAR	(IAR/KAI)-1	PTB	(PTB/KAI)-1	GSF	(GSF/KAI)-1			
		CLAB-P								
0.07-2 MeV	51.63	37.34	-27.7%	59.77	15.8%	73.67	42.68%			
		CLAB-D								
0.07-2 MeV	42.83	30.51	-28.8%	48.91	14.2%	52.27	22.04%			
		Ringhals-L								
0.07-2 MeV	355.32	130.67	-63.2%	300.71	-15.4%	347.14	-2.30%			
		KAI	NPL	(NPL/KAI)-1						
		Ringhals-A								
0.07-2 MeV	2831.30	1686.90	-40.4%			1901.80	-32.83%			

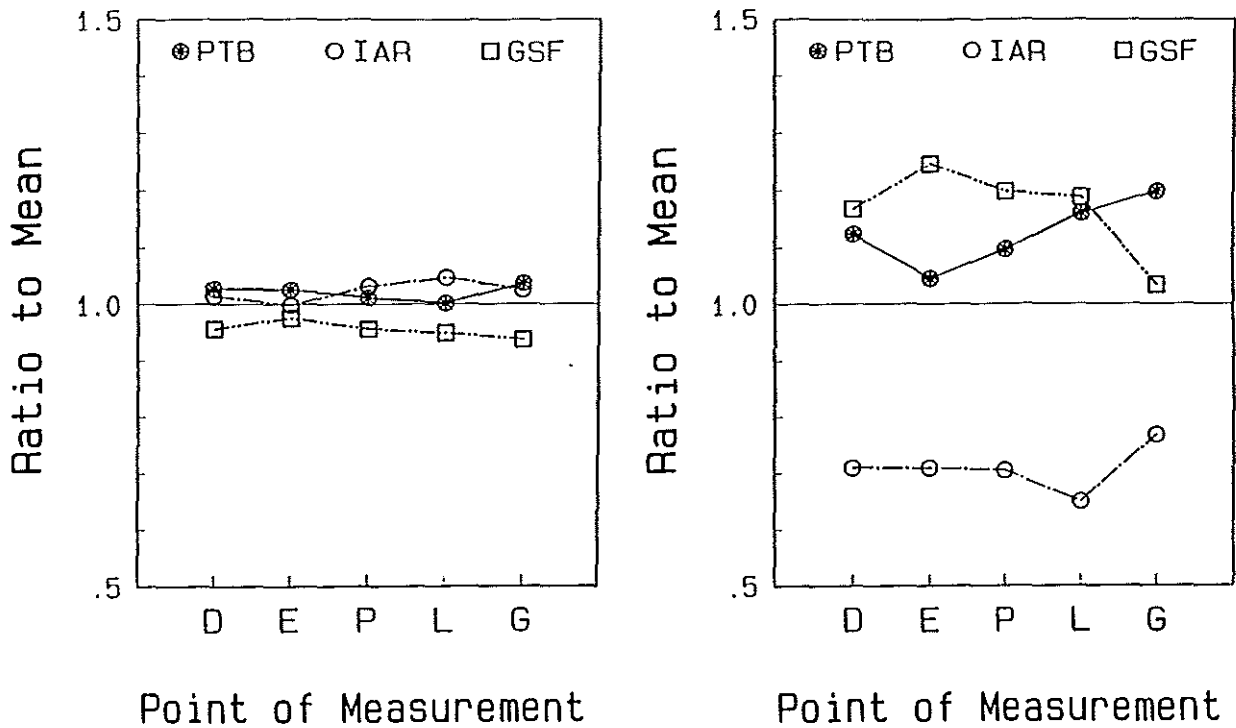


Figure 2: Ratio of the total neutron fluence (left) and dose equivalent values (right) determined by GSF, IAR and PTB at 5 positions (see Table 1) with Bonner Sphere spectrometers to their mean values.

Table 4: Relative contribution (in %) of neutrons from different energy regions to the total fluence (left) and DE (right) at the positions investigated at Ringhals (A, F, G, L) and CLAB (D, E, P)

energy region	fluence fraction (%) at		DE-fraction (%) at	
	P, D, E, L	F, G, A	P, D, E, L	F, G, A
< 0.4 eV	12 - 17	32 - 58	2 - 5	15 - 51
0.4 eV - 10 keV	52 - 64	37 - 50	8 - 17	21 - 28
10 keV - 100 keV	7 - 20	4 - 10	8 - 16	7 - 18
100 keV - 1 MeV	7 - 18	0.7 - 9	51 - 74	10 - 51
> 1 MeV	0.4 - 1.5	< 0.2	2 - 15	< 6

The reason for this unexpected result is obvious from Fig. 1, and Table 3: all IAR spectra are softer than the PTB (and the GSF) spectra such that the fluence in the two highest supergroups is about 40-90% lower for the IAR than for the PTB result. As a consequence of the strong increase of the conversion factors in the energy region from 10 keV to 1 MeV the total DE is then underestimated by 40 - 50% in the IAR spectra.

A comparison of the GSF and PTB spectra also shows some systematic differences. While the total GSF fluence is always slightly lower than the PTB fluence (4 - 8%) the GSF DE-values are generally higher than the PTB DE-results except for pos. G. These deviations are chiefly caused by the different shapes of the spectra, in particular by the deep minima of the GSF spectra in the region of 1 keV to 10 keV.

Two BS data sets were only available for positions F and A, both situated in the reactor containment building. For pos. F the IAR spectrum is much softer than the GSF result, similar to the trend observed for the other positions. At pos. A only two BSSs could be employed due to the high dose rates, namely the active system with the lowest sensitivity (GSF) and the passive BSS using Au activation for the detection of the thermal neutrons (NPL). Including the thermal fluence separately reported by the NPL (but not included in the spectrum submitted) the fluence (-5%) and DE(-15%) are both lower for the NPL result.

Finally, the high resolution data obtained by KAI with recoil proton spectrometry are compared in the overlapping region (70 keV to 2 MeV). The rather large differences of the integral fluence if compared with the PTB, GSF and NPL BS results point to a problem with the normalization of the PRS data. If, however, the shape of these spectra is only considered, reasonable agreement is observed with all BS results except for the IAR spectra.

Besides the large deviations in the DE values from the mean, some systematic differences can also be seen in shape:

- the IAR and GSF spectra show more structure (peaks and dips) than the PTB spectra, which may be caused by the selection of the guess spectra and/or too many iterations in the unfolding procedure,
- the thermal distribution used by the PTB corresponds with a somewhat higher temperature (mean energy) than those used by GSF and IAR and

- the mean energy of the fission-like distributed high energy neutrons is much lower for the IAR than for GSF and PTB (finally resulting in the much lower DE values).

Since it was not obvious from the results reported whether the differences were caused by the response matrices, the guess spectra or the unfolding procedures used, an additional unfolding was performed.

2.2 Additional Unfolding

The original version of the SAND 2 code [6] distributed by RSIC/Oak Ridge was adopted for IBM compatible and VAX computers including some supporting programs (CSTAPE, SLACTS, SLTAPE). In order to avoid possible inaccuracies in the interpolation procedure of the CSTAPE code, which prepares the response matrix library for the SAND 2 code, a new code CSTAP_EM was written. This code rewrites the response matrix with the energy bin structure supplied by the participants into the format required by the SAND 2 code.

The response matrices of PTB, GSF and IAR were originally submitted with 53, 44 or 47 bins and therefore transformed into 49 bins of the common format. The 128 bin structure used by the IAR group for the resulting spectral neutron fluence was ignored because no recipe was given for inter- or extrapolation of the original structure of the response matrix.

Various input (guess) spectra were used:

- the spectrum unfolded by the participant (submitted spectrum),
- the spectra submitted by other participants,
- the high resolution spectra of KAI, if available, extrapolated to lower energies by an $1/E$ and subsequent thermal Maxwellian distribution according to the procedure inherent in the SAND 2 code or
- the KAI spectra extrapolated by the PTB result for energies below 70 keV.

The SAND-iterations were stopped at a standard deviation $STDV=2.5$ (see [6]) or at least after 50 iterations. The standard deviation $STDV$ is calculated from:

$$\text{STDV} = \text{sqrt}((N-1)^{-1} \sum_i \text{AE}(i)/(\text{AC}(i) R - 1)^2) \quad (1)$$

with $R = N^{-1} \sum_i \text{AE}(i)/\text{AC}(i)$

and $N =$ number of spheres employed (incl. the bare detector)

$\text{AE}(i) =$ the measured rate if the i -th sphere

$\text{AC}(i) =$ the rate of the i -th sphere as calculated for the actual spectral fluence and the response matrix given.

Group and total fluence and the total dose equivalent (DE) values derived from the spectra evaluated for the different input spectra are listed in Tables 5 - 9. For simplicity only $H^*(10)$ values according to ICRP 60 [4] are given for comparison. The corresponding spectra are compared in Figures 3 - 8.

In general the limit $\text{STDV}=2.5$ was achieved before 50 iterations. The solutions obtained were stable, i.e. at the end of the iteration procedure the STDV values changed by less than 1% (preset value) between subsequent iterations. A STDV -value of 2.5 means that the differences between measured and calculated count rates are chiefly less than 1%, amount to 2% for 2 - 3 spheres and may increase up to 5% for one or two spheres in bad cases. It must be born in mind that the statistical uncertainties reported are generally less than 1% (1.5% at maximum) but the total uncertainties are in general given 2-3 times larger.

Considering the statistical compatibility of measured and calculated rates most of the resulting spectra were adequate solutions and the selection of the best result had to be based on additional information on the neutron field investigated, e.g. on the primary neutron source and the shielding material. The results obtained are discussed in sequence for the data sets measured by the various groups.

Unfolding of the data measured with the IAR-BSS (Tab. 5, Fig. 3)

Using the start spectra as reported by the participant the SAND 2 unfolding resulted in spectra rather different from those submitted. This could simply be explained by the fact that the same input parameters were differently interpreted by the SAND 2 code and the modified SANDPET version used by IAR. The systematic differences between the IAR and the PTB (and GSF) results could, however, not be resolved in this simple way.

Surprisingly, discrepancies of the ratios of measured to calculated count rates were also observed when the submitted spectra were used as the a priori information. It turned out that the input facility of the SAND 2 code (SPECTRUM TABULAR) was not fully reliable if the fine structure of the reported spectrum was transformed into the coarse common bin structure. In addition, the response matrix used by the IAR group differed from that one submitted, in particular in the thermal energy region.

Despite these problems, the submitted spectrum was confirmed in shape including the dip between the thermal and the $1/E$ distribution but not as pronounced as for the input spectrum. Although the thermal fluence decreased in most cases by 8 - 20%, the total fluence (-2%) and DE (-1%) values were only slightly influenced except for the very soft spectrum encountered at pos. G in the reactor containment building for which the total fluence (-11%) and DE (-10%) values decreased very similarly.

In the case that the three other guess spectra based on the PTB and KAI results were used the upper edge of the spectral fluence shifted to higher energies (additional tests with the GSF results which were submitted rather late were not performed because further improvements could not be expected). While the total fluence values slightly decreased by about 4% (-12% for pos. G only) the DE values considerably increased by 10 - 20% (CLAB and RINGHALS-G spectra) or even 33 - 40% for pos. L. A sufficient agreement of measured and calculated count rates was, however, not achieved and it was therefore suspected that an inadequate response matrix caused the problem at high energies, in particular the discrepancies in shape with the high resolution KAI data.

CLAB-D. IAR measurement

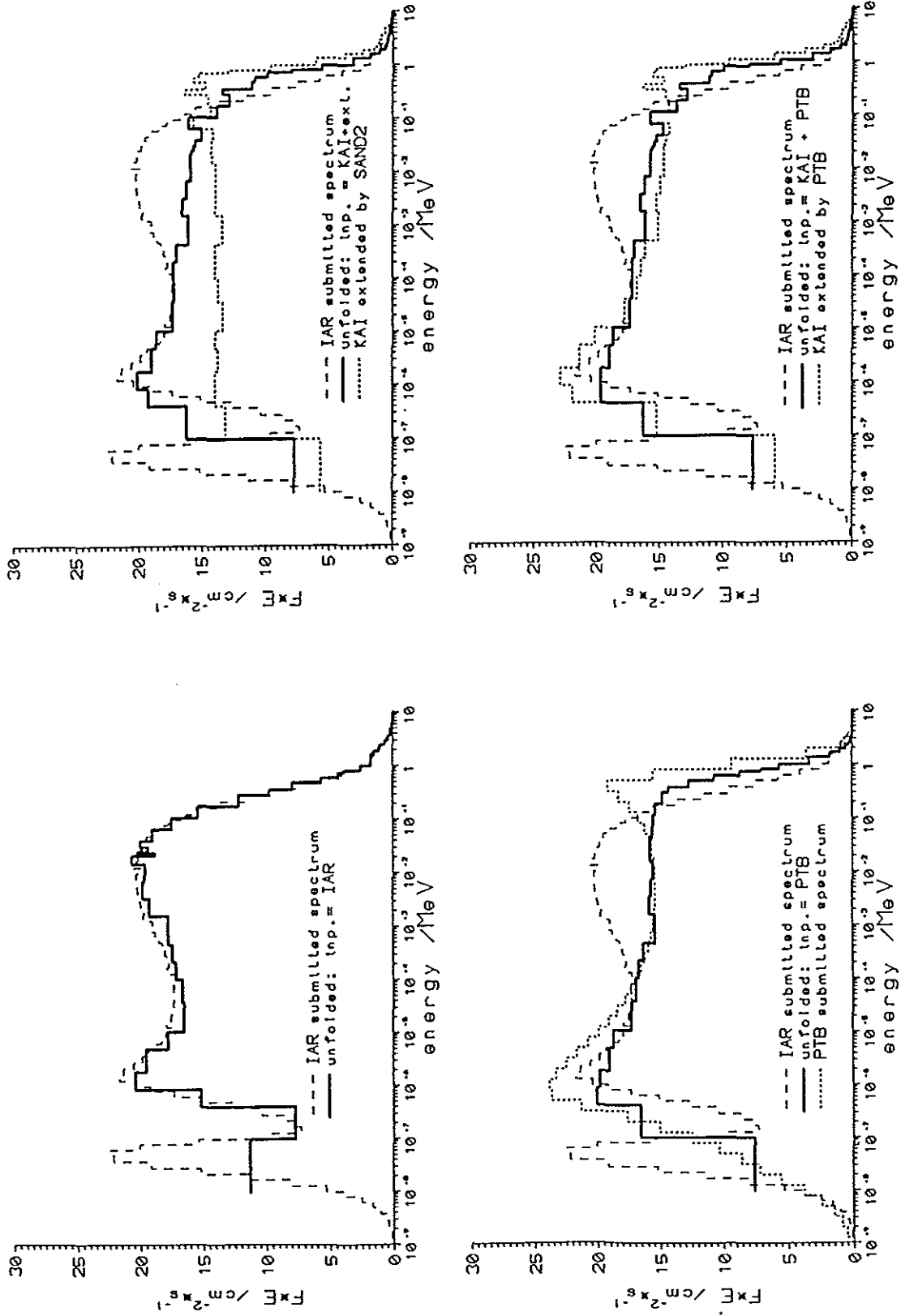


Figure 3: Unfolding of BS data sets measured by the IAR group at Ringhals (L, F, G) and CLAB (D, E, P) using different start spectra. For comparison the result submitted by IAR is shown in all figures.

CLAB-P, IAR measurement

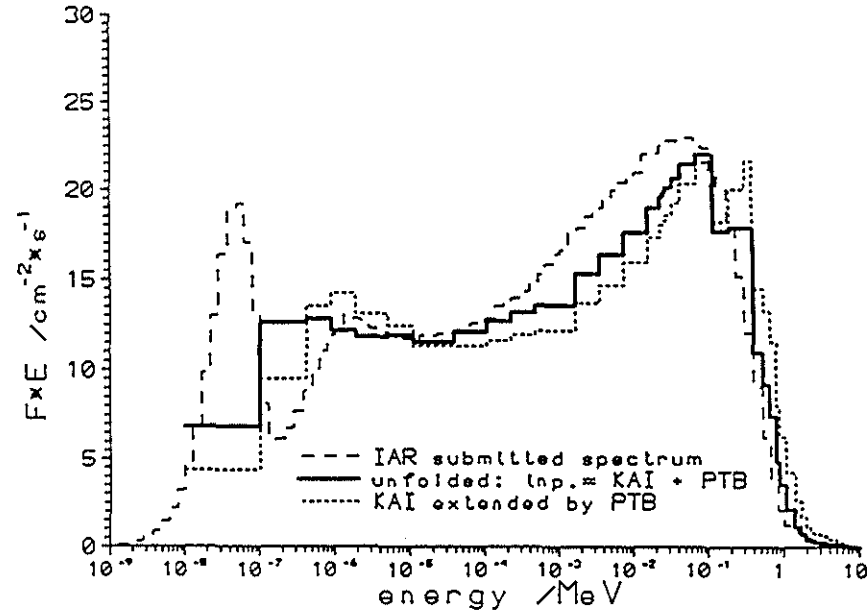
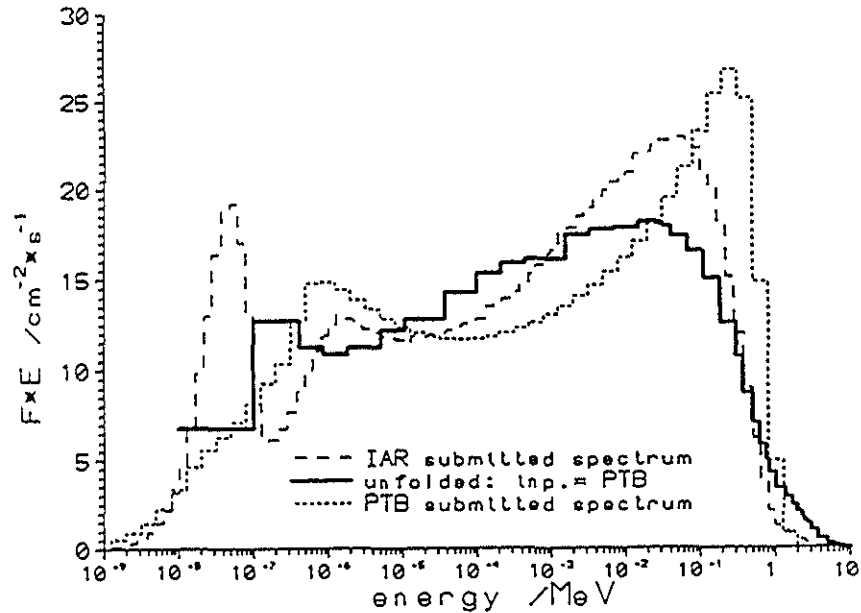
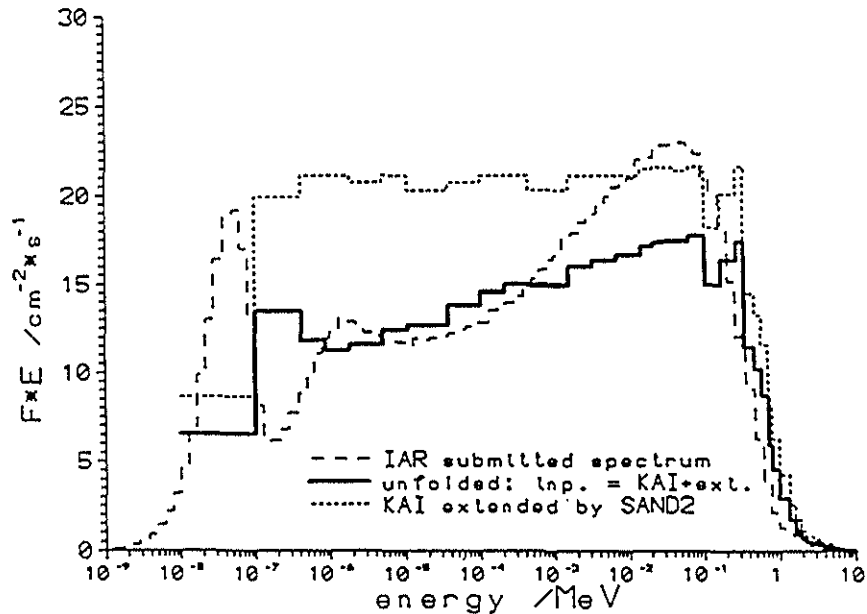
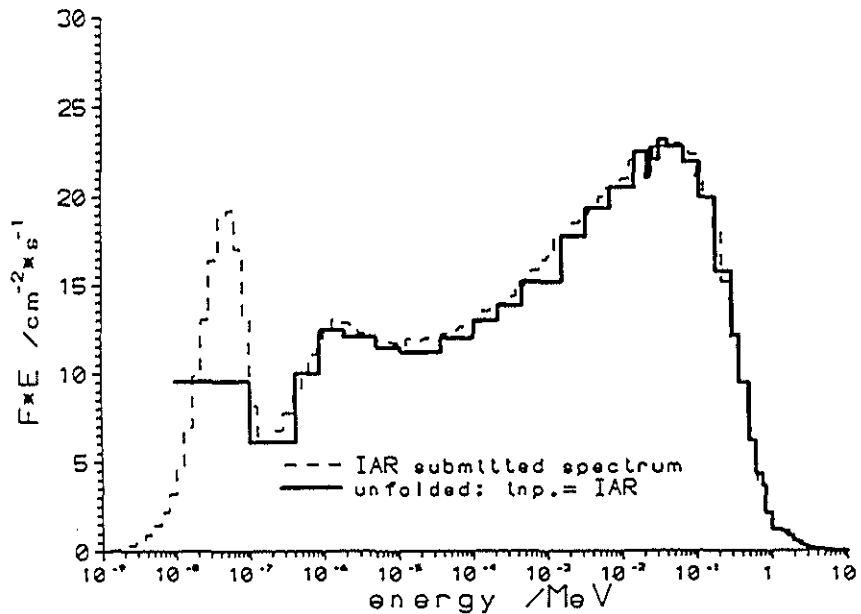


Figure 3: (continued)

Ringhals-L, IAR measurement

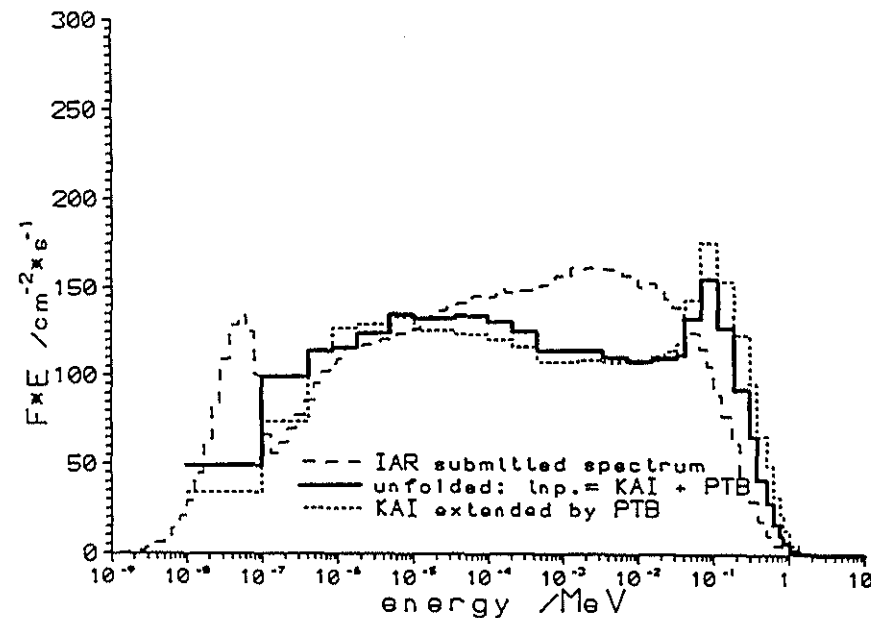
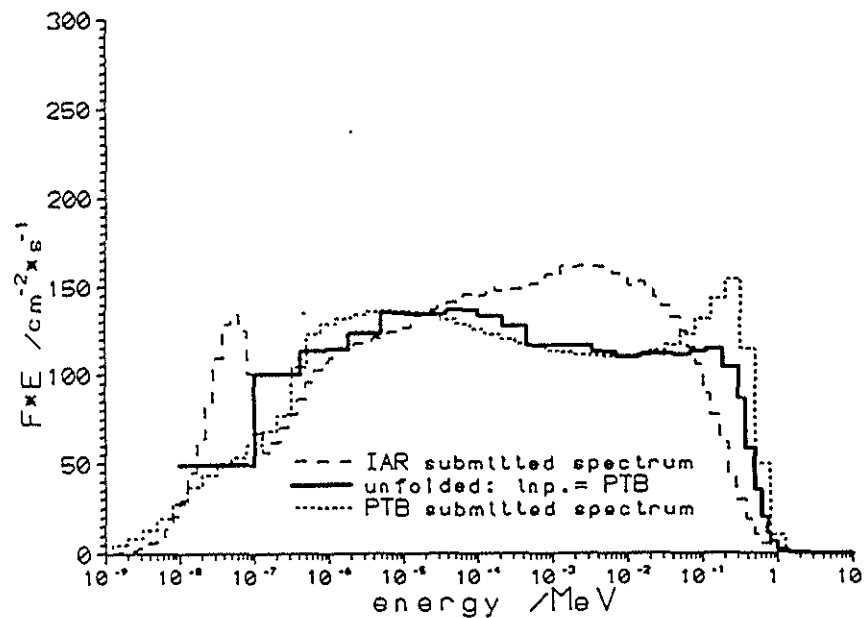
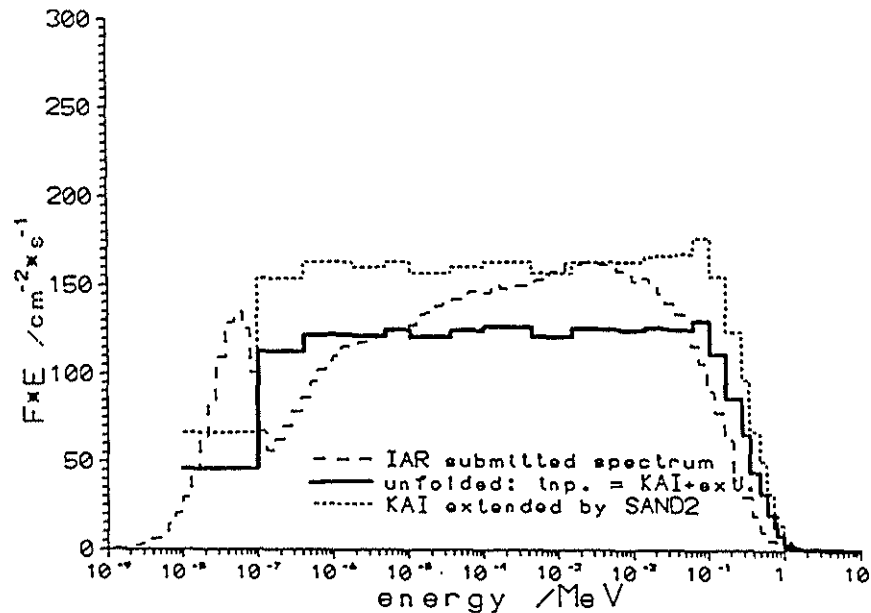
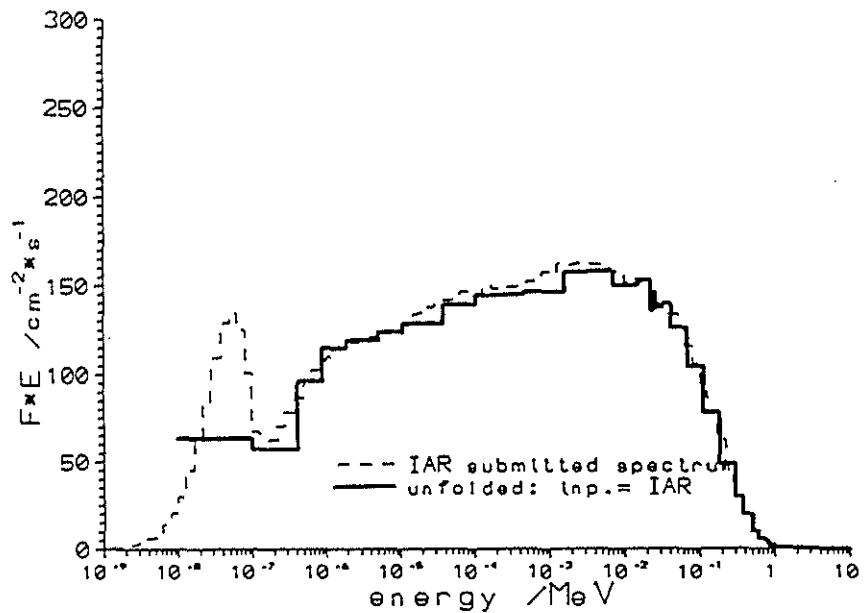


Figure 3: (continued)

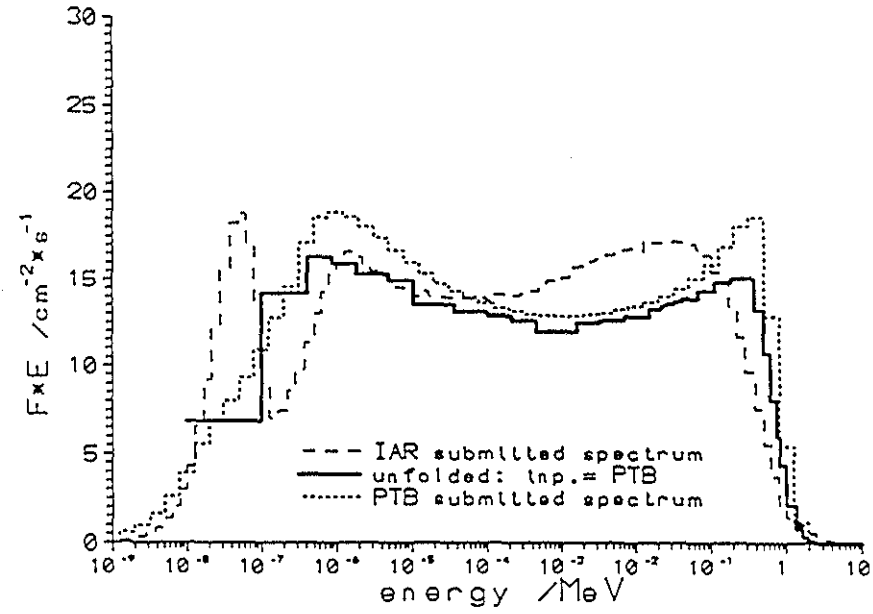
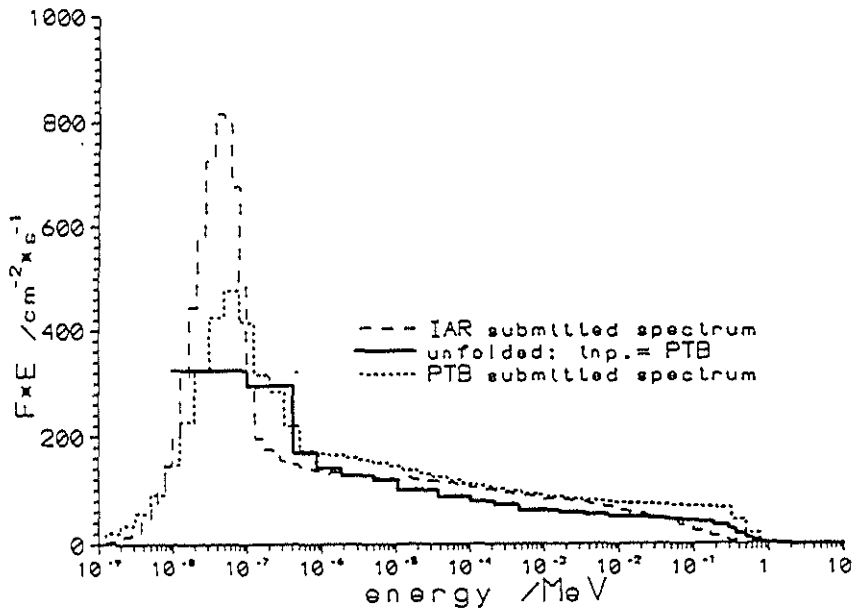
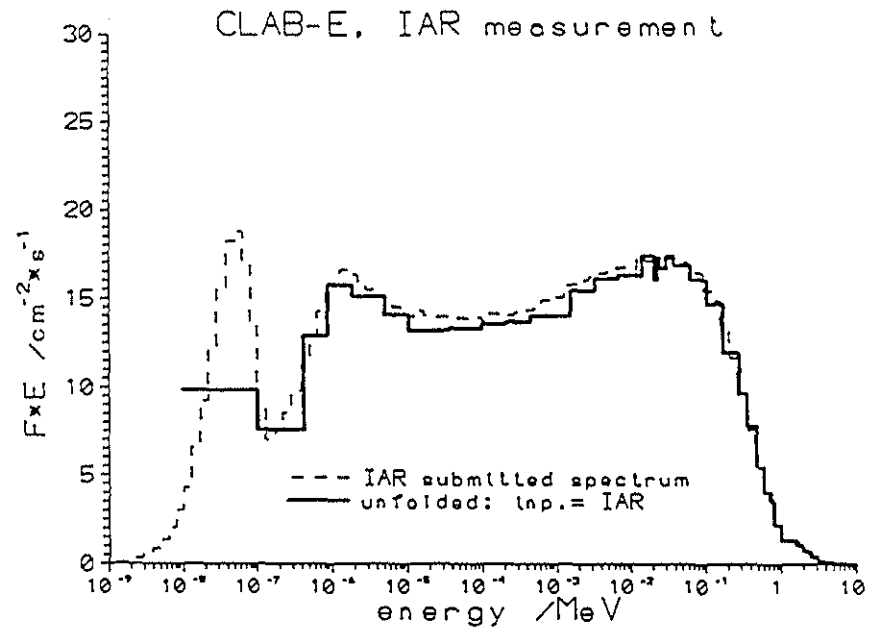
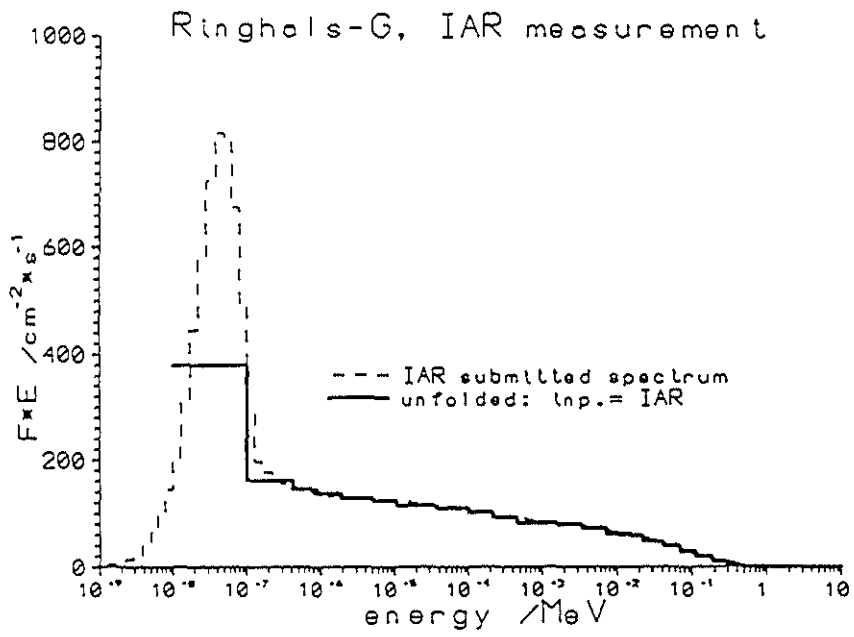
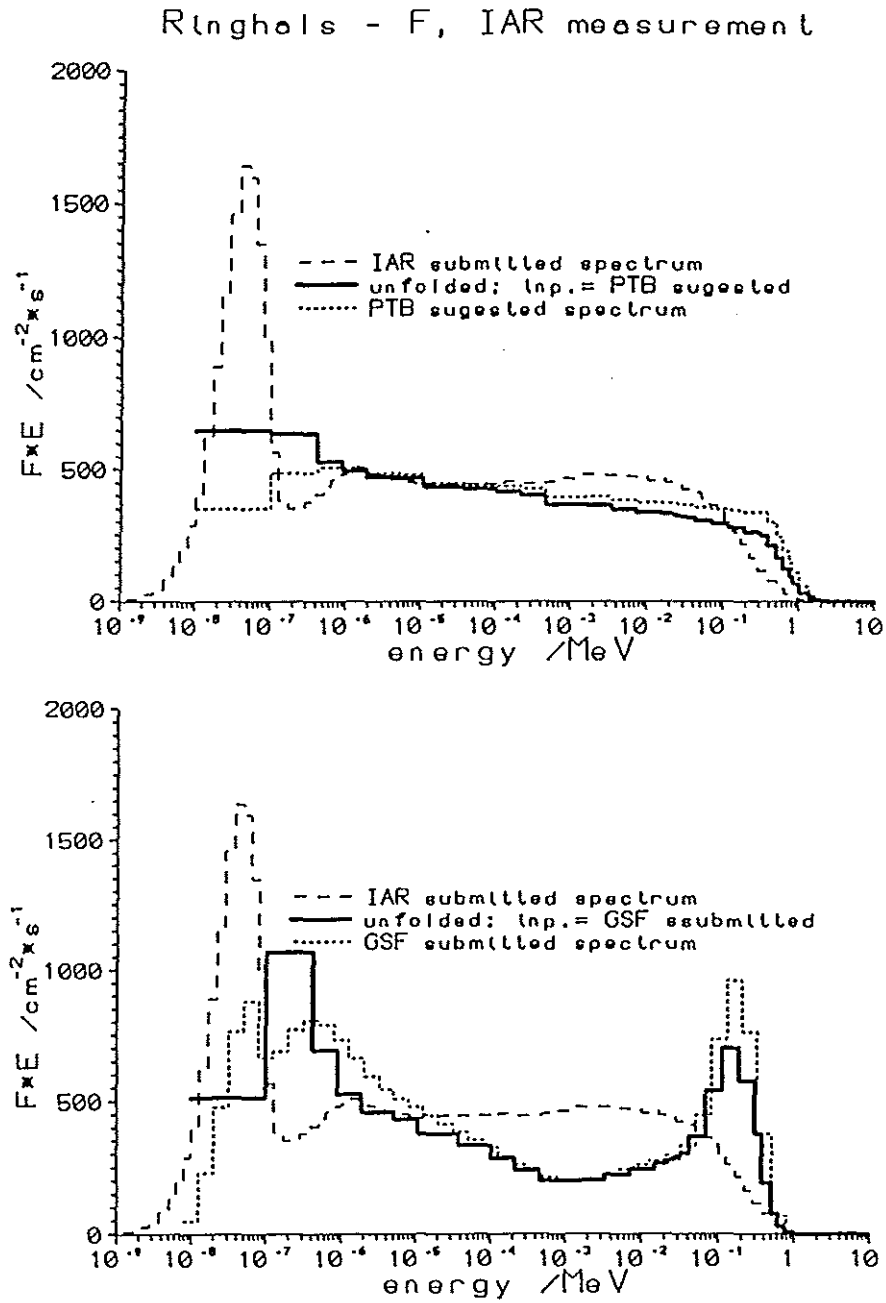


Figure 3: (continued)

Figure 3: (continued)



Unfolding of the data measured with the PTB-BSS (Table 6, Figs. 4)

Since at PTB the guess spectrum is iteratively improved in the course of the unfolding with a modified version of the SAND 2 code the submitted spectrum was directly used as input spectrum. Only small systematic shifts were observed: the fluence below 100 keV neutron energy slightly increased, and decreased above such that the total fluence was almost unchanged. In consequence the total DE values decreased by about 3%. This improvement is even questionable because rather low STDV-values (<1.5) were obtained.

Using the IAR submitted spectra as an input the general shape remains, but the thermal distribution is reduced, the epithermal part increased and the upper edge generally shifted to higher energies. The total DE values are still 15-20% lower than the original PTB results.

The spectra submitted by the GSF are generally confirmed in shape and systematic changes of the total fluence and DE values were not observed. The resulting STDV values are, however, larger than those for the other attempts.

The high resolution KAI spectra show exactly the same slope as the PTB spectra for energies above 0.5 MeV but the fluence between 70 keV and 500 keV is significantly different. Using the KAI shape with the two different extrapolations to thermal neutron energies the resulting spectra give 2 - 10% lower DE values but the discrepancies in the 70 keV to 2 MeV region remain, most obviously for pos. L. For this reason it was suspected that the KAI results suffer in normalisation problems, in particular for the measurements under severe conditions in the containment of the reactor.

Table 6: Integral fluence and DE rates ($[cm^{-2} s^{-1}]$ and $[nSv/s]$ resp.) obtained for all PTB BS data sets using different start spectra as indicated (for details see text).

PTB measurements												
	approx. rel.w. [%]	Integral values and differences from the submitted and KAI spectra [%]										
		submitted spectrum	PTB	IAR		KAI+SANDext		KAI+PTB		GSF		
CLAB-D												
< 0.4 eV	13-14	44.59	44.76	0.4%	40.89	-8.31%	48.73	9.3%	44.70	0.3%	47.60	6.8%
0.4eV-10keV	64	188.26	189.58	0.7%	192.74	2.38%	186.97	-0.7%	193.33	2.7%	184.17	-2.2%
10-100 keV	13-15	36.82	37.31	1.3%	47.494	28.99%	38.53	4.6%	36.12	-1.9%	37.60	2.1%
0.1-1. MeV	7-9	38.99	38.37	-1.6%	31.14	-20.13%	36.97	-5.2%	35.32	-9.4%	40.18	3.0%
> 1. MeV	0.6	4.37	4.06	-7.1%	4.40	0.58%	4.76	8.9%	4.80	9.8%	5.51	26.0%
0.07-2 MeV		48.91	48.08	-1.7%	41.20	-15.77%	46.84	-4.2%	44.77	-8.5%	51.19	4.7%
total fluence		313.00	314.08	0.3%	316.65	1.17%	315.96	0.9%	314.27	0.4%	315.06	0.7%
H60-PTB		17.43	17.02	-2.4%	14.66	-15.89%	17.02	-2.4%	16.55	-5.0%	18.08	3.7%
		KAI										
0.07-2 MeV		42.83	48.08	12.3%	41.20	-3.81%	46.84	9.4%	44.77	4.5%	51.19	19.5%
CLAB-E												
< 0.4 keV	15-17	39.91	40.07	0.4%	38.55	-3.4%					39.30	-1.5%
0.4eV-10keV	58-62	152.81	154.24	0.9%	156.76	2.6%					151.91	-0.6%
10-100 keV	9-13	33.37	33.93	1.7%	41.69	24.9%					25.56	-23.4%
0.1-1. MeV	8-11	36.12	35.15	-2.7%	28.47	-21.2%					42.73	18.3%
> 1. MeV	0.4-1.3	2.01	1.87	-7.1%	2.53	25.7%					2.60	29.4%
0.07-2 MeV		43.60	42.59	-2.3%	36.85	-15.5%					51.43	18.0%
total fluence		264.20	265.25	0.4%	267.98	1.4%					262.11	-0.8%
H60		14.69	14.234	-3.1%	12.25	-16.6%					16.78	14.3%
CLAB-P												
< 0.4 keV	12-14	30.71	30.87	0.5%	30.15	-1.8%	34.45	12.2%	31.23	1.7%	38.28	24.6%
0.4eV-10keV	56-60	134.85	136.27	1.1%	146.82	8.9%	145.66	8.0%	139.40	3.4%	121.81	-9.7%
10-100 keV	16-20	44.47	45.39	2.1%	48.26	8.5%	42.17	-5.2%	47.42	6.6%	43.80	-1.5%
0.1-1. MeV	9-15	50.12	48.74	-2.8%	34.97	-30.2%	39.86	-20.5%	42.25	-15.7%	60.03	19.8%
> 1. MeV	0.3-1.3	1.70	1.64	-3.3%	4.64	173.1%	3.83	125.1%	3.23	89.8%	1.04	-38.6%
0.07-2 MeV		59.77	58.50	-2.1%	45.75	-23.5%	50.23	-16.0%	53.63	-10.3%	71.03	18.8%
total fluence		261.80	262.90	0.4%	264.84	1.2%	265.97	1.6%	263.53	0.7%	264.96	1.2%
H60		18.28	17.73	-3.0%	15.28	-16.4%	16.34	-10.6%	16.54	-9.5%	19.92	9.0%
		KAI										
0.07-2 MeV		51.63	58.50	13.3%	45.75	-11.4%	50.23	-2.7%	53.63	3.9%	71.03	37.6%
Ringhals-L												
< 0.4 keV	12-13	239.12	241.13	0.8%	248.24	3.8%	278.72	16.6%	240.80	0.7%	247.00	3.3%
0.4eV-10keV	62-63	1270.20	1278.30	0.6%	1290.00	1.6%	1294.00	1.9%	1279.00	0.7%	1306.40	2.8%
10-100 keV	14-17	273.16	278.74	2.0%	357.59	30.9%	316.72	15.9%	315.35	15.4%	216.68	-20.7%
0.1-1. MeV	9-12	252.04	241.33	-4.2%	180.20	-28.5%	199.82	-20.7%	220.36	-12.6%	284.14	12.7%
> 1. MeV	< 0.3	3.04	2.99	-1.8%	5.47	79.9%	4.03	32.6%	3.62	19.1%	2.46	-19.1%
0.07-2 MeV		300.71	290.97	-3.2%	236.73	-21.3%	253.65	-15.6%	283.66	-5.7%	344.06	14.4%
total fluence		2038.00	2047.20	0.5%	2081.50	2.1%	2093.30	2.7%	2059.10	1.0%	2056.70	0.9%
H60-PTB		94.31	90.80	-3.7%	76.05	-19.4%	80.82	-14.3%	85.04	-9.8%	98.74	4.7%
		KAI										
0.07-2 MeV		355.32	290.97	-18.1%	236.73	-33.4%	253.65	-28.6%	283.66	-20.2%	344.06	-3.2%
Ringhals-G												
< 0.4 keV	52-54	1367.10	1354.50	-0.9%	1331.40	-2.6%					1410.40	3.2%
0.4eV-10keV	40-43	1269.90	1280.40	0.8%	1365.60	7.5%					1240.80	-2.3%
10-100 keV	4	170.21	171.88	1.0%	197.75	16.2%					198.11	16.4%
0.1-1. MeV	0.7-2.3	112.84	108.51	-3.8%	58.81	-47.9%					115.70	2.5%
> 1. MeV	< 0.2	1.61	1.55	-4.0%	1.01	-37.3%					0.04	-97.6%
0.07-2 MeV		139.65	135.47	-3.0%	82.62	-40.8%					154.69	10.8%
total fluence		2922.00	2916.80	-0.2%	2954.60	1.1%					2965.10	1.5%
H60-PTB		66.24	64.78	-2.2%	51.33	-22.5%					63.21	-4.6%

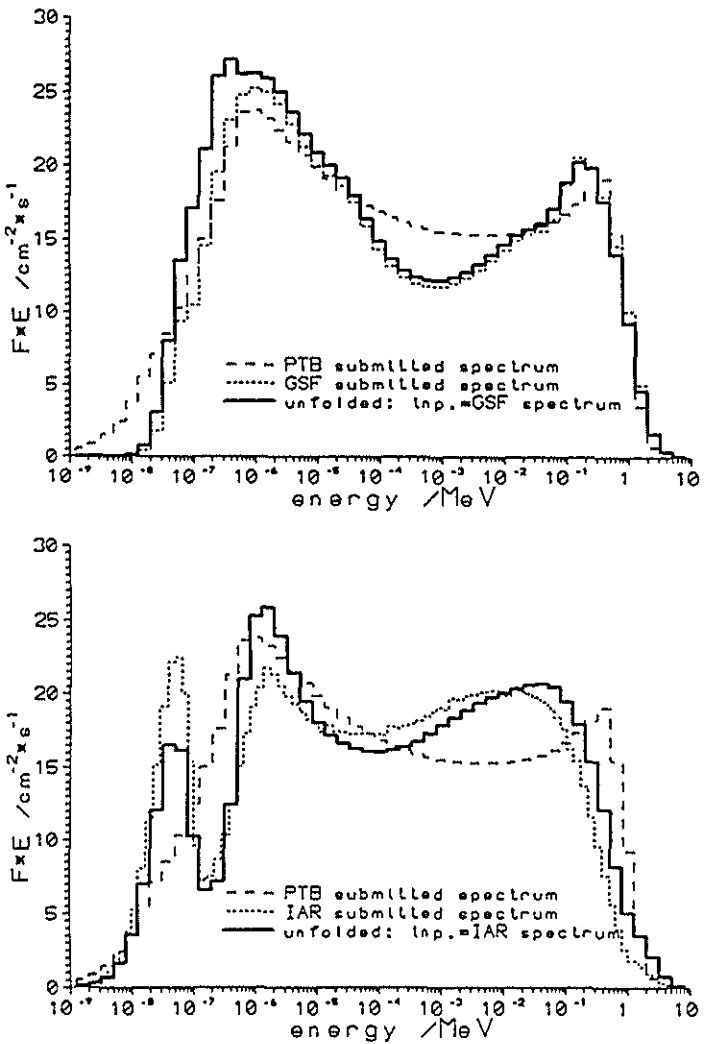
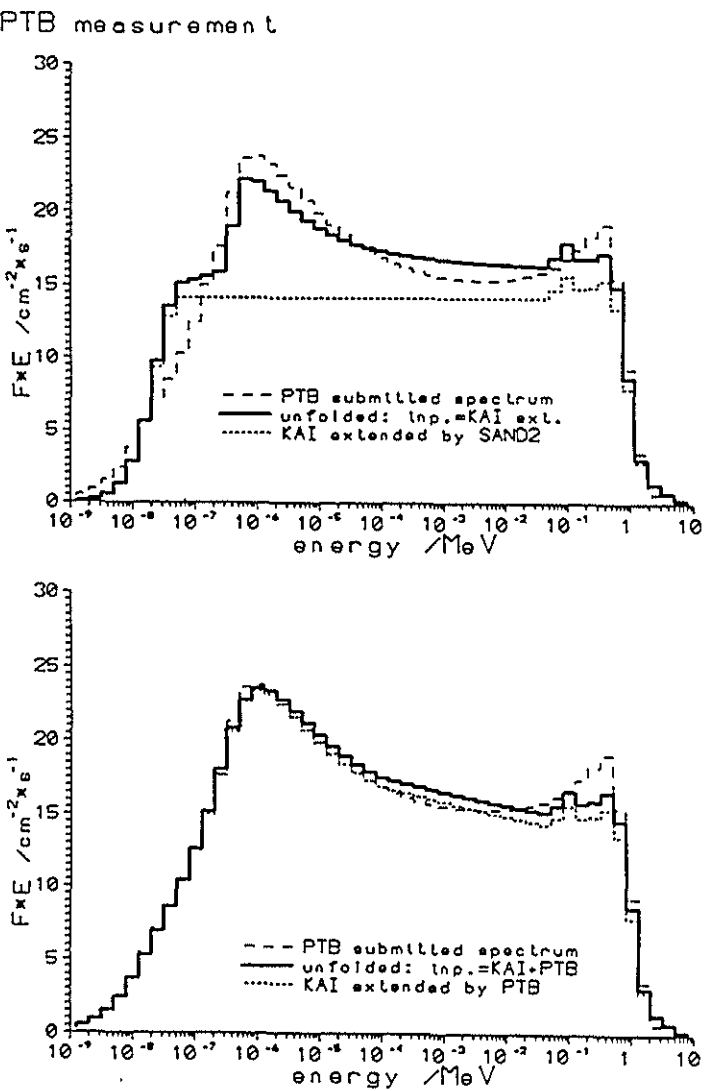


Figure 4: Unfolding of BS data sets measured by the PTB group (L, G) and CLAB (D, E, P) using different start spectra. For comparison the result submitted by PTB is shown in all figures.

CLAB-P, PTB measurement

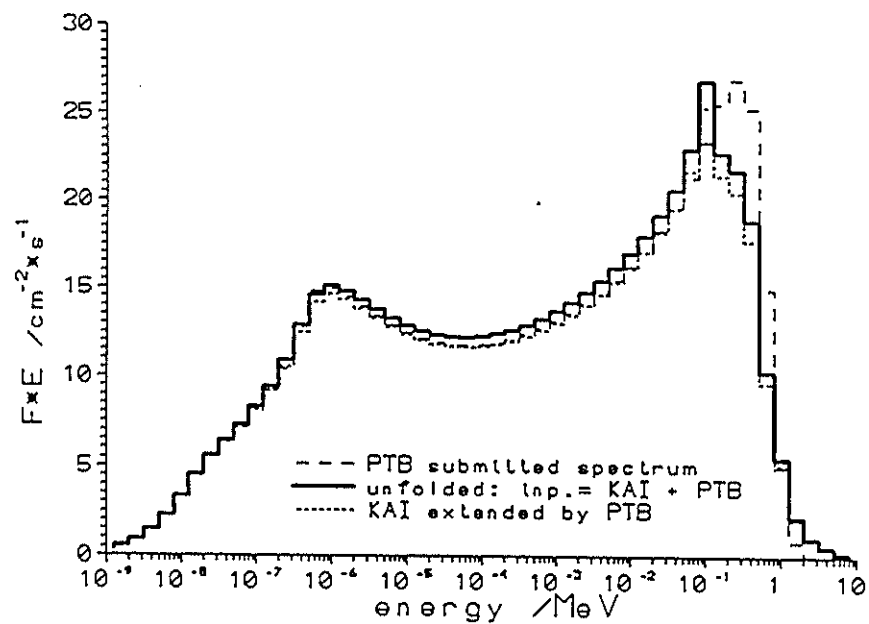
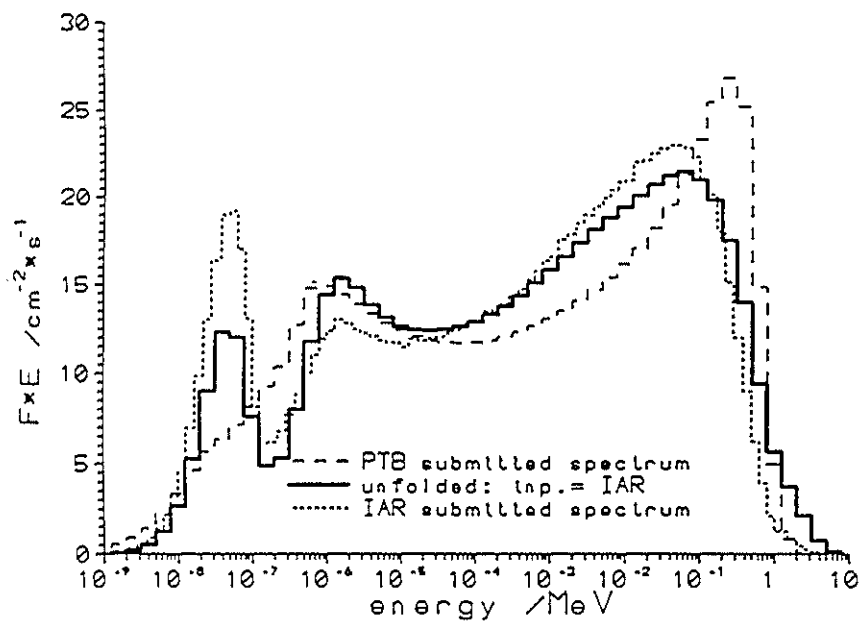
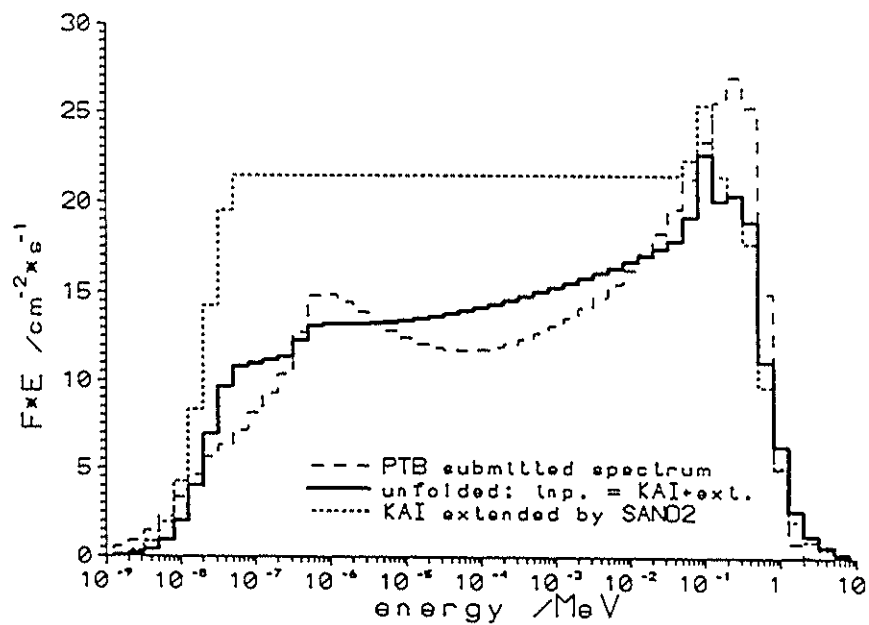
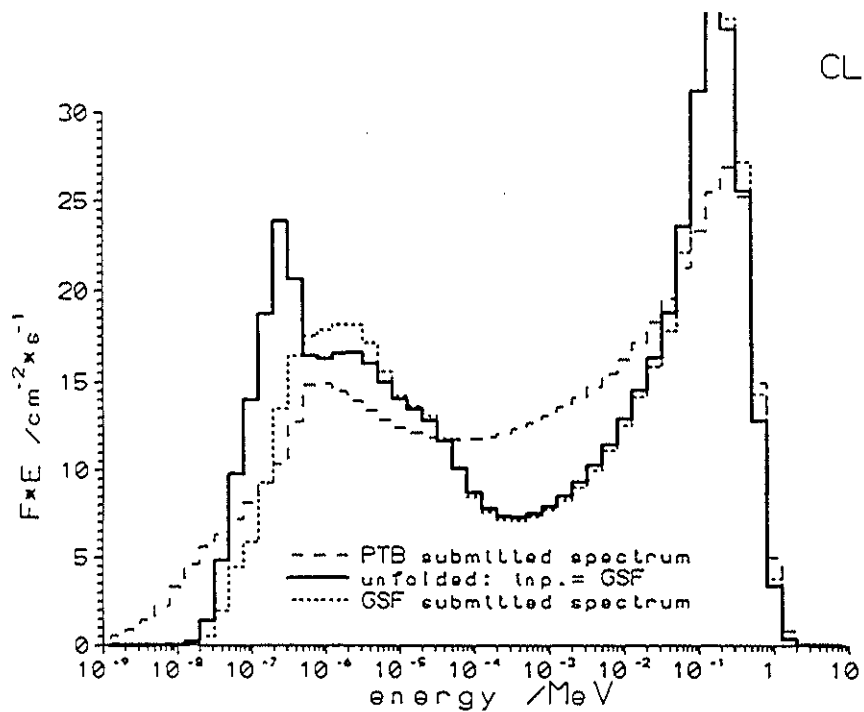


Figure 4: (continued)

Ringhals-L, PTB measurement

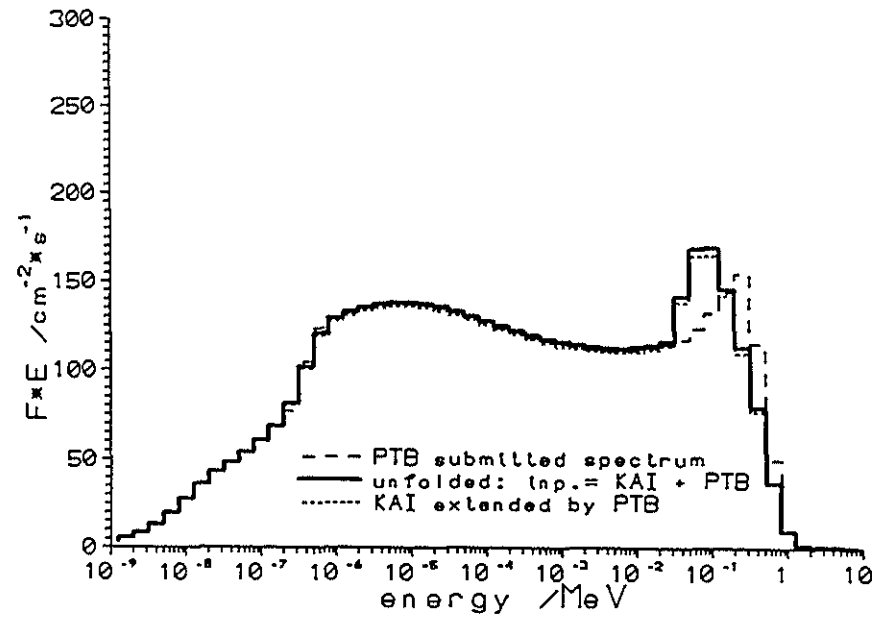
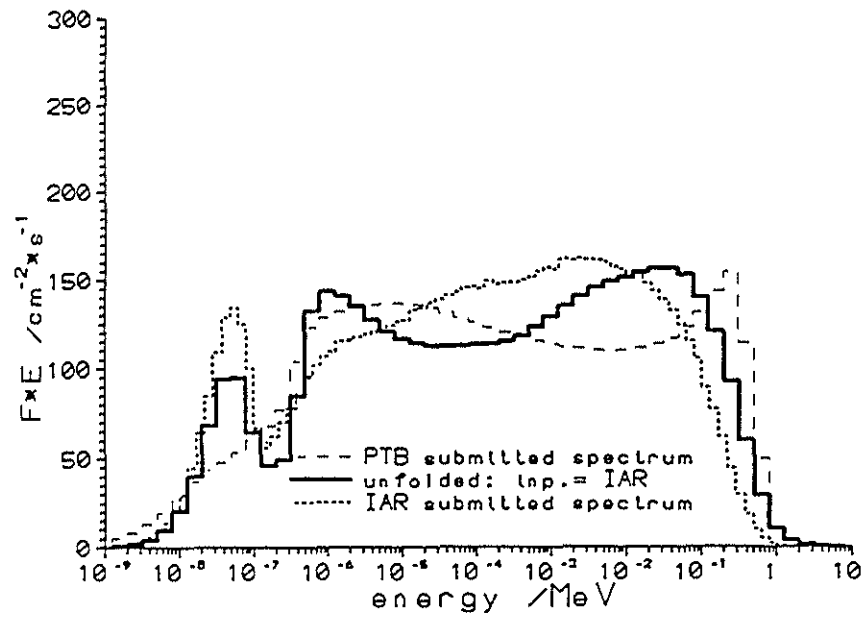
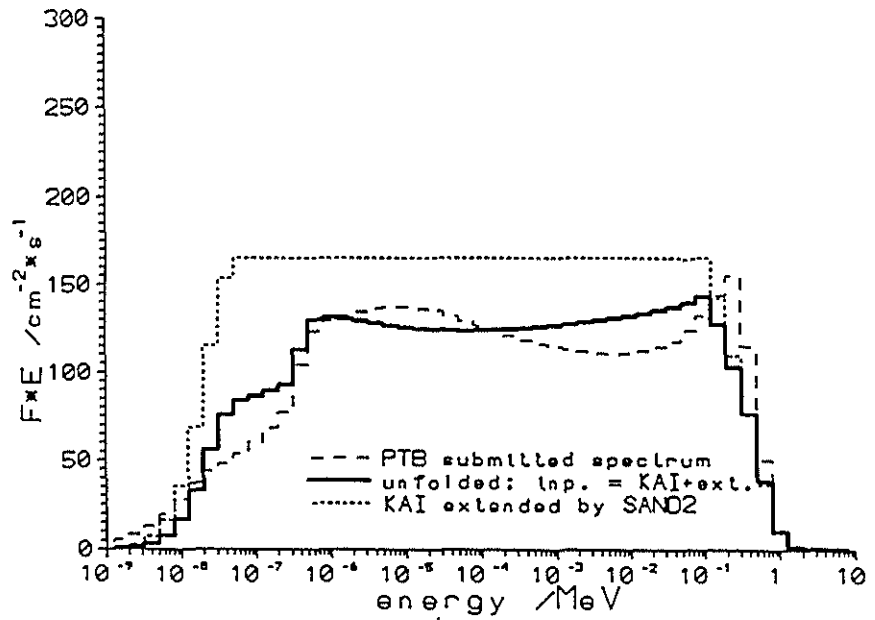
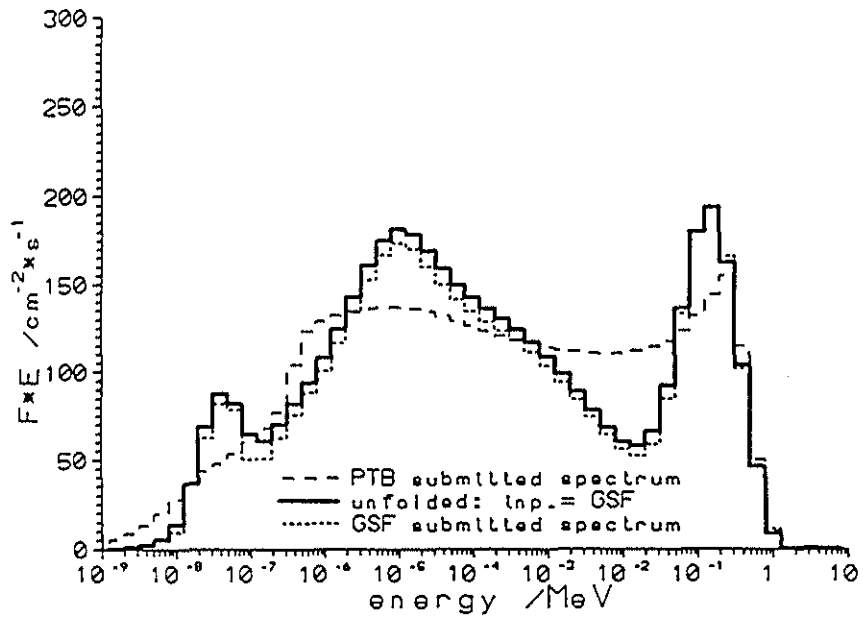


Figure 4: (continued)

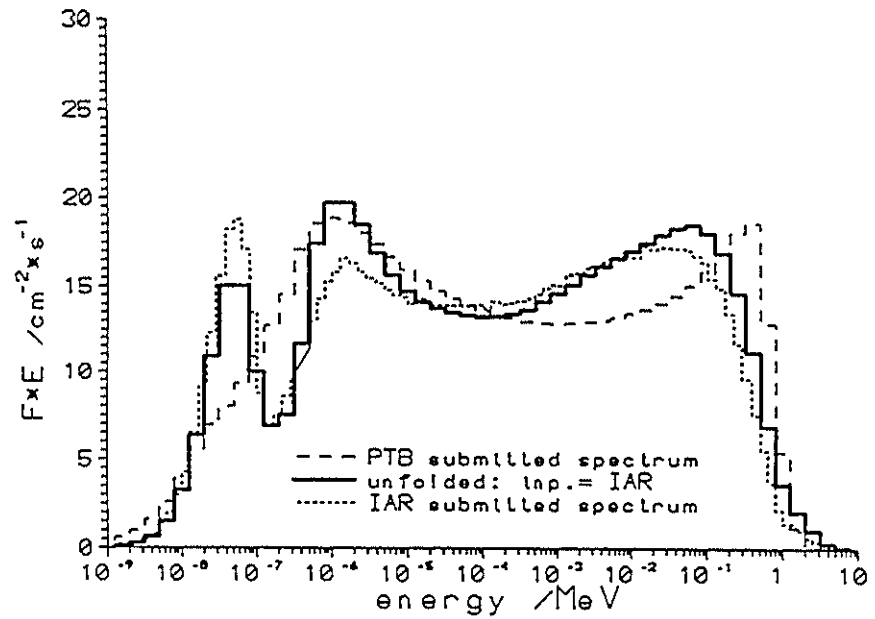
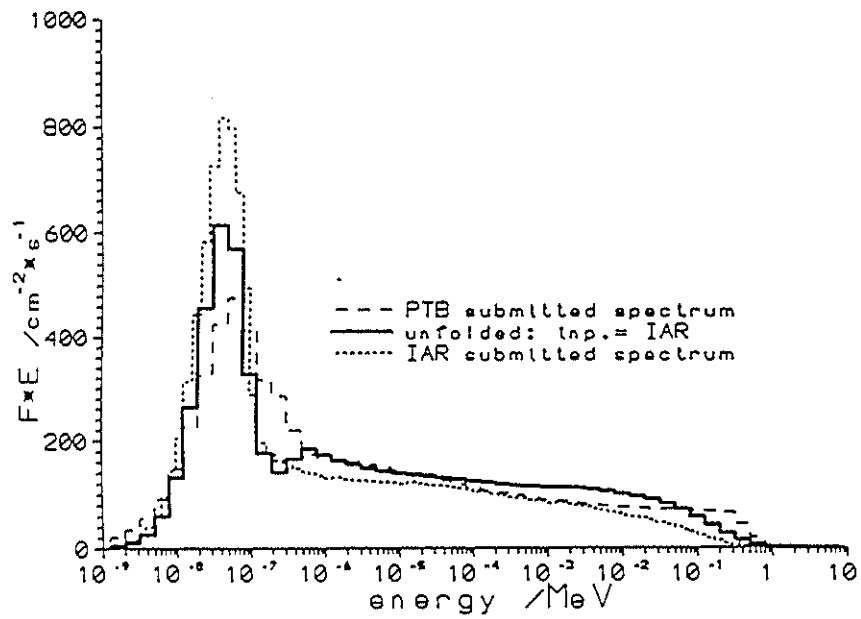
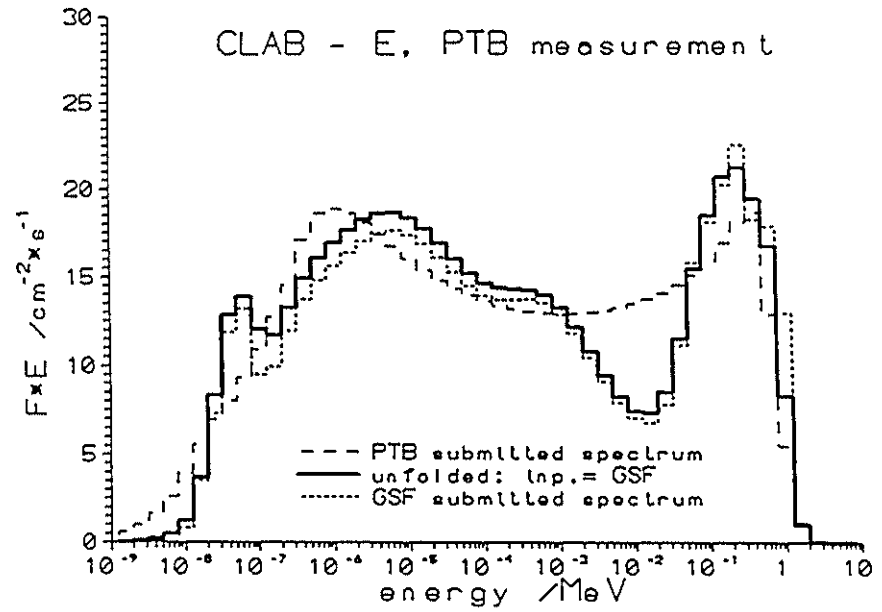
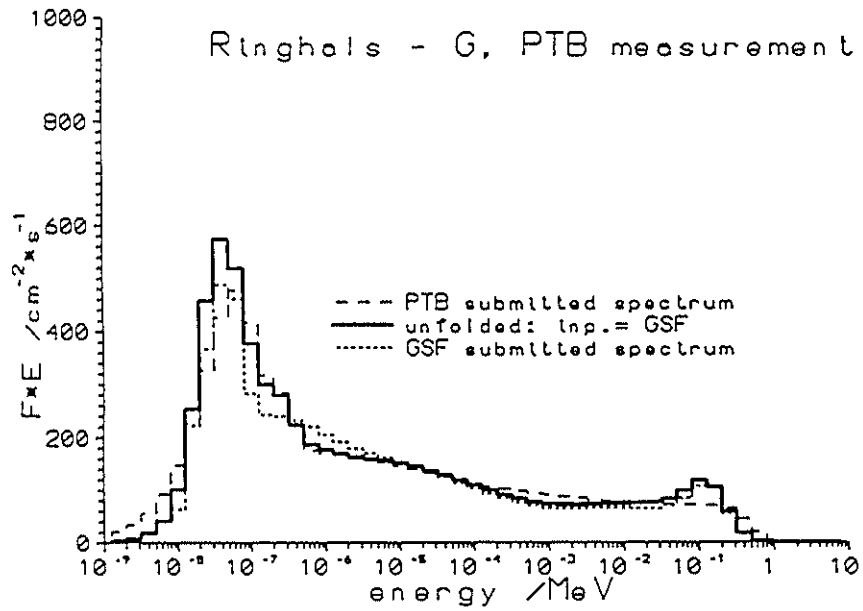


Figure 4: (continued)

Unfolding of the data measured with the GSF-BSS (Table 7, Fig 5)

Utilizing the submitted spectra as an input for the SAND 2 unfolding the shape of the spectra was generally not changed, but rather high STDV values and the comparison of measured and calculated count rates (see also Table 8 and Fig. 6) clearly indicated that the data obtained with the 10" sphere were biased for the measurements at pos. E and L.

These findings were confirmed when the PTB spectra were used. Low STDV values (2.7-3.3) after a few iterations only showed that the PTB shapes were accepted. The resulting spectra are softer than the submitted GSF results. The corresponding DE values became therefore lower than the submitted ones, except for pos. G.

The application of the extrapolated KAI spectra did not result in any improvement concerning the shape. The STDV values remained rather high (> 4) except for pos. D.

When used as input the IAR spectra were generally "hardened", the same experience as for the unfolding of the PTB data, but the total DE values are still much lower than the original GSF and PTB results. Thus, these attempts were also not satisfying.

Table 7: Integral fluence and DE rates ($[cm^{-2} s^{-1}]$ and $[nSv/s]$ resp.) obtained for all GSF BS data sets using different start spectra as indicated (for details see text).

GSF measurements										
	approx. rel.w. [%]	submitted spectrum	integral values and differences from the submitted and KAI spectra [%] corresponding to input spectrum							
			PTB	IAR	KAI+SANDext	KAI+PTB				
CLAB-D										
< 0.4 eV	12-17	33.44	39.40	17.8%	41.00	22.61%	49.09	46.8%	39.76	18.9%
0.4eV-10keV	56-62	176.89	186.06	5.2%	183.76	3.88%	168.97	-4.5%	187.96	6.3%
10-100 keV	12-16	36.62	36.57	-0.1%	50.30	37.34%	39.13	6.8%	35.08	-4.2%
0.1-1. MeV	10-14	41.00	37.93	-7.5%	31.35	-23.54%	38.45	-6.2%	34.23	-16.5%
> 1. MeV	1.3-1.9	5.98	4.06	-32.2%	3.81	-36.25%	5.14	-14.1%	4.65	-22.3%
0.07-2 MeV	13-17	52.27	47.53	-9.1%	41.36	-20.87%	49.74	-6.8%	43.34	-17.1%
total fluence		293.93	301.02	2.4%	310.22	5.54%	300.77	2.3%	301.68	2.6%
H60-PTB		18.30	16.75	-8.5%	14.30	-21.85%	17.49	-4.4%	16.01	-12.5%
0.07-2 MeV		KAI								
		42.83	47.53	11.0%	41.36	-3.43%	48.74	13.8%	43.34	1.2%
CLAB-E										
< 0.4 keV	13-15	34.51	33.83	-2.0%	38.40	11.3%				
0.4eV-10keV	54-58	144.07	144.94	0.6%	143.46	-0.4%				
10-100 keV	10-17	24.79	35.17	41.9%	45.21	82.4%				
0.1-1. MeV	13-18	43.95	41.18	-6.3%	34.32	-21.9%				
> 1. MeV	1.0-1.8	3.87	2.45	-36.9%	3.11	-19.8%				
0.07-2 MeV	17-21	53.90	49.61	-8.0%	44.03	-18.3%				
total fluence		251.19	257.56	2.5%	264.49	5.3%				
H60		17.79	16.30	-8.3%	14.27	-19.7%				
CLAB-P										
< 0.4 keV	6-11	20.06	26.85	35.1%	28.80	43.6%	27.10	35.1%	27.10	35.1%
0.4eV-10keV	50-57	123.36	133.83	18.6%	137.74	11.7%	146.28	18.6%	136.75	10.8%
10-100 keV	17-22	42.20	45.11	3.5%	58.92	39.6%	43.66	3.5%	47.16	11.8%
0.1-1. MeV	14-24	82.76	48.54	-38.7%	38.10	-36.3%	38.49	-38.7%	42.24	-32.7%
> 1. MeV	0.4-1.4	1.14	1.64	187.5%	1.93	89.6%	3.28	187.5%	3.23	183.4%
0.07-2 MeV	19-28	73.67	58.26	-20.9%	49.08	-33.4%	48.54	-34.1%	53.60	-27.2%
total fluence		249.52	255.86	2.6%	265.48	6.4%	258.75	3.7%	256.48	2.8%
H60		20.53	17.59	-14.3%	14.53	-29.2%	15.48	-24.6%	16.46	-19.8%
0.07-2 MeV		KAI								
		51.63	58.26	12.8%	49.08	-4.8%	48.54	-6.0%	53.60	3.8%
Ringhals-L										
< 0.4 keV	11-13	218.15	213.78	-2.0%	259.54	19.0%	260.24	19.3%	213.42	-2.2%
0.4eV-10keV	61-64	1236.80	1247.30	0.8%	1297.90	4.9%	1228.10	-0.7%	1244.40	0.6%
10-100 keV	11-18	204.43	269.59	31.9%	360.05	76.1%	318.59	56.3%	305.42	49.4%
0.1-1. MeV	6-14	287.17	232.83	-18.9%	133.74	-53.4%	190.02	-33.8%	212.90	-25.9%
> 1. MeV	< 0.17	3.13	2.86	-8.7%	1.78	-43.2%	3.20	2.3%	3.46	10.4%
0.07-2 MeV	9-17	347.14	280.92	-19.1%	183.19	-47.2%	243.14	-30.0%	274.17	-21.0%
total fluence		1949.70	1866.50	0.8%	2053.00	5.3%	2001.10	2.6%	1979.60	1.5%
H60-PTB		96.71	87.50	-11.4%	60.30	-38.8%	76.21	-22.8%	82.01	-16.9%
0.07-2 MeV		KAI								
		355.32	280.92	-20.9%	183.19	-48.4%	243.14	-31.6%	274.17	-22.6%
Ringhals-G										
< 0.4 keV	42-47	1149.10	1859.00	61.8%	1335.00	16.2%				
0.4eV-10keV	45-48	1253.00	1209.70	-3.5%	1310.50	4.6%				
10-100 keV	5-6.5	170.72	160.03	-6.3%	147.91	-13.4%				
0.1-1. MeV	1-4	108.80	100.22	-8.0%	30.07	-72.4%				
> 1. MeV	< 0.06	0.02	1.41	5734.9%	0.21	779.1%				
0.07-2 MeV	2-5	143.54	125.24	-12.7%	45.05	-68.6%				
total fluence		2681.80	2657.30	-0.9%	2823.70	5.3%				
H60-PTB		57.69	59.46	3.1%	41.51	-28.0%				
Ringhals-F										
< 0.4 keV	27-28	2274.80	2318.60	1.9%	2497.10	8.8%				
0.4eV-10keV	50-54	4127.40	4745.30	15.0%	4840.30	17.3%				
10-100 keV	10-13	848.35	849.86	0.2%	1157.90	36.5%				
0.1-1. MeV	5-13	1199.70	664.55	-44.6%	438.29	-63.5%				
> 1. MeV	< 0.1	0.89	31.02	3399.9%	9.45	966.6%				
0.07-2 MeV	6-16	1418.50	821.00	-42.1%	597.30	-57.8%				
total fluence		8451.20	8609.40	1.8%	8943.10	5.8%				
H60-PTB		394.40	306.56	-22.3%	227.36	-42.4%				
Ringhals-A										
< 0.4 keV	28-29	5052.70	4974.70	-1.5%	4975.40	-1.5%	5101.80	1.0%		
0.4eV-10keV	53-60	9316.69	9674.10	3.8%	9452.30	1.5%	9496.40	1.9%		
10-100 keV	8-10	1423.40	1652.30	16.1%	1744.40	22.6%	1978.50	39.1%		
0.1-1. MeV	6-8	1516.80	1270.50	-16.2%	1363.80	-10.1%	1195.40	-21.2%		
> 1. MeV	< 0.6	119.09	58.53	-50.9%	37.54	-68.5%	20.98	-82.4%		
0.07-2 MeV	8-10	1801.80	1571.70	-17.4%	1682.50	-11.5%	1525.60	-15.8%		
total fluence		17429.00	17630.00	1.2%	17573.00	0.8%	17794.00	2.1%		
H60-PTB		697.89	599.26	-14.1%	600.33	-14.0%	544.32	-22.0%		
0.07-2 MeV		KAI								
		2831.30	1571.70	-44.5%	1682.50	-40.6%	1525.60	-46.1%		

note: (*) a priori sp. = NFL submitted sp

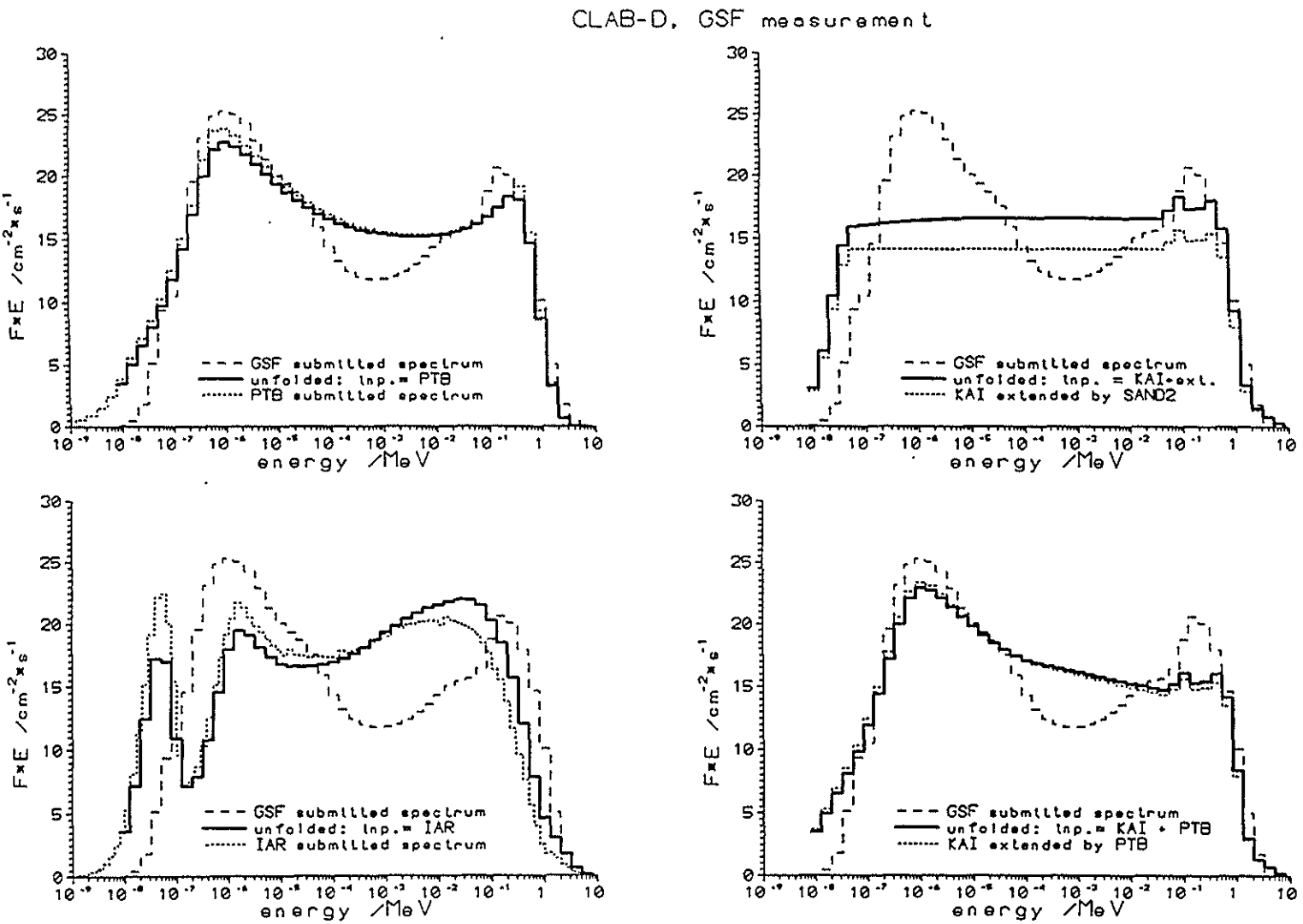


Figure 5: Unfolding of BS data sets measured by the GSF group (L, G, F, A) and CLAB (D, E, P) using different start spectra. For comparison the result submitted by GSF is shown in all figures.

CLAB-P, GSF measurement

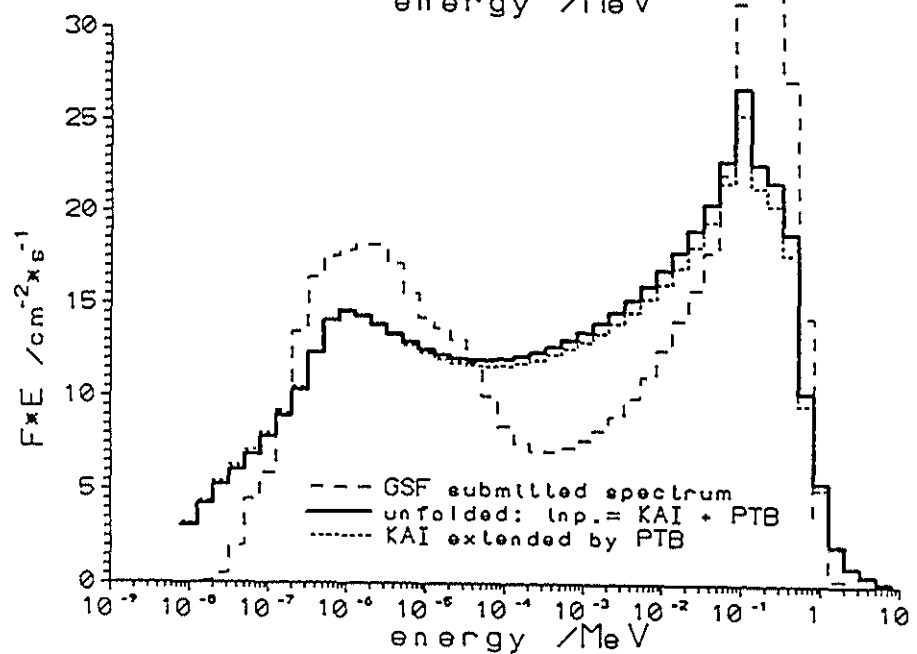
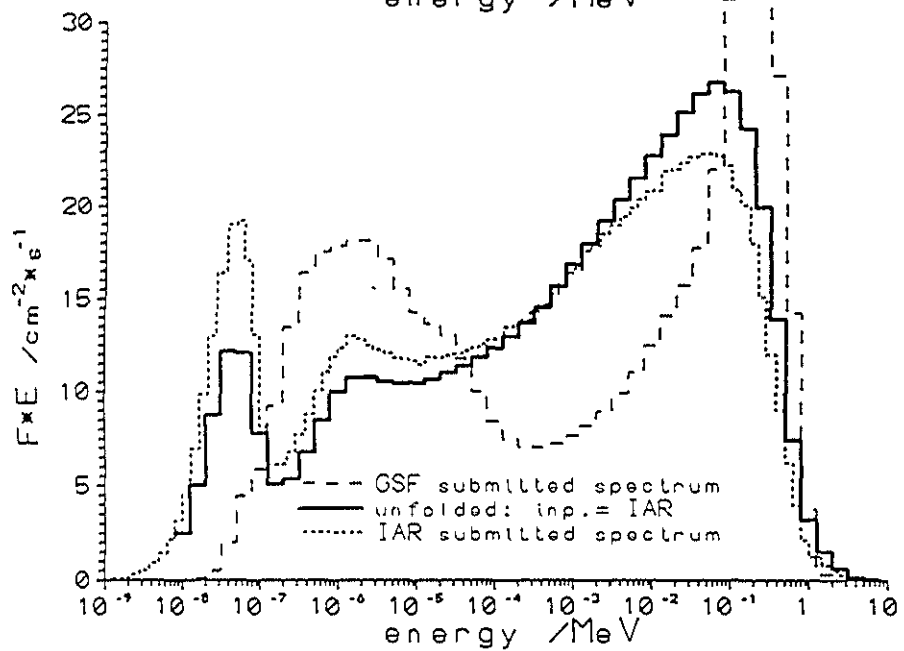
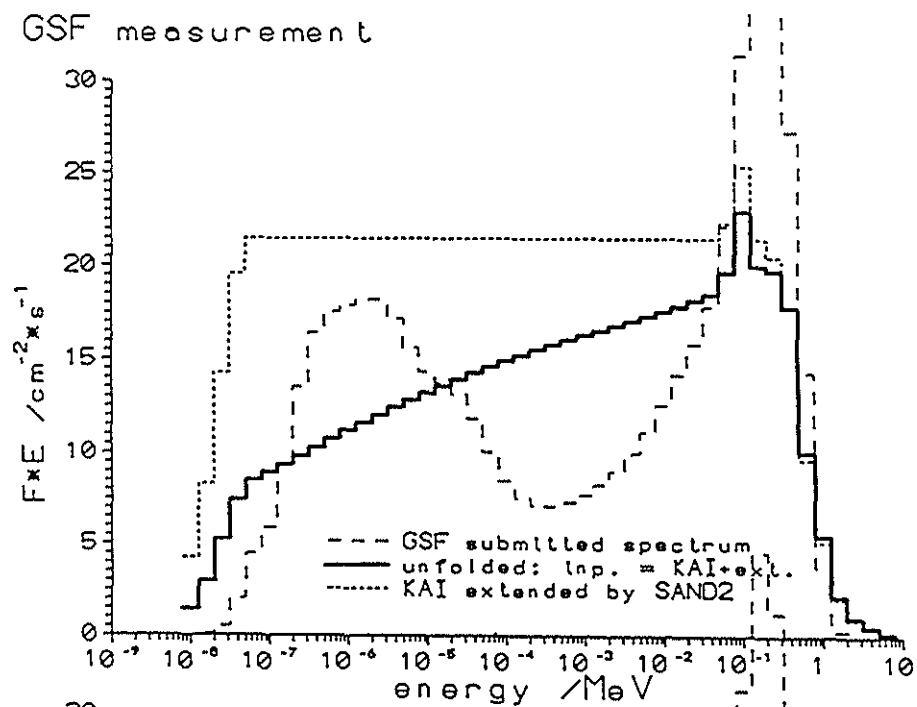
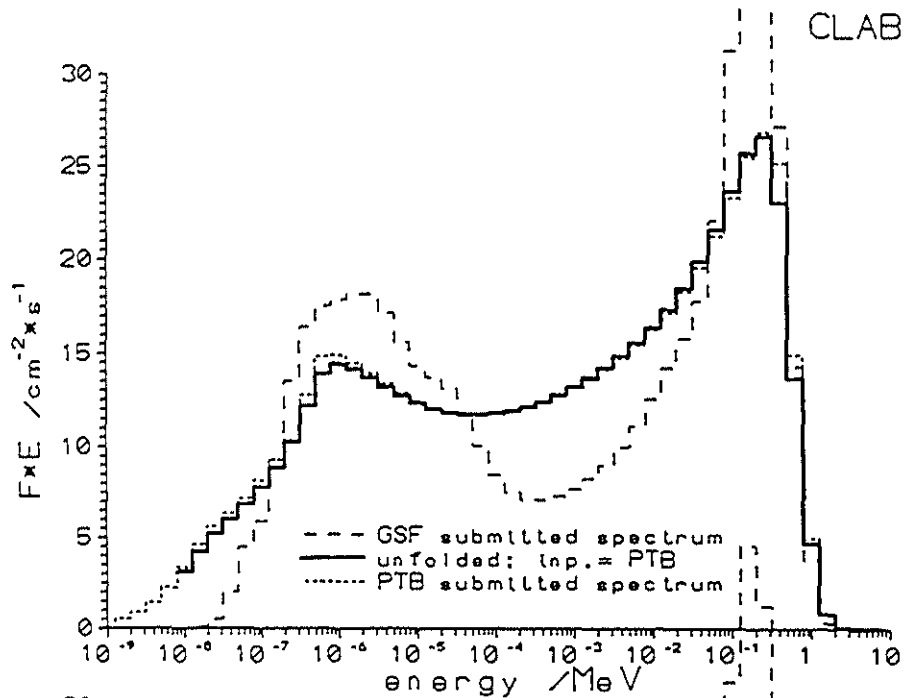


Figure 5: (continued)

Rlnghals - L, GSF measurement

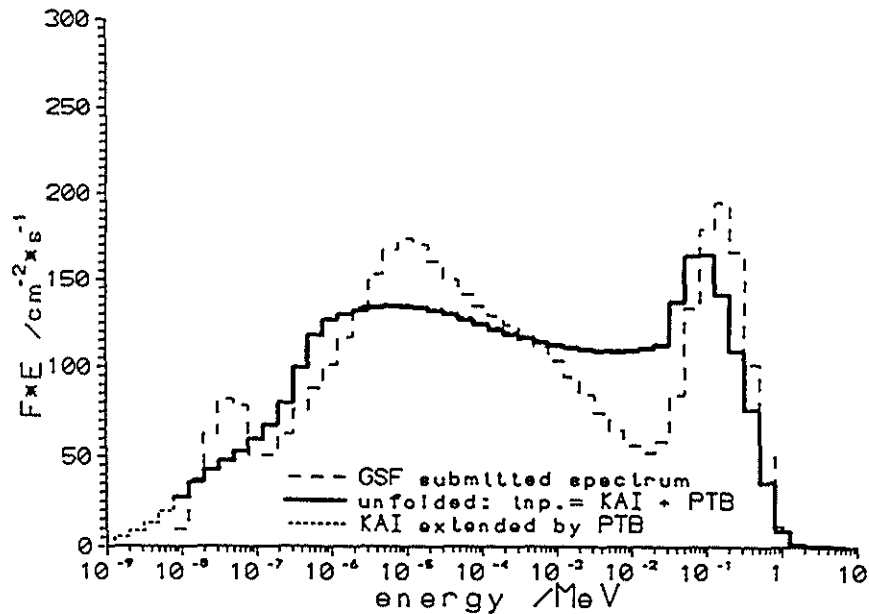
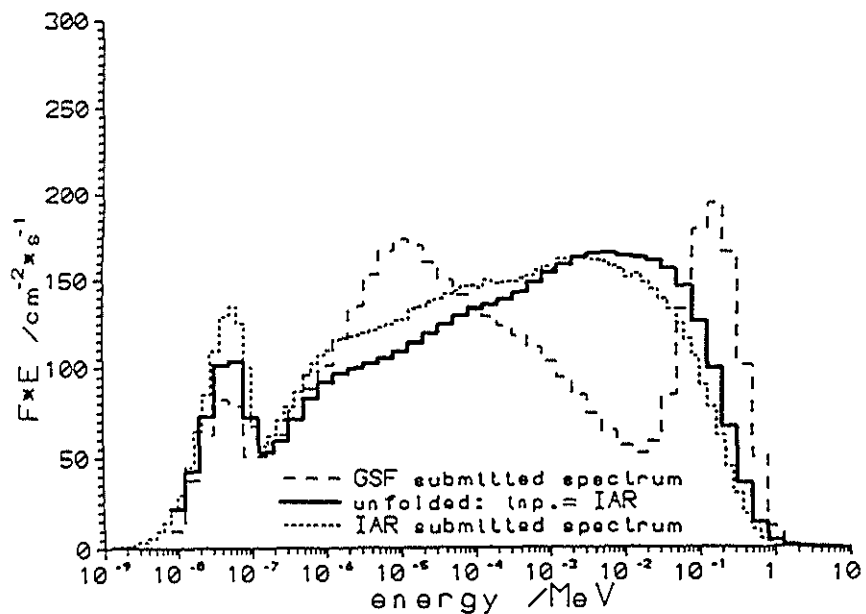
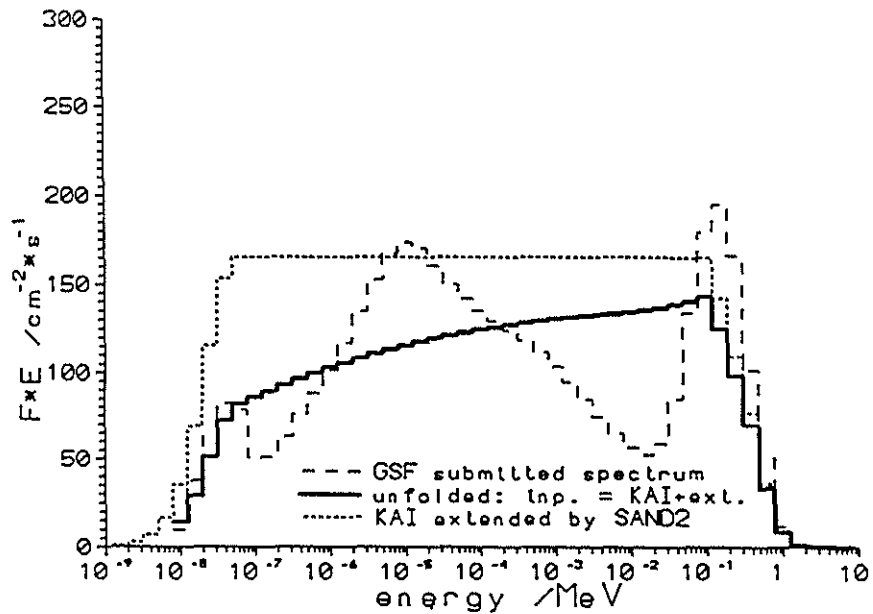
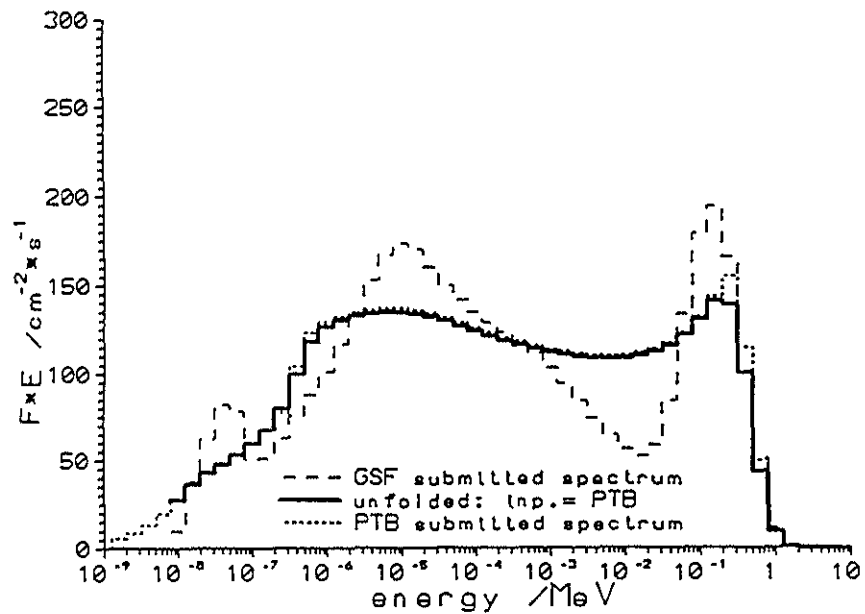
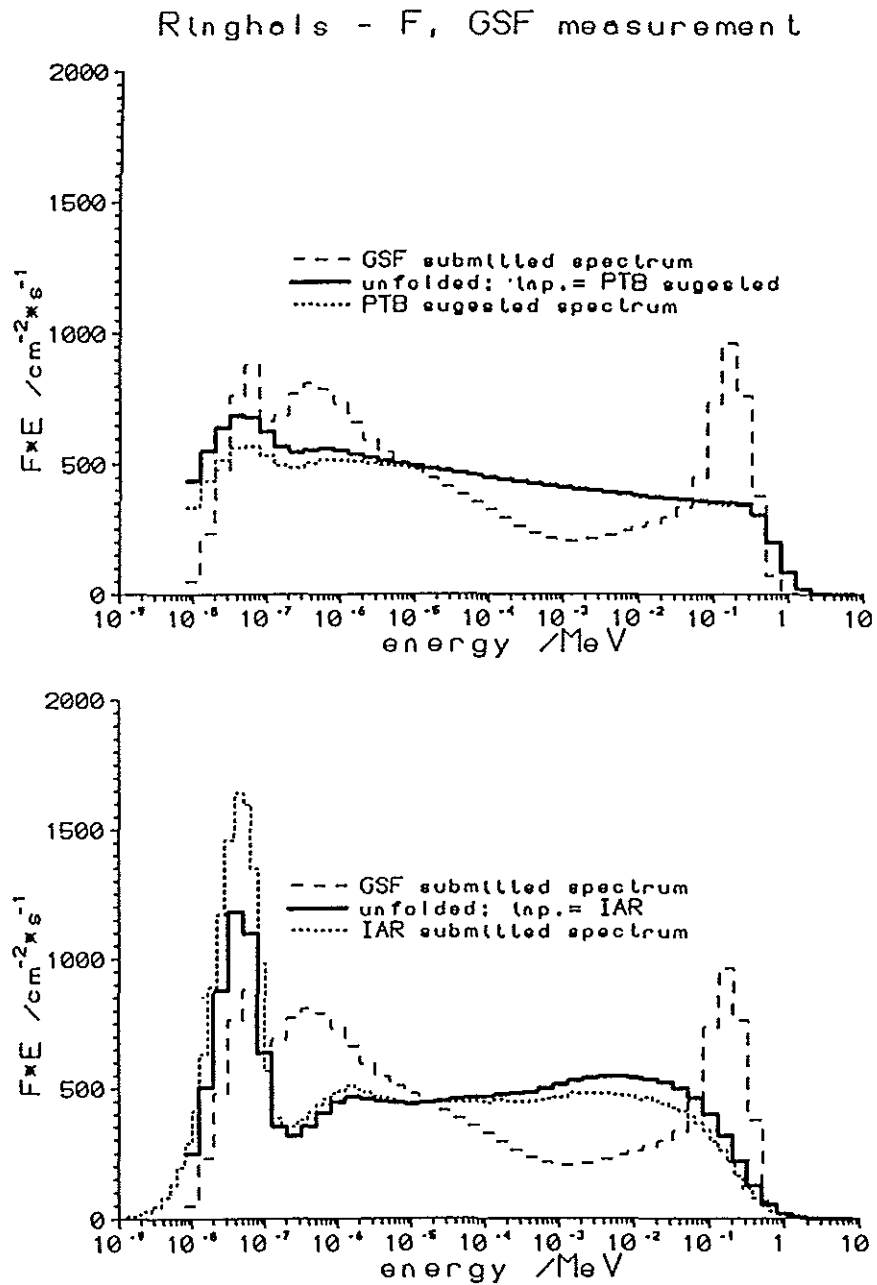
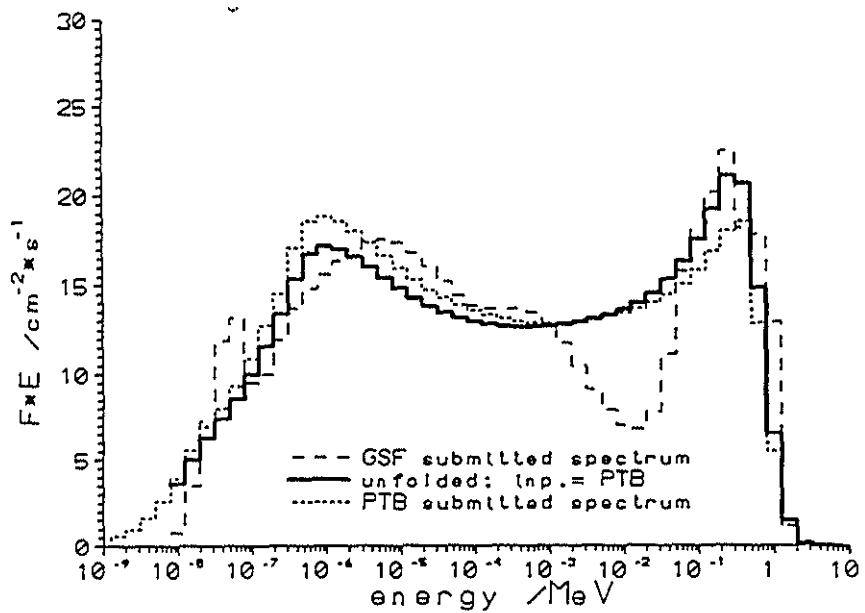


Figure 5: (continued)

Figure 5: (continued)



CLAB-E, GSF measurement



Ringhals-G, GSF measurement

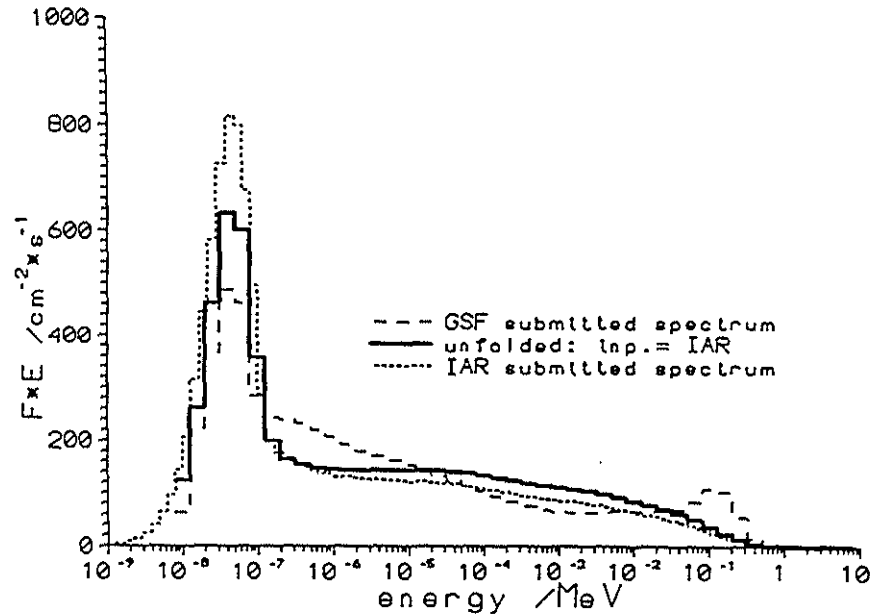
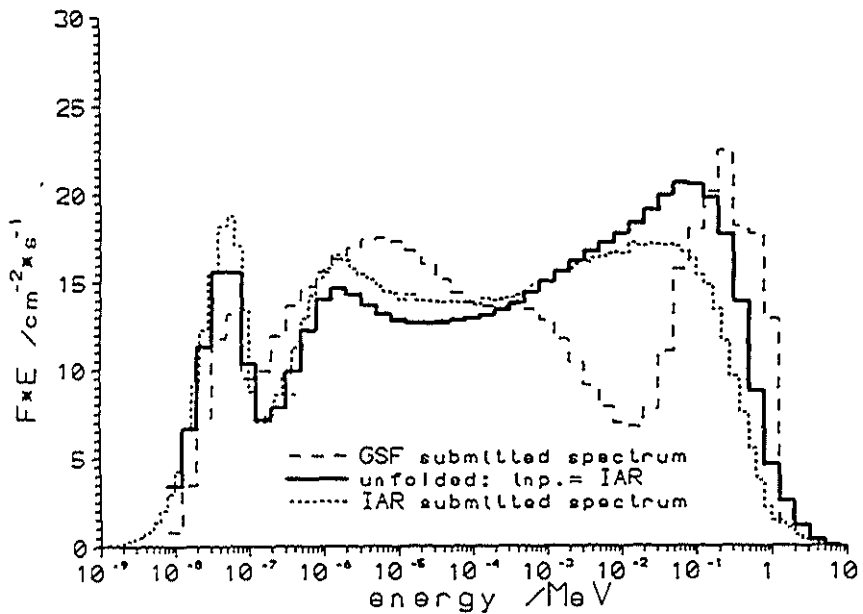
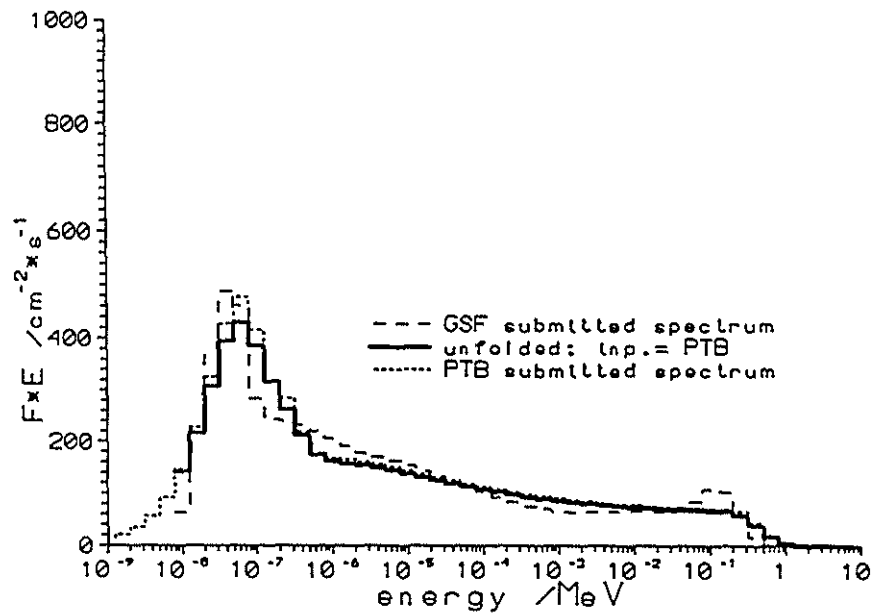
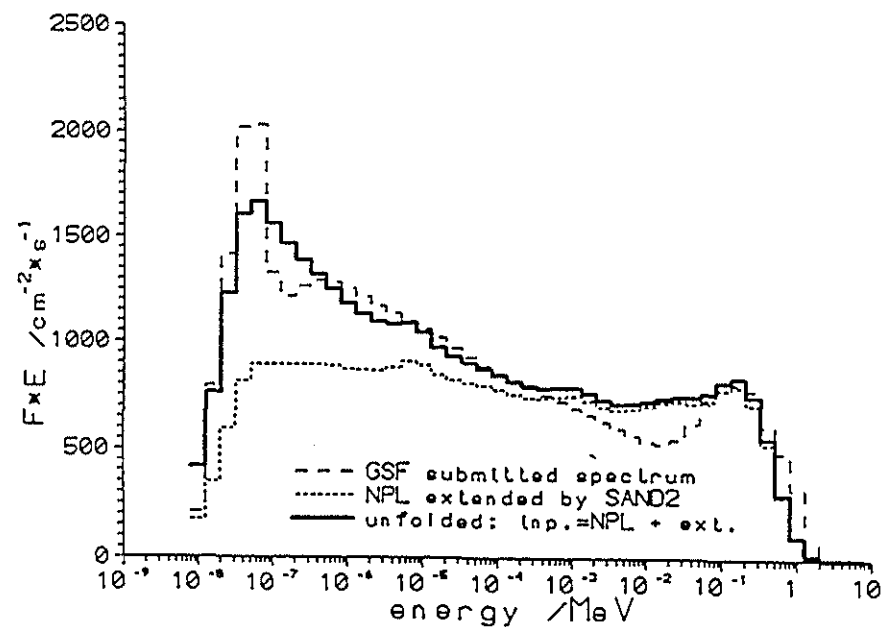
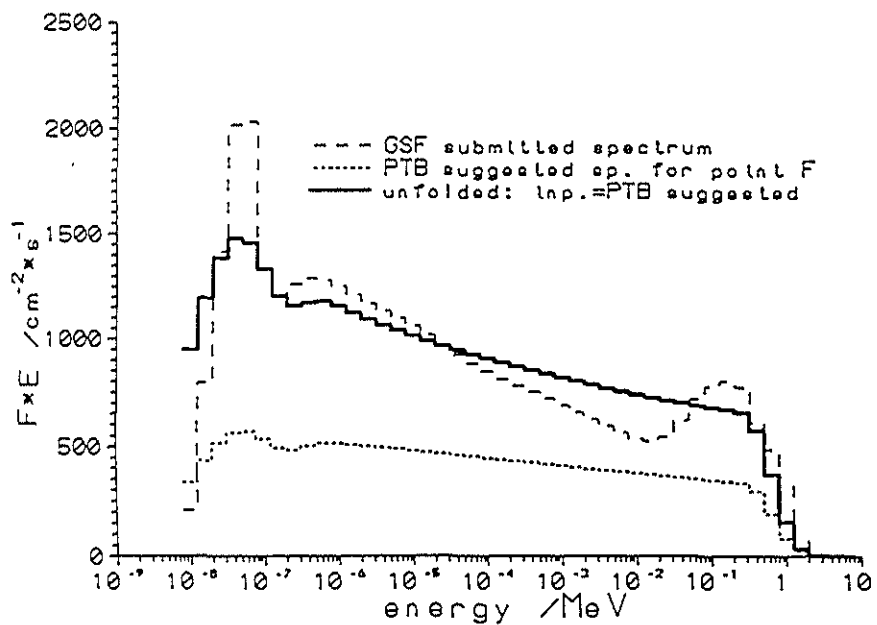
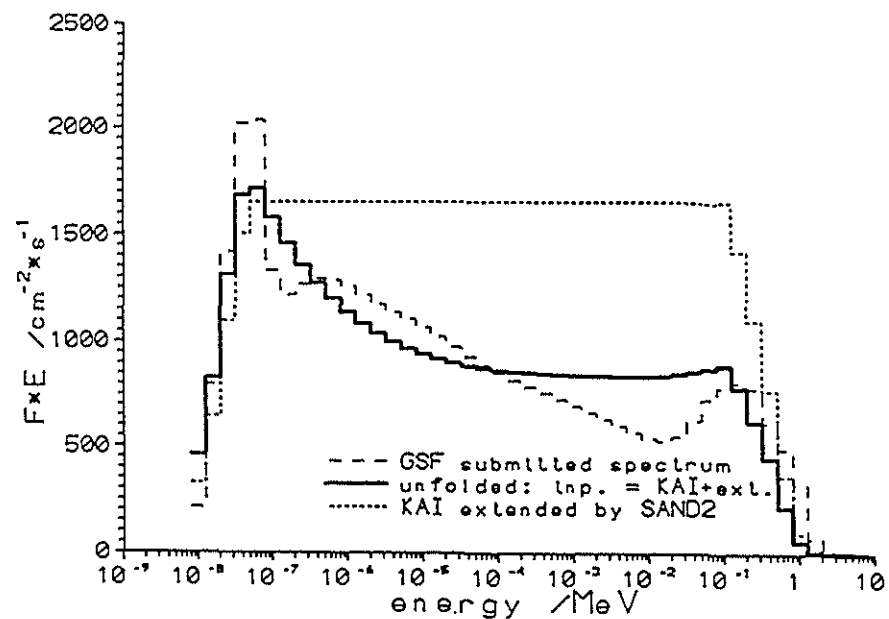


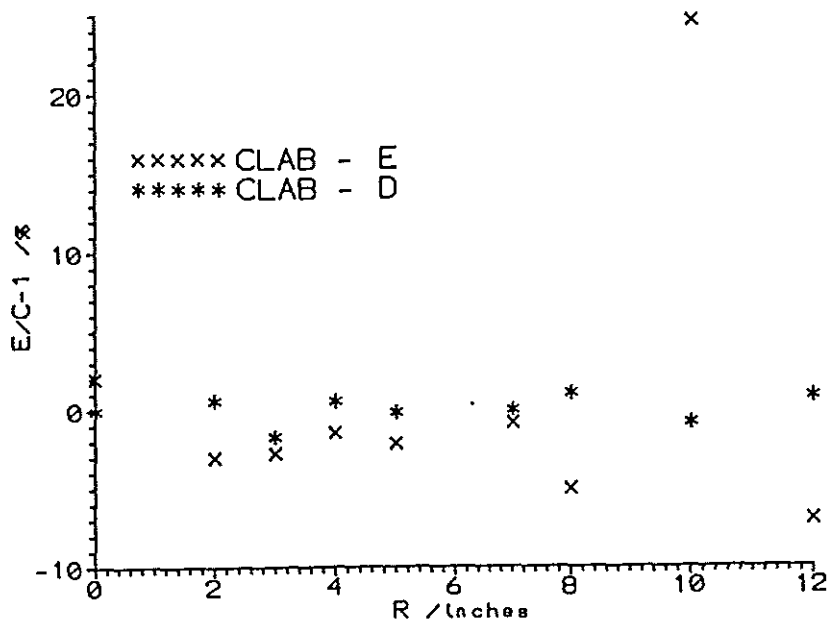
Figure 5: (continued)

Ringshals - A, GSF measurement

Figure 5: (continued)



GSc: E/C count rates for GSF submitted spectra



GSc: E/C count rates for PTB submitted spectra

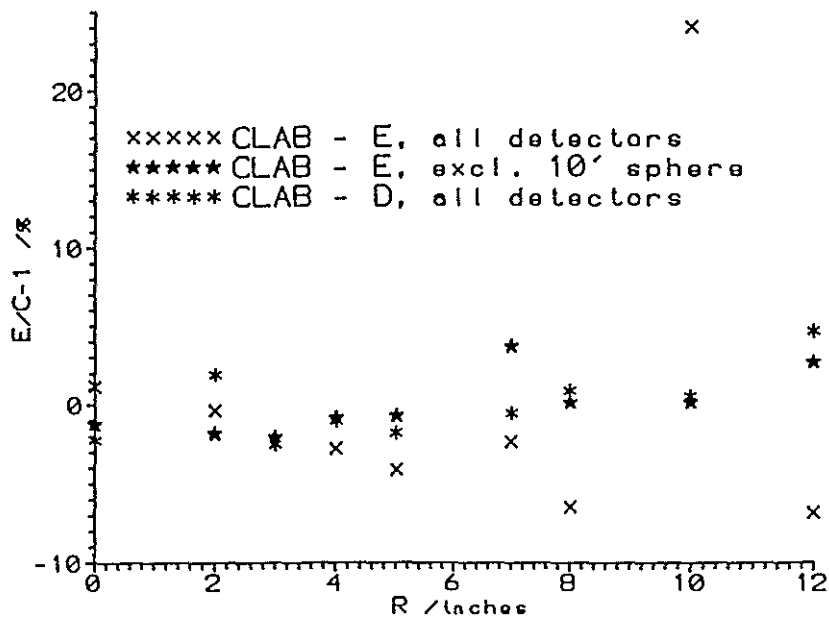


Figure 6: Deviation of measured (E) from calculated (C) BS count rates (in %) for different spheres with diameter R employed at positions E and D at CLAB.

Unfolding of the data measured with the NPL-BSS (Table 9, Fig. 7)

The NPL data were analysed not taking into account the thermal neutron fluence which was later reported separately. Best agreement with the NPL submitted results was obtained when the GSF submitted and a PTB guess spectrum were used, while the extrapolated KAI spectrum resulted in a significantly lower DE value. The lowest STDV value was obtained with the smooth PTB guess spectrum.

Table 9: Integral fluence and DE rates ($[\text{cm}^{-2} \text{s}^{-1}]$ and $[\text{nSv/s}]$ resp.) obtained for all NPL BS data sets using different start spectra as indicated (for details see text).

NPL measurements										
	approx. rel.w. [%]	submitted spectrum	Integral values and differences from the submitted and KAI spectra [%]							
			PTB (**)	corresponding to input spectrum			submit.val			
				GSF	KAI+SANDext.					
					Ringhals-A					
0.4eV-10keV	72-75	8000.30	8329.90	4.1%	8361.10	4.5%	8212.4	2.7%	7999	-0.0%
10-100 keV	12-17	1696.10	1563.30	-7.8%	1342.10	-20.9%	1923.60	13.4%	1696	-0.0%
0.1-1. MeV	10-13	1377.00	1209.00	-12.2%	1380.90	0.3%	1079.20	-21.6%	1377	0.0%
> 1. MeV	<0.4	39.82	58.00	45.7%	91.45	129.7%	17.75	-55.4%	39.81	-0.0%
0.07-2 MeV	12-15	1686.90	1495.90	-11.3%	1718.90	1.9%	1389.20	-17.6%		
*total fluence		11113.00	11160.00	0.4%	11176.00	0.6%	11233.00	1.1%	11110	-0.0%
*H60-PTB		525.68	502.55	-4.4%	566.52	7.8%	428.61	-18.5%		
		KAI								
0.07-2 MeV		2831.30	1495.90	-47.2%	1718.90	-39.3%	1389.20	-50.9%		

note: * means without thermal neutrons

(**) PTB spectrum suggested for F point

Ringhols - A, NPL measurement

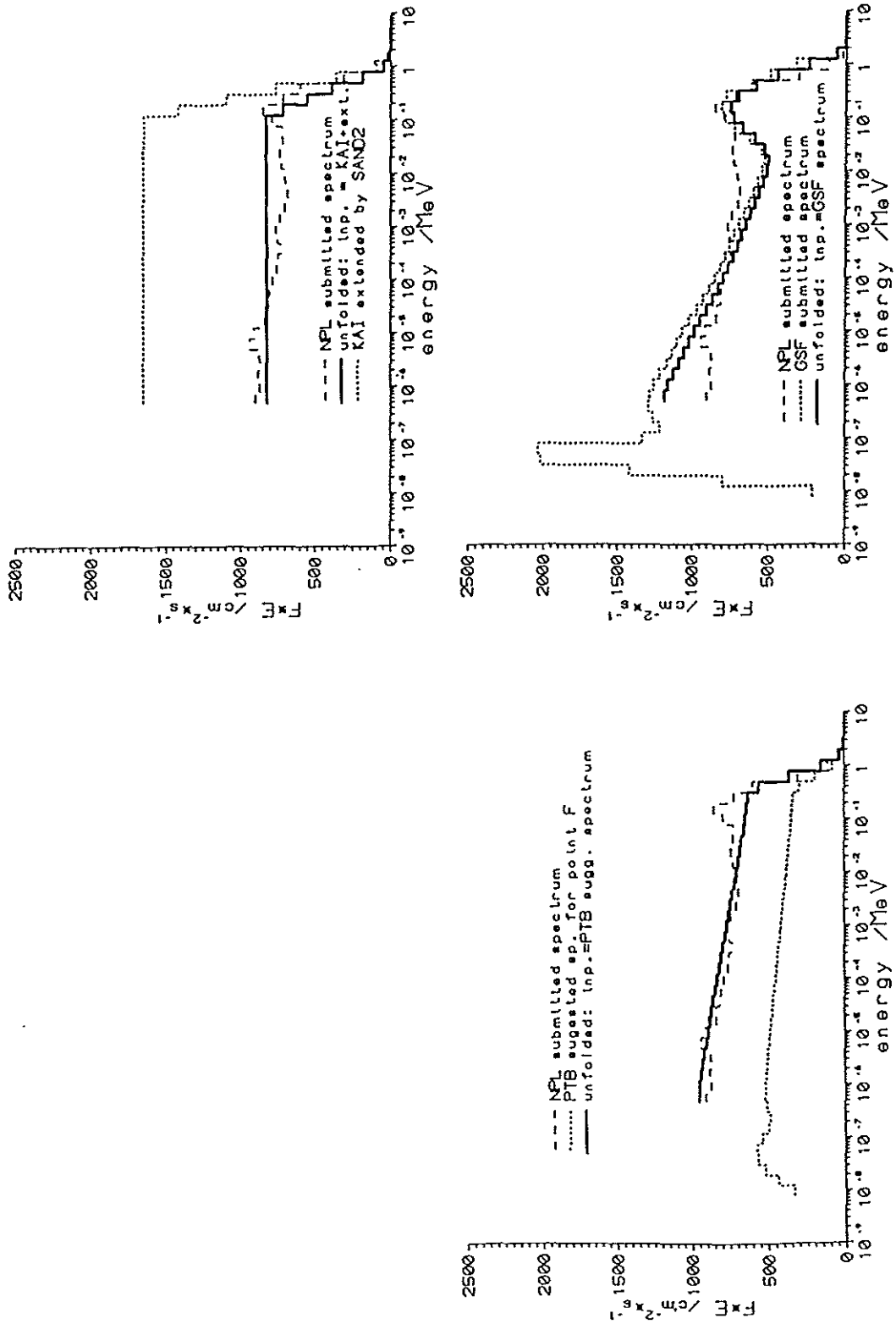


Figure 7: Unfolding of BS data sets measured by the NPL group (A) using different start spectra. For comparison the result submitted by NPL is shown in all figures.

2.3 Selection of the Recommended Solution

Originally the intention was to determine the recommended final spectra as the (weighted) average of the submitted data, although at maximum three full range spectra from BSSs and one high resolution spectrum from the PRS were available for the same position. After the thorough evaluation the IAR data sets had to be excluded from this analysis because the systematic deviations from the other results could not be solved during the time the evaluation was performed. Since the absolute scaling of the KAI high resolution data was also questionable, finally only two spectrometric data sets remained for each position (except for pos. F where only the GSF data remained acceptable).

For five (of seven) positions GSF and PTB results were available. In the course of the additional unfolding of the PTB measurements all trials resulted in spectra compatible with the measured count rates at reasonable STDV values. These spectra formed the class of acceptable spectra. The GSF measured count rates did not considerably change the PTB spectral shape for pos. D,P and G at acceptable STDV values (< 2.2 , see Table 8). In contrary, the PTB measured rates were not as well compatible with the GSF submitted shape. In addition, rather high STDV-values (5-10) were obtained if the GSF data sets for pos. E and L were unfolded with the PTB submitted spectra, but the GSF results itself were as worse. The ratios of measured and calculated count rates shown in Fig. 6 for the GSF data set measured at pos. E, clearly indicate a problem with the 10" count rate which was then omitted from the analysis. The PTB submitted spectra were selected as the final recommended results for the pos. D,E,P,L and G because these spectra were statistically compatible with all PTB and GSF data accepted, but vice versa a similar result was not achieved with the GSF spectra.

For pos. A and F another solution had to be found. Since the results submitted for pos. A and F showed large differences in shape and integral quantities, smooth spectra suggested in similarity to the other results were used for the additional unfolding (Fig. 8). In this way the differences of the GSF and NPL DE-values for pos. A could be reduced from 25% to 16% (Table 10). The additional unfolding of the GSF and NPL data sets with these smooth guess spectra were attained as the final result.

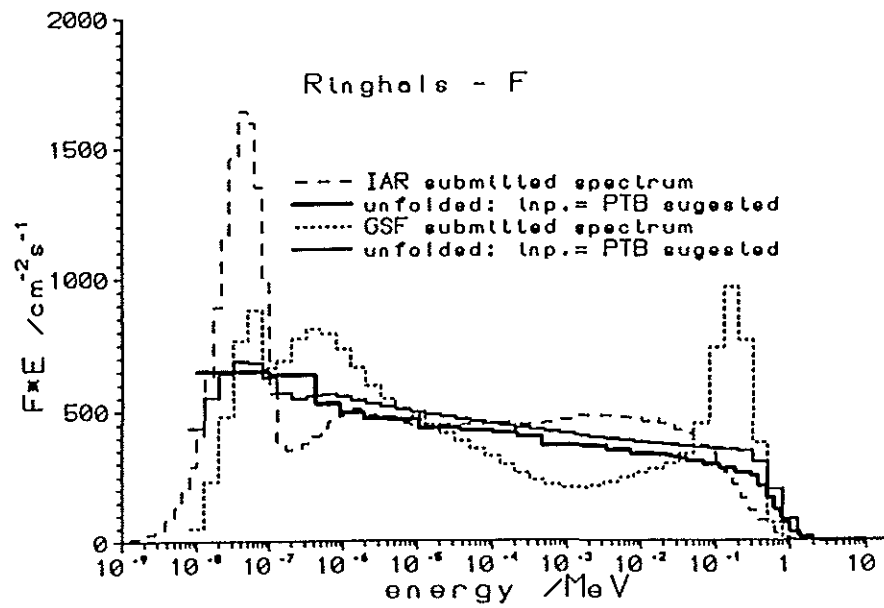
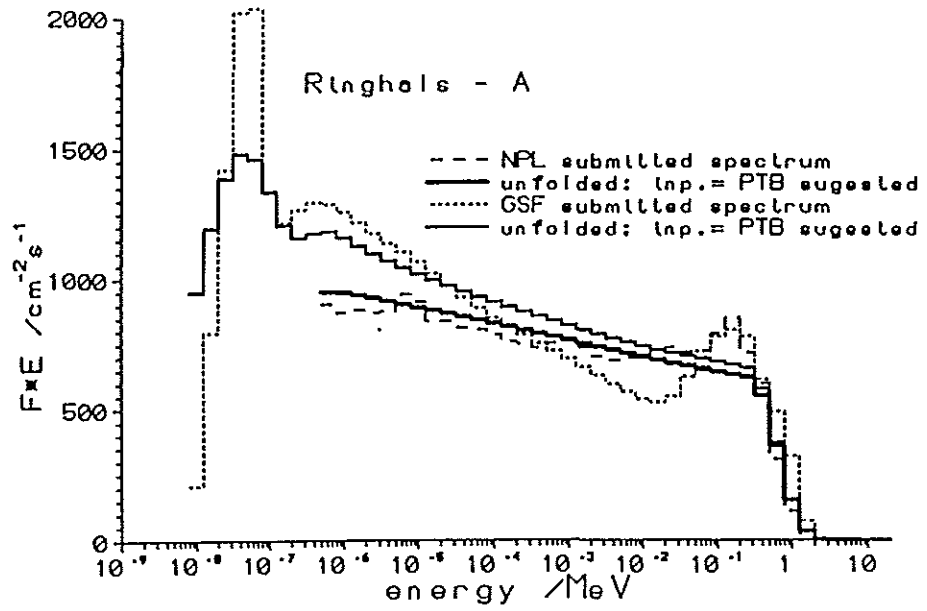


Figure 8: Additional unfolding of BS data sets measured at Ringhals positions A and F using different start spectra (see also Table 10).

Table 10: Integral fluence and DE rates ($[\text{cm}^{-2} \text{s}^{-1}]$ and $[\text{nSv/s}]$ resp.) obtained by additional unfolding of BS data sets measured at positions F and A using different start spectra.

Ringsals - F						
	submitted	submitted		PTB suggest.	PTB suggest.	
	IAR	GSF	IAR/GSF-1	IAR	GSF	IAR/GSF-1
< 0.4 keV	3363.50	2274.90	47.9%	2785.10	2318.60	20.1%
0.4eV-10keV	4675.30	4127.40	13.3%	4456.30	4745.30	-6.1%
10-100 keV	962.30	848.35	13.4%	753.88	849.96	-11.3%
0.1-1. MeV	319.02	1199.70	-73.4%	502.79	664.55	-24.3%
> 1. MeV	4.74	0.89	434.4%	14.61	31.02	-52.9%
0.07-2 MeV	449.38	1418.50	-68.3%	618.54	821.00	-24.7%
total fluence	9324.80	8451.20	10.3%	8512.70	8609.40	-1.1%
H60-PTB	200.91	394.40	-49.1%	251.02	306.56	-18.1%
STDV input	10.19	1.72		17.52	5.06	
STDV output	2.72	1.67		3.8	2.81	
Ringsals - A						
	submitted	submitted		(**) PTB suggest.	(**) PTB suggest.	
	NPL	GSF	NPL/GSF-1	NPL	GSF	NPL/GSF-1
< 0.4 keV		5052.70			4974.70	
0.4eV-10keV	8000.30	9316.60	-14.1%	8329.90	9674.10	-13.9%
10-100 keV	1696.10	1423.40	19.2%	1563.30	1652.30	-5.4%
0.1-1. MeV	1377.00	1516.80	-9.2%	1209.00	1270.50	-4.8%
> 1. MeV	39.82	119.09	-66.6%	58.00	58.53	-0.9%
0.07-2 MeV	1686.90	1901.80	-11.3%	1495.90	1571.70	-4.8%
total fluence*	11113.00	12375.89	-10.2%	11160.00	12655.43	-11.8%
H60-PTB	525.68	697.99	-24.7%	502.55	599.26	-16.1%
STDV input	1.91	5.25		2.46	8.48	
STDV output	1.90	5.21		2.38	5.18	

note:* means without thermal neutrons

(**) PTB spectrum suggested for F point

Fig. 9 shows the recommended spectra to be used for any further evaluation of the dosimetric measurements. The corresponding group and integral data are listed in Table 11-14. The uncertainties of the spectra could not be evaluated. Advanced unfolding procedures as the STAY'SL or BASACF code which include the propagation of uncertainties were not applied (except by the NPL group for pos.A measurements) and could also not be used for the additional unfolding because the uncertainties of the input data, in particular those of the response matrices, were not sufficiently specified, if at all. Therefore, the scatter of the results not rejected from the analysis for certain reasons may serve as the basis for a rough estimate of the accuracy achieved. The uncertainties of the total fluence and DE values may be about 5% and < 20% respectively.

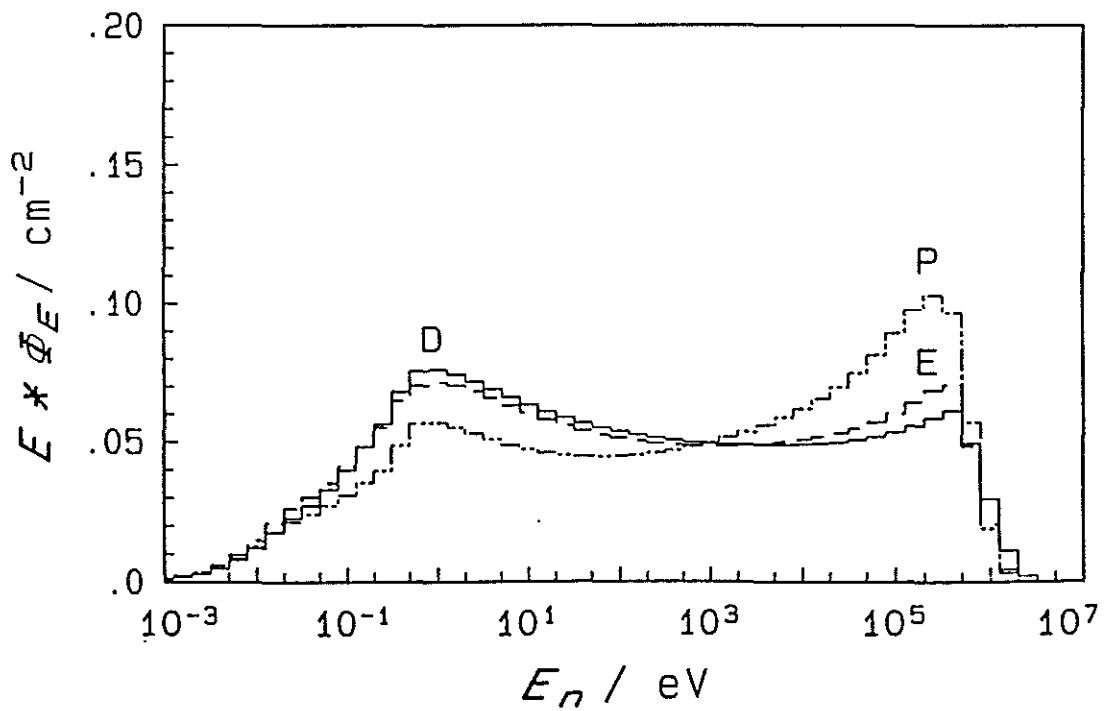
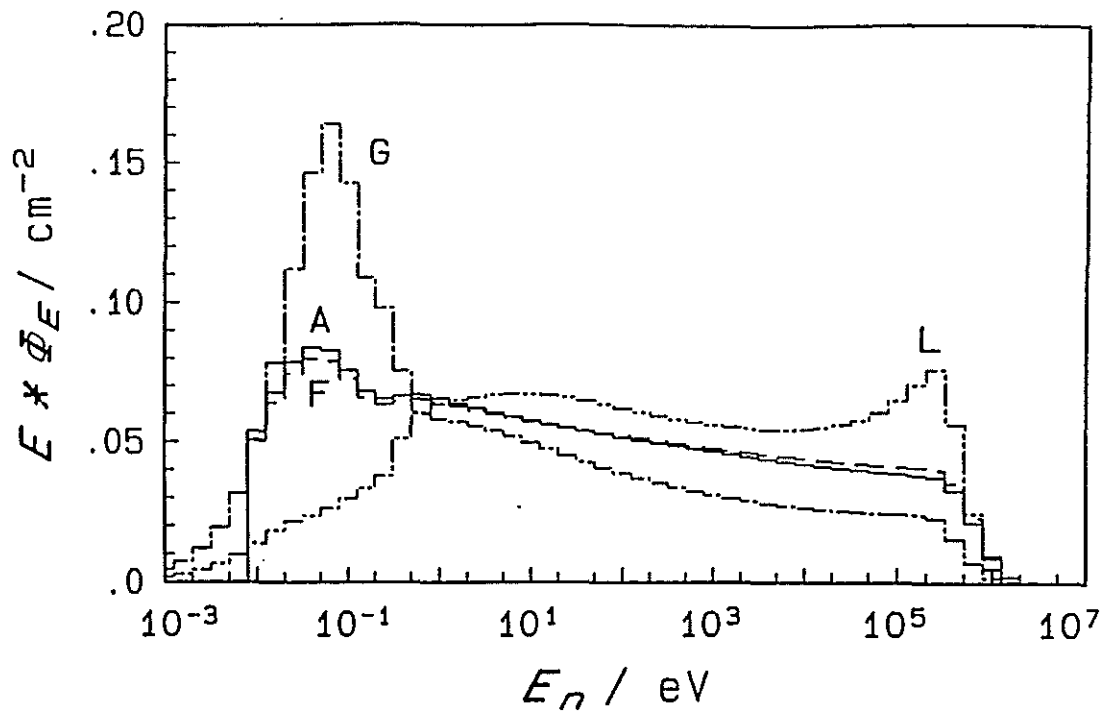


Figure 9: Evaluated spectral neutron fluence, normalized for unit fluence, for various positions at pressurized water reactors in Ringhals (A, F, G, L) and in the environment of a transport cask with spent fuel elements at CLAB in Oskarshamn (D, E, P).

Table 11: Fluence and DE rates, either absolute or as percentual fraction, of the evaluated neutron spectra (see Figure 9).

group and total fluence rates [$\text{cm}^{-2} \text{s}^{-1}$]

SPECTRUM	Group limits in eV					TOTAL
	1.000E-03 4.000E-01	4.000E-01 1.000E+04	1.000E+04 1.000E+05	1.000E+05 1.000E+06	1.000E+06 1.000E+08	
CLAB-D.REC	4.4526E+01	1.8826E+02	3.6818E+01	3.8986E+01	4.3722E+00	3.1296E+02
CLAB-E.REC	3.9829E+01	1.5281E+02	3.3371E+01	3.6123E+01	2.0054E+00	2.6414E+02
CLAB-P.REC	3.0635E+01	1.3485E+02	4.4471E+01	5.0116E+01	1.6999E+00	2.6177E+02
RING-A.REC	4.9746E+03	9.6741E+03	1.6523E+03	1.2704E+03	5.8514E+01	1.7630E+04
RING-F.REC	2.3185E+03	4.7454E+03	8.4994E+02	6.6453E+02	3.1016E+01	8.6094E+03
RING-G.REC	1.3644E+03	1.2699E+03	1.7021E+02	1.1284E+02	1.6093E+00	2.9190E+03
RING-L.REC	2.3839E+02	1.2702E+03	2.7315E+02	2.5204E+02	3.0402E+00	2.0368E+03

percentual values of group fluence rates

SPECTRUM	Group limits in eV					TOTAL
	1.000E-03 4.000E-01	4.000E-01 1.000E+04	1.000E+04 1.000E+05	1.000E+05 1.000E+06	1.000E+06 1.000E+08	
CLAB-D.REC	14.23 %	60.15 %	11.76 %	12.46 %	1.40 %	99.98 %
CLAB-E.REC	15.08 %	57.85 %	12.63 %	13.68 %	.76 %	99.97 %
CLAB-P.REC	11.70 %	51.51 %	16.99 %	19.14 %	.65 %	99.97 %
RING-A.REC	28.22 %	54.87 %	9.37 %	7.21 %	.33 %	100.00 %
RING-F.REC	26.93 %	55.12 %	9.87 %	7.72 %	.36 %	100.00 %
RING-G.REC	46.74 %	43.50 %	5.83 %	3.87 %	.06 %	99.91 %
RING-L.REC	11.70 %	62.36 %	13.41 %	12.37 %	.15 %	99.96 %

Table 11: (continued)

group and total dose equivalent (DE) rates H21 [Sv/s)

SPECTRUM	Group limits in eV					
	1.000E-03 4.000E-01	4.000E-01 1.000E+04	1.000E+04 1.000E+05	1.000E+05 1.000E+06	1.000E+06 1.000E+08	TOTAL
CLAB-D.REC	5.0804E-10	2.1571E-09	9.7651E-10	5.7851E-09	1.5441E-09	1.0971E-08
CLAB-E.REC	4.5184E-10	1.7470E-09	8.9635E-10	5.1422E-09	6.8881E-10	8.9262E-09
CLAB-P.REC	3.4604E-10	1.5191E-09	1.2313E-09	6.7925E-09	5.7858E-10	1.0467E-08
RING-A.REC	5.5780E-08	1.1076E-07	4.2704E-08	1.6997E-07	2.0151E-08	3.9937E-07
RING-F.REC	2.6012E-08	5.4227E-08	2.2002E-08	8.9130E-08	1.0687E-08	2.0206E-07
RING-G.REC	1.5221E-08	1.4718E-08	4.3978E-09	1.3526E-08	5.4173E-10	4.8404E-08
RING-L.REC	2.6835E-09	1.4446E-08	7.3480E-09	3.1357E-08	1.0151E-09	5.6850E-08

percentual values of group DE rates H21

SPECTRUM	Group limits in eV					
	1.000E-03 4.000E-01	4.000E-01 1.000E+04	1.000E+04 1.000E+05	1.000E+05 1.000E+06	1.000E+06 1.000E+08	TOTAL
CLAB-D.REC	4.63 %	19.66 %	8.90 %	52.73 %	14.07 %	99.99 %
CLAB-E.REC	5.06 %	19.57 %	10.04 %	57.61 %	7.72 %	99.99 %
CLAB-P.REC	3.31 %	14.51 %	11.76 %	64.89 %	5.53 %	99.99 %
RING-A.REC	13.97 %	27.73 %	10.69 %	42.56 %	5.05 %	100.00 %
RING-F.REC	12.87 %	26.84 %	10.89 %	44.11 %	5.29 %	100.00 %
RING-G.REC	31.44 %	30.41 %	9.09 %	27.94 %	1.12 %	99.95 %
RING-L.REC	4.72 %	25.41 %	12.93 %	55.16 %	1.79 %	99.99 %

Table 11: (continued)

group and total DE rates H39 [Sv/s]

SPECTRUM	Group limits in eV					TOTAL
	1.000E-03 4.000E-01	4.000E-01 1.000E+04	1.000E+04 1.000E+05	1.000E+05 1.000E+06	1.000E+06 1.000E+08	
CLAB-D.REC	4.1285E-10	1.6010E-09	1.0256E-09	7.1653E-09	1.5207E-09	1.1725E-08
CLAB-E.REC	3.6575E-10	1.2960E-09	9.4350E-10	6.4464E-09	6.8274E-10	9.7345E-09
CLAB-P.REC	2.7922E-10	1.1203E-09	1.3029E-09	8.6013E-09	5.7485E-10	1.1878E-08
RING-A.REC	4.4991E-08	8.1880E-08	4.4635E-08	2.1439E-07	1.9960E-08	4.0586E-07
RING-F.REC	2.0989E-08	4.0029E-08	2.3004E-08	1.1240E-07	1.0584E-08	2.0701E-07
RING-G.REC	1.2219E-08	1.0999E-08	4.5973E-09	1.7389E-08	5.3979E-10	4.5744E-08
RING-L.REC	2.1587E-09	1.0598E-08	7.7398E-09	4.0339E-08	1.0138E-09	6.1849E-08

percentual values of group DE rates H39

SPECTRUM	Group limits in eV					TOTAL
	1.000E-03 4.000E-01	4.000E-01 1.000E+04	1.000E+04 1.000E+05	1.000E+05 1.000E+06	1.000E+06 1.000E+08	
CLAB-D.REC	3.52 %	13.65 %	8.75 %	61.11 %	12.97 %	100.00 %
CLAB-E.REC	3.76 %	13.31 %	9.69 %	66.22 %	7.01 %	100.00 %
CLAB-P.REC	2.35 %	9.43 %	10.97 %	72.41 %	4.84 %	100.00 %
RING-A.REC	11.09 %	20.17 %	11.00 %	52.82 %	4.92 %	100.00 %
RING-F.REC	10.14 %	19.34 %	11.11 %	54.30 %	5.11 %	100.00 %
RING-G.REC	26.71 %	24.04 %	10.05 %	38.01 %	1.18 %	99.97 %
RING-L.REC	3.49 %	17.14 %	12.51 %	65.22 %	1.64 %	99.99 %

Table 11: (continued)

group and total DE rates H60 [Sv/s]

Group limits in eV						
SPECTRUM	1.000E-03 4.000E-01	4.000E-01 1.000E+04	1.000E+04 1.000E+05	1.000E+05 1.000E+06	1.000E+06 1.000E+08	TOTAL
CLAB-D.REC	6.4047E-10	2.4665E-09	1.6028E-09	1.0844E-08	1.9697E-09	1.7524E-08
CLAB-E.REC	5.6753E-10	1.9954E-09	1.4764E-09	9.8259E-09	8.9469E-10	1.4760E-08
CLAB-P.REC	4.3335E-10	1.7179E-09	2.0447E-09	1.3210E-08	7.5600E-10	1.8162E-08
RING-A.REC	6.9871E-08	1.2619E-07	6.9574E-08	3.2929E-07	2.6130E-08	6.2105E-07
RING-F.REC	3.2595E-08	6.1665E-08	3.5863E-08	1.7259E-07	1.3853E-08	3.1657E-07
RING-G.REC	1.8977E-08	1.6990E-08	7.1663E-09	2.7150E-08	7.1299E-10	7.0997E-08
RING-L.REC	3.3507E-09	1.6318E-08	1.2115E-08	6.2768E-08	1.3432E-09	9.5894E-08

percentual values of group DE rates H60

Group limits in eV						
SPECTRUM	1.000E-03 4.000E-01	4.000E-01 1.000E+04	1.000E+04 1.000E+05	1.000E+05 1.000E+06	1.000E+06 1.000E+08	TOTAL
CLAB-D.REC	3.65 %	14.08 %	9.15 %	61.88 %	11.24 %	100.00 %
CLAB-E.REC	3.85 %	13.52 %	10.00 %	66.57 %	6.06 %	100.00 %
CLAB-P.REC	2.39 %	9.46 %	11.26 %	72.73 %	4.16 %	100.00 %
RING-A.REC	11.25 %	20.32 %	11.20 %	53.02 %	4.21 %	100.00 %
RING-F.REC	10.30 %	19.48 %	11.33 %	54.52 %	4.38 %	100.00 %
RING-G.REC	26.73 %	23.93 %	10.09 %	38.24 %	1.00 %	99.97 %
RING-L.REC	3.49 %	17.02 %	12.63 %	65.45 %	1.40 %	99.99 %

3. Measurements with Tissue Equivalent Proportional Counters (TEPC)

Six detector systems based on Tissue Equivalent Proportional Counters (TEPC) participated in the intercomparison. Of the six, five systems (AECL, KFA CEA-Gren., CEA-Font. and PTB-Handi) measure the distributions of pulse heights due to single energy deposition events in the counters sensitive volume. The sixth system (SSI) measures the current and its variance in the detector using an electrometer. Table 12 summarises some characteristics of the systems.

Table 12: Physical characteristics of the TEPCs used in this comparison exercise.

	AECL	KFA	CEA-Gren.	CEA-Font.	PTB-Handi	SSI
Containment						
Shape	cylindrical	cylindrical	cylindrical	cylindrical	cylindrical	thimble
Diameter (mm)	150	127	150	76	88.8	220
Height (mm)	180	190	180	100	100	300
Wall material	aluminium	polyethylene	aluminium	nickel	stainl. steel	aluminium
Wall thickness (mm)	1.27	14	1.27	0.3	0.76	2
Sensitive Volume						
Shape	spherical	cylindrical	spherical	cylindrical	spherical	spherical
Diameter (mm)	125.7	70	125.7	50	59	184
Height		70		50		
Wall material	A-150	A-150	A-150	A-150	A-150	A-150
Wall thickness (mm)	2.29	1	2.29	4	2.5	6.26
Volume (cm ³)	1039.93	269.4	1039.93	98.17	107.54	3300
TE-Gas based on	propane	methane	propane	propane	propane	methane
Sim. Diameter (μm)	2	1	2	3	2	2/4.5 ¹

¹ 2μm Counter B/ 4.5μm Counter A

Counter Operation and Calibration in Terms of Lineal Energy

The pulse height distributions measured by five of the systems are calibrated in terms of lineal energy, y , which is defined as the quotient of the energy imparted by a single charged particle and the average chord length of the sensitive counter volume [7]. The analysis of microdosimetric spectra measured with different systems reveals, whether the systems worked properly and had been calibrated correctly in terms of lineal energy, y . Figure 10 shows as a representative example the microdosimetric dose distributions, $yd(y)$, versus the logarithm of

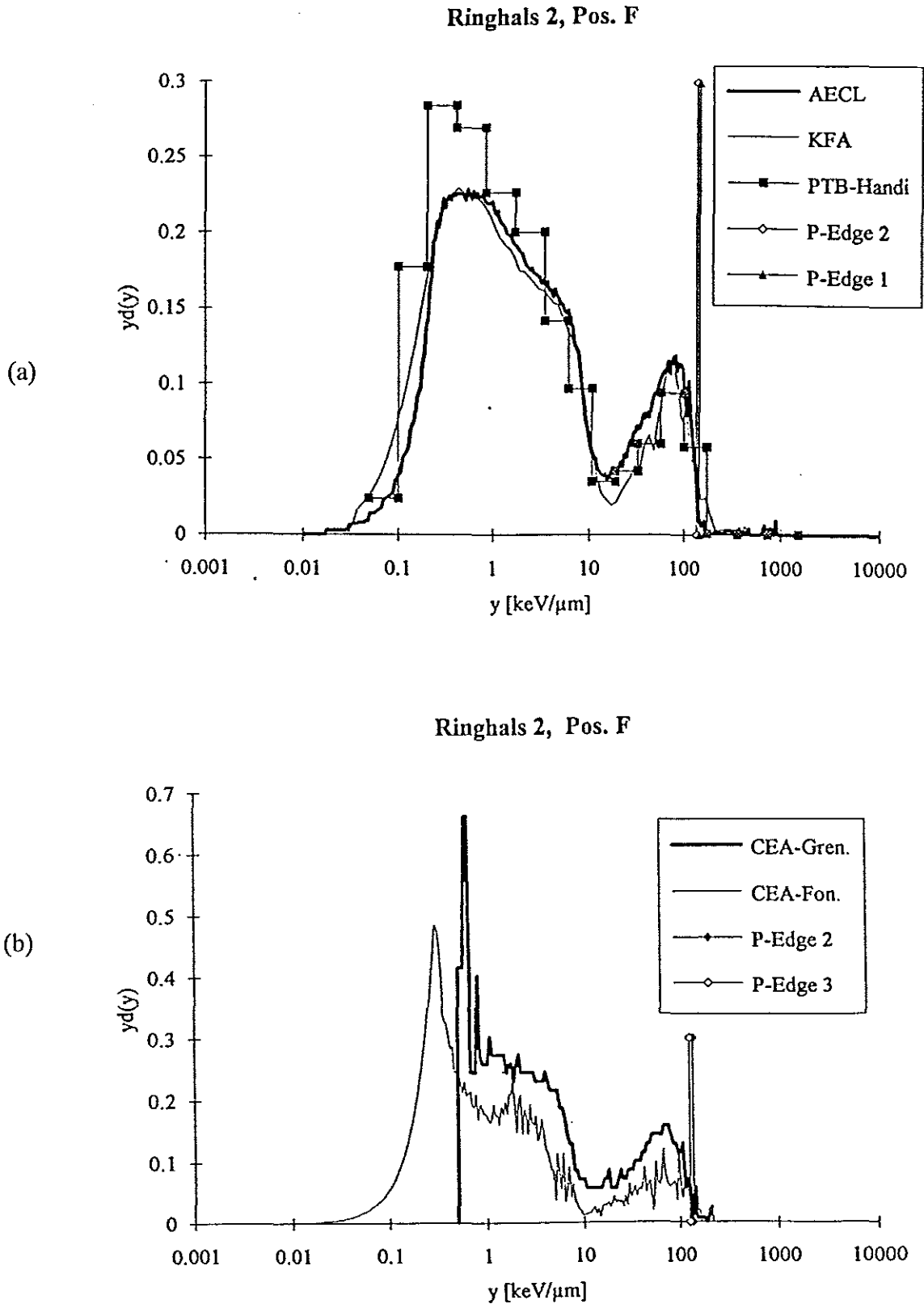


Figure 10: Dose frequency distribution, $y d(y)$, versus the logarithm of the lineal energy, y , as measured by various groups at position F in Ringhals. The proton edges are indicated for each system.

lineal energy, y , derived for reactor 2 in Ringhals at position F. The spectra of AECL, KFA and PTB-Handi (Figure 10a) are consistent with respect to the general shape. The part of the distribution below lineal energies of about $10 \text{ keV}/\mu\text{m}$ is due to electrons generated in interactions of photons with the counter wall (photon events). Events with lineal energies above $10 \text{ keV}/\mu\text{m}$ are produced by protons and heavier charged particles released in neutron interactions (neutron events).

The photon parts of the spectra measured by CEA-Gren. and CEA-Font. deviate in shape considerably from the other three detectors (Fig. 10b). For the CEA-Gren system, the edge of this part at about $10 \text{ keV}/\mu\text{m}$ is visible. In the case for the CEA-Font. system it seems to be shifted to lower values. The reasons for this deviation in spectrum shape cannot be resolved. Consequently, results of the two CEA systems were not included in the calculations of recommended values, which contain the photon parts.

A good parameter to check the calibration of counters in terms of lineal energy is the position of the so called proton edge in the dose distribution [8]. It is due to protons, which deposit the maximum possible energy in the counters sensitive volume. The lineal energy of the proton edge depends on the simulated diameter and on the geometry of the detection volume. For spherical and right-cylindrical counters the proton edge should appear at $146 \text{ keV}/\mu\text{m}$, $136 \text{ keV}/\mu\text{m}$ or $126 \text{ keV}/\mu\text{m}$ for $1 \mu\text{m}$ (KFA), $2 \mu\text{m}$ (AECL, CEA-Gren., PTB-Handi) and $3 \mu\text{m}$ (CEA-Font.) simulated site size respectively. The positions were calculated using the range tables from ICRU 49 (ICRU 1993). The analysis of the spectra shows that the calibration of the participating systems in terms of lineal energy is consistent (Fig. 10).

Data Evaluation

The dosimetric quantities, absorbed dose, quality factor and dose equivalent are derived from an evaluation of the measured pulse height spectra. The separation of neutron dose and photon dose use the fact that these two contributions are separable in the distribution as can be seen in Figure 10 [1, 9, 10].

Absorbed doses, D , are reported by most of the systems as doses to the tissue equivalent wall of the detector's sensitive volume, i.e. as tissue doses. SSI however reported tissue KERMA values free in air.

Quality factors, Q , are derived by folding the $q(\text{LET})$ relationship given by ICRP¹ with measured microdosimetric spectra [1] and dose equivalents are derived according to its definition

$$H = Q \cdot D. \quad (2)$$

In this exercise, values of ambient dose equivalent, $H^*(10)$, were requested. Effectively, it is defined as the product

$$H^*(10) = Q \cdot D^*(10) \quad (3)$$

where $D^*(10)$ denotes ambient absorbed dose measured in 10 mm depth in the ICRU sphere in an expanded and aligned field. In principle, TEPC readings may be corrected or calibrated in a known field to give $D^*(10)$. However, the relation between $D^*(10)$ and dose to the counters tissue wall is quite energy dependent due to the differences in neutron transport in the ICRU sphere and a TEPC. Therefore, this correction is not applied. In the way the TEPC instruments work the determined quality factors are independent on whether the dose reading is scaled in terms of $D^*(10)$ or not, since it depends only on the spectral distribution of dose in terms of lineal energy and its proper calibration (see above) and not on its absolute value.

The difference between tissue KERMA free in air and $D^*(10)$ in monoenergetic neutron fields may be up to 25% for energies above 500 keV and around 5% to 10% for energies around 100 keV [9].

The SSI system, which uses the variance technique, is calibrated in terms tissue kerma free in air in a standard photon field but the reading of $H^*(10)$ is adjusted by a factor of 1.4 obtained

¹ In this evaluation, the $q(\text{LET})$ definition according to ICRP Report 21 [2] was used, since it is still in effect legally. Dose equivalent values using the new $q(\text{LET})$ relation according to ICRP Report 60 [4] are given in the first report on this comparison exercise [1].

from a calibration in a D_2O -moderated ^{252}Cf -field. The quality factor is derived from a measurement of the dose average lineal energy \bar{y}_D [1], and the relation

$$Q = a + b \cdot \bar{y}_D \quad (4)$$

The value of the parameters a and b in this relation were determined from measurements at PTB, in beams for which the value of the quality factor is known [11].

Absorbed Dose

The total dose rates measured by AECL, KFA, PTB-[Handi] and SSI at the different locations are given in Table 13. The other two systems were omitted due to the inconsistency in the photon part of their distributions. AECL, PTB-Handi and SSI use comparable detectors with respect to wall thickness and simulated tissue diameter. Therefore, the measured dose values of AECL and PTB-Handi should agree within about 10%. This uncertainty is related to the internal α -source calibration method used by the systems [12]. Since SSI is calibrated in terms of tissue KERMA free in air, reported dose values could be expected to be close to those for the other systems. The detector of the KFA system applies a thicker wall, in order to shape the counter response [13]. The wall attenuates and moderates the incident neutron spectrum, especially at low and intermediate neutron energies. This could result in somewhat lower dose readings as compared to the other systems [14].

Table 13: Total dose rates measured at Ringhals reactors and CLAB with TEPCs (AECL, KFA, PTB-HANDI) and the variance system (SSI).

Position	AECL Abs. D/t [$\mu\text{Gy/h}$]	KFA D/t [$\mu\text{Gy/h}$]	PTB-HANDI D/t [$\mu\text{Gy/h}$]	SSI D/t [$\mu\text{Gy/h}$]
Reac. 4, L	52.49	52.92	63.20	54.70
Reac. 4, A	334.73	327.09	418.00	330.33
Reac. 2, F	195.43	231.85	230.00	198.00
Reac. 2, G	65.37	67.76	79.40	64.00
CLAB, D	26.91	26.19	28.80	24.45
CLAB, E	19.95	20.49	23.30	19.35
CLAB, P	23.23	22.22	25.90	22.40

It cannot be expected that the differences between the systems due to differences in calibration and detector design are pronounced since first, the measurements were performed in mixed neutron-gamma radiation fields and second, the neutron components had broad energy ranges. The dose is dominated by the photon contribution of the incident fields (see tables 4.5-4.11 in [15]) and the differences between the detector responses with respect to photons is negligible [16]. Therefore, it is concluded that the reported results on total dose should agree within an uncertainty of about 10%.

Table 13 reveals a good agreement between the measured dose values of AECL, KFA and SSI. The PTB-Handi system, on average gives 17% higher values than AECL. This result is surprising since, as stated earlier, the calibration of the system is consistent with AECL, and no special weighting is performed in the evaluation of the spectrum. The dose equivalent readings of PTB-Handi are also consistently about 20% higher than those of e.g. AECL (see below). Even though this is a systematic deviation, no firm explanation can be given. The average values for absorbed dose rate, given in Table 18 as recommended results, therefore, include only data of AECL, KFA and SSI. Also given are the standard deviations of the mean, which are below 10% for all positions.

Dose Equivalent and Quality Factor

Comparing the dose equivalent values of the TEPC systems is more difficult, since several parameters can be adjusted. As stated above and described in [1], generally, for systems registering pulse height distributions, the $q(\text{LET})$ relationship is folded into the microdosimetric spectrum. Then the mean quality factor, Q , for the radiation can be determined, and the dose equivalent reading, H , is calculated simply by equation (2). Since lineal energy, y , is not LET, an assumption about the relation of the two quantities has to be assumed. The two relations generally used are: $\text{LET} = y$ (AECL, KFA, CEA-Gren. PTB-Handi) and $\text{LET} = 8/9 y$ (CEA-Font.) and the equation for Q becomes

$$Q = \int_0^{\infty} q(y) \cdot d(y) dy, \quad (5)$$

where $d(y)$ denotes the microdosimetric dose distribution.

Furthermore, the possibility of neutron gamma discrimination is used to correct the dose equivalent response of the systems with respect to ambient dose equivalent, $H^*(10)$. This is advisable, since the ambient dose equivalent response of TEPCs measuring microdosimetric spectra becomes significantly lower than 1 for neutron energies below about 100 keV [17]. Therefore the total dose equivalent reading is calculated in the following way:

$$H_n H = H_\gamma + K \cdot H'_n \quad \text{with} \quad = K \cdot H'_n \quad (6)$$

where H_γ and H'_n are calculated according to

$$H_\gamma = D \int_0^{y_{\gamma,n}} q(y) \cdot d(y) dy, \quad H'_n = D \int_{y_{\gamma,n}}^{\infty} q(y) \cdot d(y) dy, \quad (7)$$

($y_{\gamma,n}$ denotes the threshold value for discriminating the neutron and photon part of the distribution) and K is a correction factor which is derived from a measurement in the radiation field of a calibration neutron source, e.g. a D_2O moderated ^{252}Cf source. The factor is determined in such a way that the total dose equivalent reading of the system in the calibration field is equal to the reference ambient dose equivalent, $H^*(10)$, value for this source. The quality factors are then calculated according to

$$Q = H/D, \quad Q_\gamma = H_\gamma/D_\gamma \quad \text{and} \quad Q_n = H_n/D_n \quad (8)$$

The value of K depends on the neutron/gamma discrimination, the detector design and the calibration field. With respect to the neutron/gamma discrimination a fitting method (AECL) and a threshold method (KFA, PTB-Handi, CEA-Gren., CEA-Font.) are used [9, 10]. With the threshold method, the discrimination value is a parameter that is determined empirically. PTB-Handi uses 6 keV/ μm , KFA and CEA-Font. 7 keV/ μm and CEA-Gren. 10 keV/ μm . The detector geometry in particular the wall thickness is important, since it moderates the incident neutron field and consequently the measured microdosimetric distribution [13, 9, 10]. The K factors used are 1.27 (AECL), 1.5 (KFA), 1.75 (CEA-Gren.) and 1.41 (PTB-Handi).

CEA-Font. didn't report the factor used. However, the system was calibrated in runs of ambient dose equivalent in an external neutron calibration field (Am-Be).

Table 14: Deviations of dose fractions determined for a threshold of 10 keV/ μm to those for a threshold of 7 keV/ μm , averaged for all measurements with the KFA-TEPC.

Fraction	dD [%]	dH [%]	dQ [%]
Photon	3.8	8.0	
Neutron	-26.4	-7.6	26.3
Total	0.0	-1.5	-1.5

The data of KFA were used to study the influence of the threshold value $y_{\gamma,n}$ on the dose, dose equivalent and quality factor fractions due to neutrons and photons. Two values for $y_{\gamma,n}$ were used, namely 7 keV/ μm (usually applied by KFA) and 10 keV/ μm . Table 14 gives the average deviations (averaged over all positions measured in this intercomparison) of the dose, dose equivalent and quality factor fractions for a threshold of 10 keV/ μm relative to a threshold of 7 keV/ μm . Whereas the gamma dose is only weakly affected by the threshold value (about 4%) the neutron dose changes significantly (about -26%), since the main contribution to the dose comes from photons. The total dose equivalent readings are shifted by about 1.5% if 10 keV/ μm is used as threshold. The photon dose equivalent rate changes by 8% and the neutron dose equivalent rate by almost -8 %. The latter is lower by about 5% in the reactor fields and by about 9.7% in the fields at CLAB. The quality factor decreases slightly by about 1.5%, however the neutron quality factor is higher by about 26%.

The SSI system determines the average quality factor according to equation (4) and the dose equivalent according to equation (2). SSI cannot perform a separation of neutron dose and gamma dose from the current measurement. The gamma dose is measured separately with a GM counter and subtracted from the dose equivalent reading of the system to get the neutron dose fraction.

Due to the weighting with the quality factor, the differences in neutron gamma discrimination and the factor K, the uncertainty in the dose equivalent readings are higher than for the dose readings. Even higher uncertainties have to be accepted, when only neutron dose equivalents are discussed.

Table 15: Total dose equivalent rates determined with TEPCs (AECL, KFA, PTB-HANDI) and the variance system (SSI).

Position	AECL H/t [$\mu\text{Sv/h}$]	KFA H/t [$\mu\text{Sv/h}$]	PTB-Handi H/t [$\mu\text{Sv/h}$]	SSI H/t [$\mu\text{Sv/h}$]
Reac. 4, L	185.64	167.69	229.00	155.00
Reac. 4, A	1239.27	1242.53	1590.00	1014.50
Reac. 2, F	659.31	827.57	822.00	593.00
Reac. 2, G	141.82	169.33	162.00	136.00
CLAB, D	63.50	55.57	72.20	54.15
CLAB, E	46.87	43.11	61.50	43.00
CLAB, P	55.00	46.34	72.40	51.40

Table 15 lists the total dose equivalent rates reported by AECL, KFA, PTB-Handi and SSI. The CEA systems are not included due to the problems in the photon part of the distribution. The values for AECL, PTB-Handi and SSI should ideally agree, whereas KFA, due to its wall could deviate. PTB-Handi is consistently about 20% higher than AECL, as in the case of absorbed dose and no explanation can be given from the analysis of the data. SSI is consistently lower than AECL by on average 10%. The reason for this might be due to the different assessment of the quality factor.

From the above discussion it is concluded that the differences between AECL, KFA and SSI are statistically not significant. Therefore, the recommended average values, given in Table 18 include those three systems.

Table 16 shows the gamma dose equivalent rate readings of AECL, KFA, PTB-Handi and the GM counter used separately by SSI. The data of the TEPC systems agree within about 10%, whereas the GM counter is significantly higher in the reactor fields. The reason for this is the presence of high energy gamma rays (up to 7 MeV) in the incident field. GM counters are known to over respond to photons of this energy.

Table 17 lists the neutron dose equivalent rate readings of AECL, KFA, CEA-Gren., CEA-Font and PTB-Handi. SSI was not included, since the determination of the photon component using the GM counter leads to an underestimation of the neutron dose equivalent for this system. The readings of AECL and CEA-Gren. are consistent within about 20%. PTB-Handi,

Table 16: Gamma dose equivalent rates measured with the TEPCs and a Geiger-Mueller counter (SSI).

Position	AECL Hg/t [μ Sv/h]	KFA Hg/t [μ Sv/h]	PTB-Handi Hg/t [μ Sv/h]	SSI Hg/t [μ Sv/h]
Reac. 4, L	47.43	46.34	50.00	71.00
Reac. 4, A	297.30	276.42	327.00	490.00
Reac. 2, F	179.88	199.58	184.00	310.00
Reac. 2, G	67.97	63.04	71.50	115.00
CLAB, D	27.52	25.31	25.20	33.00
CLAB, E	20.46	19.62	20.10	22.00
CLAB, P	23.76	21.08	22.00	23.00

Table 17: Neutron dose equivalent rates evaluated from various TEPC measurements.

Position	AECL Hn/t [μ Sv/h]	KFA Hn/t [μ Sv/h]	CEA-Gren. Hn/t [μ Sv/h]	CEA-Font. Hn/t [μ Sv/h]	PTB-Handi Hn/t [μ Sv/h]
Reac. 4, L	138.21	121.35	165.00		179.00
Reac. 4, A	941.97	966.10	786.60	521.04	1260.00
Reac. 2, F	479.43	627.98	426.00	239.65	639.00
Reac. 2, G	73.85	106.29			90.80
CLAB, D	35.97	30.26	39.10	21.38	47.10
CLAB, E	26.41	23.49	30.90	20.66	41.50
CLAB, P	31.24	25.26	40.20	19.85	50.50

Table 18: Recommended dose and dose equivalent rates evaluated from TEPC and variance measurements performed at Ringhals and CLAB.

Position	Average D/t [μ Gy/h]	Std.Dev %	Average H/t [μ Sv/h]	Std. Dev. %	Average Hn/t [μ Sv/h]	Std. Dev. %
Reac. 4, L	53.37	2%	169.44	7%	141.52	13%
Reac. 4, A	330.72	1%	1165.43	9%	898.22	9%
Reac. 2, F	208.43	8%	693.29	14%	511.14	17%
Reac. 2, G	65.71	2%	149.05	10%	90.07	18%
CLAB, D	25.85	4%	57.74	7%	35.11	10%
CLAB, E	19.93	2%	44.33	4%	26.93	11%
CLAB, P	22.62	2%	50.92	7%	32.23	19%

is consistently more than 30% higher than AECL, except at reactor 2, location G. CEA-Font. is generally more than 20% lower than AECL, except for reactor 2, location F. Both systems are therefore not included in the calculation of the average values given in Table 18.

The dose equivalent responses ($H_{TEPC}/H^*(10)$) per fluence as a function of incident neutron energy of KFA and PTB-Handi were measured in well defined quasi monoenergetic neutron

fields during two EURADOS intercomparisons [9, 10, 14]. These responses were used to calculate from the spectral fluence information derived from the Bonner sphere measurements expected dose equivalent readings for these two TEPCs. The TEPC response functions included the factor K (see equation 6) to calibrate the dose equivalent reading in terms of ambient dose equivalent on the basis of a measurement in a D₂O moderated ²⁵²Cf source. The result is shown in Figure 11.

Figure 11a compares the experimental response, $H_{\text{TEPC}}/H_{\text{BS}}$: reference Bonner Sphere values for ambient dose equivalent, $H^*(10)$ of PTB-Handi and AECL to the calculated response, H_C/H_{BS} , for PTB-Handi. PTB-Handi and AECL use detectors which differ mainly in size (Table 12) and therefore, the response of these two detectors is expected to be very similar due to the same TE-diameter simulated. In fact, the experimental response of AECL agrees on average better with the calculation than does PTB-Handi, which in particular at CLAB seems to give higher results as would be expected. Figure 11b shows the same comparison for KFA. The agreement between calculation and experiment is rather well.

This comparison indicates on the one hand that the TEPC (KFA, AECL) and Bonner sphere measurements are consistent. On the other hand it supports the judgement that the dose equivalent values delivered by PTB-Handi are too high and, therefore, the decision to omit the PTB-Handi data for the calculation of the recommended average values of dose equivalent and in particular neutron dose equivalent in Table 18.

The recommended values for neutron dose equivalent, given in Table 18 include AECL KFA and CEA-Gren. KFA could also be excluded, since the response of this system differs from that of the others due to the thicker wall (Figure 11). However, in the broad fields encountered in this intercomparison, this difference is not very significant.

The standard deviation of the recommended average values are between 7% and 14% for the total dose equivalent rate and between 9% and 19% for the neutron dose equivalent rate and the neutron quality factor.

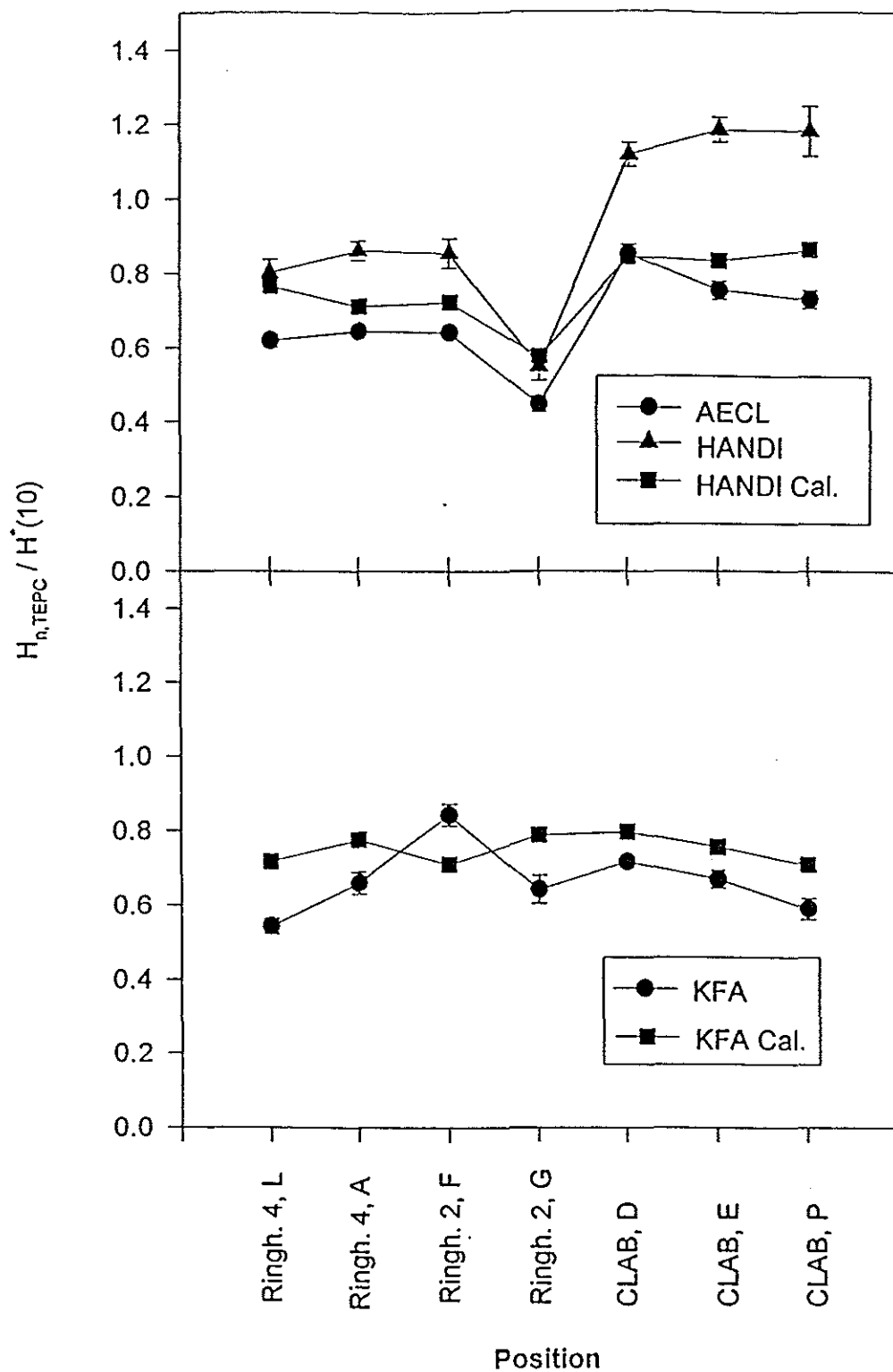


Figure 11: Ratio of the measured neutron DE values to the reference values obtained from the recommended neutron spectra for the KFA (lower) and AECL and HANDI (upper) TEPCs. For comparison the responses calculated for these neutron spectra and the corresponding fluence response functions are shown (KFA and HANDI cal.)

4. Personal Dosimeters on Phantoms

4.1 Estimation of the Directional Characteristics of the Radiation Fields

The angular proportions of the neutron and photon fluence are estimated from the readings of personal dosimeters positioned on different sides of a slab phantom or on the surface of a spherical phantom. The assumption was made that the phantom shielded the dosimeter completely from radiation from the rear (this assumption is considered to be robust at the 5% level).

There is some information indicating a shift to lower energies for neutrons incident on dosimeters not directly facing the reactor or used fuel. This information comes mainly from the differences in readings between different dosimeter types as the tested dosimeters have different energy responses. The results in the following tables and figures are derived mainly from the angular distribution of neutrons with energies above 70 keV although this can lead to a slight over estimation of the dose equivalent rates. It is assumed that the energy spectral distribution, established by means of the Bonner spheres and the proton recoil instruments, is the same for each direction component of the field.

The simple approximation analysis proceeds as follows for neutron irradiation:

1. It is assumed that the radiation field consists of a dominant direction (identified beforehand in the cases considered and designated by A-P direction) plus an isotropic component and/or a rotational component.
2. The readings of the track dosimeters as tracks for the non-A-P directions were averaged with some judgement exercised (based on experience of measurements with the different types of track dosimeters) to obtain the tracks produced by the isotropic (and/or rotational component(s)). Where there was not a dominating direction, the average value of the tracks for all direction was used. This average reading was converted to the isotropic (and/or rotational) component of fluence using the fluence response characteristics of the dosimeters for isotropic (and/or rotational) fields (obtained for on-phantom irradiation). The A-P component was obtained by subtracting

the average "isotropic" tracks from the "A-P" tracks and then converting to A-P fluence using the normal incidence response characteristics. Thus the direction components of fluence were established (with some degree of approximation).

The readings of TL/albedo dosimeters for the non A-P directions were averaged and converted to the isotropic component of the dosimeter readings. The A-P component was obtained by subtracting the average isotropic readings from the A-P reading. The TL/albedo readings from dosimeters placed on a phantom can be considered as relative measurements of the directional dose equivalent (or the fluence if the neutron spectra are direction independent).

This is a relatively crude approach. There are difficulties associated with the large dependence on angle of the fluence response characteristics of some of the personal dosimeters. When the neutrons are incident normally on a phantom face the response of dosimeters is low but when the neutron direction is not normal to a phantom face several dosimeters will respond, this makes the estimation of the angular proportions uncertain..

3. The fluence directional characteristics of the radiation field may be converted into relevant radiological protection quantities (see Table 19 for conversion coefficients). A comparison of the estimate of $H^*(10)$ obtained by this approach with values obtained from the multisphere spectrometers and from the (corrected) readings of survey instruments is given in Table 26 (see section 5).

Part of the reason for the adoption of this simple approach is that the availability of data on the relationships of quantities is limited on the main, to simple field geometries; there is limited data on the response characteristics of dosimeters and instruments; there are relatively large uncertainties in some of the measured data; the practical consideration that occupationally exposed persons move around in the radiation fields and therefore they are exposed to average directional characteristics of the fields rather than to extreme directional characteristics.

A similar approach is applied to the estimation of the directional components of the photon fields. However the photon fields include photons with energies up to 7.6 MeV which implies that the phantoms were not thick enough to shield the dosimeters from irradiation through the phantoms. This means that the photon directional components are uncertain for the high energy part of the photon fields.

The estimated angular proportions are presented in Table 19 for neutrons and in Table 20 for photons. The values of the angular proportions in position E were derived from measurement at position D at CLAB and an extra measurement at positions similar to positions D and E on another transport cask at Ringhals.

The direction "A-P" stands for positioning the phantom or a person (simulated with a calculated anthropomorphoid phantom) with the anterior side facing the direction with the highest neutron dose equivalent.

The estimated values of the angular proportions in 6 directions of the fluence or ambient dose equivalent are shown together with a calculation of the proportions from isotropic irradiation (ISO) and irradiation with direction from the reactor or the transport cask to the front of a person (A-P) respectively. The separation into two components is used in the estimation of the direction weighted dosimetric quantities below.

4.2 Calculated Dosimetric Quantities

4.2.1 Calculation for Neutrons

The calculated dosimetric quantities for neutrons are presented in Table 21.

The calculations are based on the measured neutron energy spectra which are presented in section 3 of part 1 and which are commented in section 2 of part 2. The calculations are also based on conversion coefficients from neutron fluence at monoenergetic energies to:

Table 19: Measured angular proportions of the neutron fluence on the six major sides of the phantoms. The results are based on all available dosimeter readings.

ANGAVG2.XLS

Part 1. Separation in six directional components.								
Direction	Position	A	F	G	L	D	E	P
		%	%	%	%	%	%	%
AP (Front)		31	46	21	33	38	39	68
PA (Back)		12	7	18	4	6	6	1
Lat 1)		13	15	15	15	14	14	11
Top		24	9	24	22	14	14	4
Bottom		7	8	7	11	14	13	6
1) Lat is the average from readings on the right and left side.								
Part 2. Separation in two directional components. Calculated from part 1 above.								
Proportions in %								
Direction	Position	A	F	G	L	D	E	P
		%	%	%	%	%	%	%
AP		17	35	4	20	25	26	61
ISO		83	65	96	80	75	74	39

Part 1. Separation in six directional components.								
Direction	Position	A	F	G	L	D	E	P
		%	%	%	%	%	%	%
AP (Front)		19	23	16	26	20	22	33
PA (Back)		15	13	17	14	9	9	7
Lat 1)		17	17	18	14	18	18	15
Top		17	18	19	18	17	16	Not measu
Bottom		15	12	12	14	18	17	Not measu
1) Lat is the average from readings on the right and left side.								
Part 2. Separation in two directional components. Calculated from part 1 above.								
Proportions in %								
Direction	Position	A	F	G	L	D	E	P
		%	%	%	%	%	%	%
AP		3	8		11	4	6	20
ISO		97	92	100	89	96	94	80

Table 20: Measured angular proportions of H*(10) for photons on the six major sides of the phantoms. The results are based on all available dosimeter readings.

Table 21: Calculated fluence weighted conversion coefficients (pSv/cm²).

Quantity	Sources			Ringhals				CLAB			
	Am-Be	Cf-252	Cf + D ₂ O	F	L	A	G	D	E	P	
MaDE	374	338	91.6	23.3	27.8	22.5	16.4	35.0	33.7	39.9	
H*(10) old Q(L)	381	342	93.2	23.8	30.3	22.8	15.4	37.3	36.7	45.3	
H _p (10) old Q(L)	A-P	375	332	91.2	24.6	30.9	23.5	16.0	38.2	37.5	45.8
	ROT	215	161	42.4	8.35	10.4	7.98	5.23	13.5	13.0	15.8
	ISO	196	144	37.4	6.64	8.29	6.34	4.08	10.9	10.5	12.7
H*(10) ICRP 60, ICRU 49 S/p	391	384	105	30.0	38.1	28.7	19.3	46.9	46.3	57.1	
H _p (10) ICRP 60 Q(L), ICRU 49 S/p	A-P	426	413	113	31.6	39.8	30.2	20.4	49.5	48.6	59.6
	ROT	246	200	52.3	10.7	13.5	10.2	6.63	17.5	16.9	20.7
	ISO	224	177	45.9	8.58	10.8	8.18	5.20	14.3	13.7	16.7
H ₂	A-P	273	195	51.1	9.17	10.9	8.82	6.25	14.3	13.5	16.0
	ROT	177	112	29.4	4.43	5.06	4.29	3.19	6.74	6.30	7.25
E	A-P	407	331	94.2	23.8	29.2	23.0	16.1	35.0	34.0	40.1
	ROT	278	207	58.7	13.5	16.4	13.0	9.20	19.7	19.0	22.3
	ISO	223	162	45.7	9.92	12.2	9.56	6.67	14.6	14.1	16.7

1. MADE, the maximum dose equivalent in a 60 cm tall, 30 cm diameter, tissue equivalent cylinder, based on ICRP 21 convention. [2],
2. $H^*(10)$ with old $Q(L)$, the ambient dose equivalent as calculated by Wagner et al. based on ICRU 39 [3],
3. H_E , the effective dose equivalent taken from ICRP 51. [18],
4. $H_p(10)$ with old $Q(L)$, the personal dose equivalent in an ICRU tissue slab as calculated by R. Hollnagel based on ICRU 39 and old $Q(L)$. [19], [3]
5. $H^*(10)$ with new $Q(L)$, the ambient dose equivalent as calculated by B.R.L. Siebert and H. Schumacher based on ICRP 60 with new $Q(L)$ and new stopping power data from ICRU 49. [21], [4] and [22],
6. E, the effective dose. [4],
7. $H_p(10)$ with new $Q(L)$, the personal dose equivalent in an ICRU tissue slab as calculated by R. Hollnagel. The calculations are based on ICRP 60 with new $Q(L)$ and new stopping power data from ICRU 49. [19], [4] and [22].

The results of weighting the calculated dosimetric quantities with the measured angular proportions are presented in Table 22, while Table 23 shows the calculated dose equivalent rates for the different quantities and positions.

Calculations for position A, based on a separation of the angular distribution into 6 directions and on the more isotropic angular proportions for low energy neutrons, show that $H_p(10)$ with old $Q(L)$ will decrease by 8% and H_E will decrease by 23% as compared with the values presented in Tables 22 and 21 respectively.

For the energy and angle distributions determined for position A, calculations show that both $H_p(10)$ and H_E will decrease when a person turns $90^\circ/270^\circ$ (lateral) or 180° (P-A) from the A-P-direction. For the lateral and P-A irradiations $H_p(10)$ will be higher than H_E .

4.2.2 Calculation for Photons

The measurements in the different positions show that the fields to a large degree are isotropic with only up to 20 percent from the AP direction.

Table 22: Conversion coefficients for positions A, F, G, L at Ringhals and D, E, P at CLAB.

Position and direction	Dosimetric quantities			Effective dose equivalent	Effective dose ICRP 60 + ICRU 49	Hp(10)slab old Q(L)	Hp(10)slab ICRP 60 + ICRU 49
	MaDE	H*(10) Old Q(L)	H*(10) ICRP 60 + ICRU 49				
	pSv/cm2	pSv/cm2	pSv/cm2				
A AP	22,5	22,8	28,7	5,06	11,84	9,26	11,92
F AP	23,3	23,8	30	6,09	14,78	12,93	16,64
G AP	16,4	15,4	19,3	3,31	7,05	4,56	5,81
L AP	27,8	30,3	38,1	6,23	15,60	12,81	16,60
D AP	35	37,3	46,9	8,63	19,70	17,73	23,10
E AP	33,7	36,7	46,3	8,17	19,27	17,52	22,77
P AP	39,9	45,3	57,1	12,59	30,97	32,89	42,87

Table 23: Neutron dose equivalent rates for positions A, F, G, L at Ringhals and D, E, P at CLAB, based on measured neutron fluence and calculated conversion coefficients as presented in Table 22.

Position and direction	microsievert per hour			Effective dose equivalent rate	Effective dose rate ICRP 60 + ICRU 49	Hp(10)slab/t Old Q(L)	Hp(10)slab/t ICRP 60 + ICRU 49
	MaDE/t	H*(10)/t Old Q(L)	H*(10)/t ICRP 60 + ICRU 49				
	A AP	1427	1446				
F AP	722	738	930	189	458	401	516
G AP	173	162	203	35	74	48	61
L AP	204	222	280	46	114	94	122
D AP	39	42	53	10	22	20	26
E AP	32	35	44	8	18	17	22
P AP	38	43	54	12	29	31	40

The major part of the dose equivalents are from photons with energies between 60 keV and 7.6 MeV.

The calculations of dosimetric quantities are based on conversion coefficients from photon fluence at monoenergetic energies to:

1. $H^*(10)$ from ICRU 47. [20],
2. H_E from ICRP 51. [18],
3. $H_p(10)$ from ICRU 47. [20],
4. $H'(10)$ from ICRP 51. [18].

In the energy range between 60 keV and 7.6 MeV the ratio between the dose equivalent $H'(10)$ for isotropic irradiation (ISO) and parallel A-P directed irradiation increases from 0.49 to 0.89, with a ratio of 0.69 at 511 keV which is one of the dominating energies. $H_p(10)$ can be approximated by $H'(10)$ for photon fields, when phantoms other than the ICRU sphere is used additional conversion factors should be applied which include differences mainly in back scatter between the phantom in use and the ICRU sphere [20].

In this energy range the ratio between the effective dose equivalent H_E for ISO and A-P varies between 0.49 at 60 keV and 0.85 at 7.6 MeV with a ratio of 0.65 at 511 keV which is one of the dominating energies.

For isotropic irradiation $H'(10)$ overestimates H_E with a factor 1.32, 1.20 and 1.07 at the energies 60 keV, 511 keV and 7.6 MeV respectively. For A-P irradiation the overestimation is similar.

The energy spectra at the different positions are not well known and therefore a detailed calculation can not be performed.

One can however conclude that H_E from photon irradiation in the measurement positions A to P will be overestimated when the dose equivalent is measured with a dosimeter with good energy and directional response in terms of $H_p(10)$.

4.3 Comparison of Dosimeter Readings with Calculated Quantities

4.3.1 Comparison for Neutron Measurements

The ratio between the measured dose equivalents and the calculated $H_p(10)$ with old $Q(L)$ are presented in Table 24 and in figure 12 for dosimeters on the front face of the phantom. The calculated ratios $H_E/H_p(10)$ is also presented in figure 12 for comparison.

The results from the test of the different dosimeters are presented below:

The PTB track dosimeter showed little deviation from the calculated $H_p(10)$ values at the 4 positions where measurements were performed (90% to 120%).

The PTB albedo dosimeter read 29 to 45% high compared with the calculated $H_p(10)$ values at 3 of the 4 positions where measurements were performed, in position D the albedo dosimeter read twice the calculated $H_p(10)$ value.

The NRPB PADC-track dosimeter read 8 to 38% low compared with the calculated $H_p(10)$ values at the 3 positions where measurements were performed. The readings were still higher than the calculated H_E values.

The readings of the ENEA track and TL-dosimeters were added together. The ENEA dosimeters showed little deviation from the calculated $H_p(10)$ values at the position A and P (99 - 129 %) but overresponded at positions D and L (300 - 325 %).

The AECL track dosimeter showed little deviation from the calculated $H_p(10)$ values at the 3 positions where measurements were performed (100 - 129 %).

The Neutrometer dosimeter (Apfel bubble detector) overresponded at position L (245 %).

The overestimations with the Ringhals dosimeters is mainly due to that the responses are related to remcounter readings in real fields inside the containments, similar to positions A, F

Table 24: Ratio of measurements of $H_p(10)$ (for slab and sphere) and calculated effective dose equivalent/effective dose to calculated $H_p(10)_{slab}$.

Direction AP refers to the reading on the side of the phantom with the highest neutron dose equivalent.										
Dosemeter reading or calculated dose equivalents as proportions of $H_p(10)$ old Q(L)										
	PTB	PTB	NRPB	AECL	Ringhals	Ringhals	ENEA	Apfel	Effective	Effective
	Track	Albedo	Track	Track	TLD	Albedo	Track	Bubble	dose	dose
							+ TLD	detector	equivalent	
Position										
Direction										
G AP					3,34				0,73	1,55
L AP			0,62	1,17	1,49	1,70	3,25	2,45	0,49	1,22
A AP	0,90	1,45	0,66	1,29	2,28	2,33	0,99		0,55	1,28
F AP	1,02	1,35	0,92	1,00	1,60	1,75			0,47	1,14
D AP	1,10	2,00					3,00		0,49	1,11
P AP	1,20	1,29					1,29		0,38	0,94

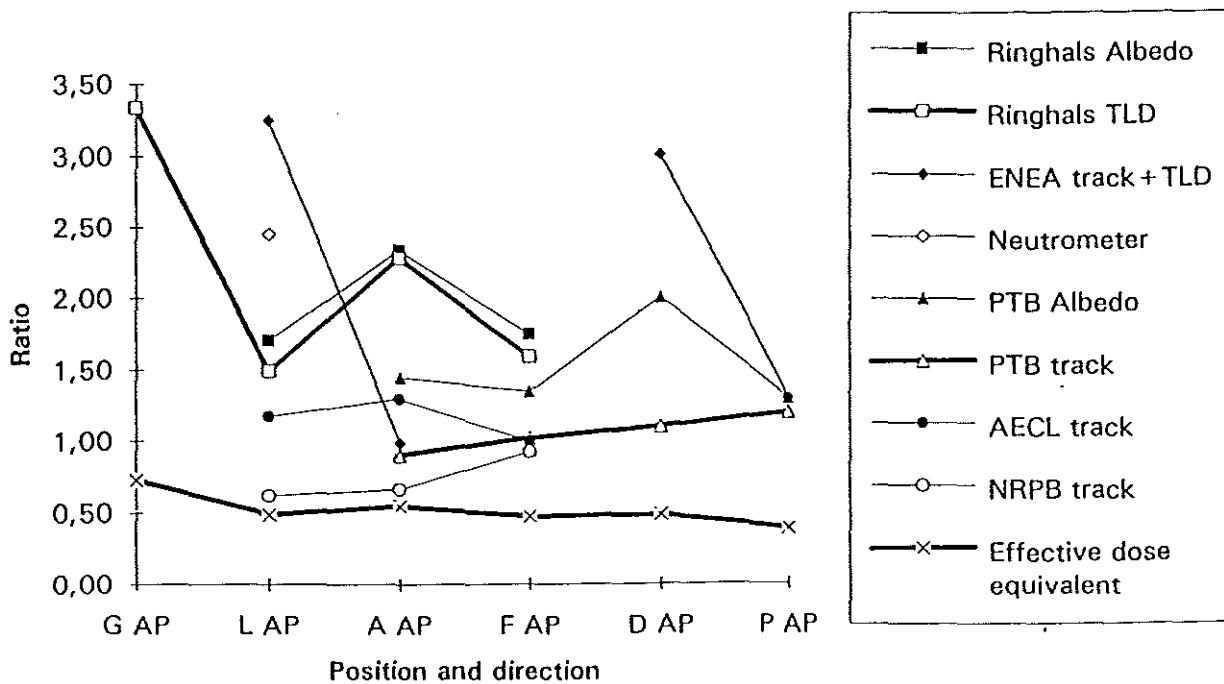


Figure 12: Ratio of dosimeter readings and calculated effective dose equivalent to $H_p(10)_{slab}$.

and G, hence the dosimeter readings are closer to $H^*(10)$ than to $H_p(10)$. The TL-dosimeters read 149 - 334 % of the calculated $H_p(10)$ values while the albedo dosimeters read 170 - 233% of the calculated $H_p(10)$ values. The highest deviation is shown in position G where the field is almost isotropic, at this position $H^*(10)$ is 3.31 times higher than $H_p(10)$. The ratios between the Ringhals dosimeter readings and $H^*(10)$ are 0.93 for TLD and 0.95 for albedo at position A, 0.87 for TLD and 0.95 for albedo at position F, 0.99 for TLD at position G, 0.63 for TLD and 0.72 for albedo at position L.

If the neutron field is separated into 3 components (A-P, ISO and ROT(front only)) instead of 2 components (AP and ISO) for position L there is a better correspondence between the readings for the NRPB PADC-track dosimeter and the measured fluence rate. The estimation of the fluence rate from NRPB dosimeter measurement increases from $1.5 * 10^3 \text{ n * cm}^{-2} * \text{s}^{-1}$ to $1.8 * 10^3 \text{ n * cm}^{-2} * \text{s}^{-1}$ when a change is made from 2 to 3 components, while the estimation from Bonner sphere measurements was $2.0 * 10^3 \text{ n * cm}^{-2} * \text{s}^{-1}$.

Table 25 shows the separation into 2 and 3 components and the corresponding calculations of total fluence.

Additional improvements in correspondence between calibrations and measurements in real fields can probably be achieved if calculations and measurements were to be based on separation of the neutron spectra into 6 or more directional components and if the shift to lower neutron energies for non A-P directions, as compared to A-P direction, can be measured.

4.3.2 Comparison for Photon Measurements

By convention the conversion coefficients for neutron irradiations are based on the incident neutron energy and hence n; γ induced photons should not be included in the photon part of the dose equivalent. Especially in low energy neutron fields n; g reactions in a human body or in a phantom will increase the photon component where the dosimeter is placed, this can lead to erroneous evaluations of the photon induced dose equivalent. In a separate test TL-dosimeters on different phantoms were irradiated with neutrons from a ^{252}Cf source (see section 5 in part 1). The test showed that the reading (in terms of $H_p(10)$) of the photon sensitive dosimeter-pellets (TLD-700) were 17% higher (1.3% of the estimated dose

Table 25: NRPB results at position L.

Irradiation time in position L was 43740 s. Calibrations were performed in different directions and with different neutron energies, see the text in section 5.2 of part 1. From these calibrations and the table above the field quantities F and H*(10) can be estimated.

Part 1. Separation into 3 components

Face of phantom	mSv	tracks	tracks		
			ISO	ROT	AP
			(forward direction)		
Front	700	90	10	60	20
Back	65	10	10	-	-
Right	200	25	10	30	-
Left	360	45	10	30	-
Top	490	60	10	30	-
Bottom	220	30	10	30	-

Field quantities			
	ISO	ROT(2 π)	AP
F	$1.5 * 10^7$	$5.8 * 10^7$	$4.8 * 10^6$
H*(10)	450 mSv	1750 mSv	150 mSv

Part 2. Separation into 2 components

Face of phantom	mSv	tracks	tracks		
			ISO	ROT	AP
Front	700	90	35	-	55
Back	65	10	35	-	-
Right	200	25	35	-	-
Left	360	45	35	-	-
Top	490	60	35	-	-
Bottom	220	30	35	-	-

Field quantities			
	ISO	ROT	AP
F	$5.3 * 10^7$		$1.3 * 10^7$
H*(10)	1605 mSv		400 mSv

equivalent from neutrons) when the dosimeters were on a pure paraffin phantom as compared to on a boron-paraffin phantom. This difference in reading gives an approximate value for the contribution to the dose equivalent from photons originating from neutron interactions in the phantom.

The response of photon measuring instruments and dosimeters to neutrons were estimated by several researchers. Alberts and colleagues have tested the response to slow neutrons. They measured excess readings of several different dosimeters and a GM-counter due to thermal neutrons. The slow neutron response ranged from 6% for the GM-counter free in air to 130% for a film badge dosimeter on a phantom, this value contains a contribution from photons generated by neutron interactions in the phantom, the slow neutron response was calculated as the measured ^{60}Co dose equivalent value to the thermal neutron dose equivalent value. [23].

A high purity Ge detector was used in positions A and L to give information of the photon energy fluences. The detector was used without a collimator. The measurements showed that a substantial part of the energy fluence was due to photons with energies between 2.2 MeV and 7.6 MeV, from $n;\gamma$ reactions with hydrogen atoms and iron atoms respectively. There was also a substantial amount of low energy photons at least down to 60 keV due to multiple scattering. The presence of low and high energy photons means that the readings of different dosimeters will depend much more on the atomic number of the dosimeter material and the material surrounding the dosimeter than when the energy fluence is dominated by 500 keV to 2 MeV photons. Additionally the presence of high energy photons can produce photo-nuclear reactions which can influence both photon sensitive and neutron sensitive detectors. A more precise evaluation of the photon energy fluences or photo-nuclear reactions will not be included in this report.

The ratio between the measured dose equivalents (normally expressed as $H_p(10)$) and the estimated $H_p(10)$ values are presented in table 4.3.2.1 for dosimeters on the front face of the phantom. Only values at positions A, F and L are presented as there are only very few results in the other positions. The dosimeter readings are as a first attempt compared with the reading of the Siemens electronic personal dosimeter (EPD) in position A and L, which is considered to closely measure $H_p(10)$, however the EPD overresponds by 30% to 4.4 to 7 MeV photons. The reading of the Ringhals LiF-based dosimeter is 23% higher than the reading of the EPD

in those 2 positions and it is considered to be reading 23% high also in position F. According to the first comment above the reading of the EPD should be up to 20% too high due to n;g reactions in the phantom. The readings of the EPD should also be a few percent too high due to the overresponse to 4.4 to 7 MeV photons.

The results from the test of the different dosimeters are presented below:

The Siemens EPD was considered to read $H_p(10)$ correctly at the two measured positions A and L. (But in this case $H_p(10)$ includes neutron induced photons in addition to direct and back scattered photons).

The PTB albedo dosimeter read 1% high compared with the estimated $H_p(10)$ value at position A and 12% low at position F.

The Ringhals LiF dosimeters overestimated $H_p(10)$ with 5 to 24% at the positions A, F and L. The readings of the LiF pellets in the albedo holder was on the average 8% lower than the readings of the LiF pellets in the plastic holder.

The ENEA TL-dosimeter underestimated $H_p(10)$ with 18% at position A and with 4% at position L.

The Rados RAD 80 overestimated $H_p(10)$ with 65% at position A. 35% of the overestimation is due to the use of a "large phantom correction factor" as the dosimeters were placed on the combined PMMA-slab + boron-paraffin-slab. More measurements need to be done to get a more exact value of the overresponse of the RAD80 dosimeter.

5. Comparison of all Dosimetric Data

In the previous sections the results obtained with different categories of instruments have been dealt with in detail and a best estimate of the result has been calculated for each category in terms of $H^*(10)$. The mean values are presented in Table 26. For reasons discussed above DE reference values $H^*(BS)$ were obtained from the Bonner spheres spectra (basically the result obtained by the PTB group). However, the differences between the results from the various Bonner spheres systems have not been considered significant. For the personal dosimeters the directional dependence of the dosimeter needs to be known to derive the ambient dose equivalent result from the personal dose equivalent result. For that reason the mean values $H^*(PDM)$ in Table 26 are calculated from the NRPB and the PTB dosimeter results only. The remmeter results shown $H^*(remc)$ were obtained with a Leake-type instrument used by the PTB group. The main argument for choosing this instrument result was the good agreement between estimated results (as calculated from the fluence measurements) and the reported results of the instrument (see Table 28). The table also gives the values for the effective dose equivalent rate H_E as well as the personal dose equivalent rate $H_{p,slab}$ calculated from the reference results. The results relative to the reference results are shown in Fig. 13. It shows

Table 26: Reference and mean values for the neutron component of the operational dose equivalent quantities $H^*(10)$ and $H_{p,slab}(10)$ as obtained with different instruments. Calculated values of the effective dose equivalent rate (H_E) and the personal dose equivalent rate ($H_{p,slab}$) are also shown. For details, see the text.

	L $\mu\text{Sv/h}$	A $\mu\text{Sv/h}$	F $\mu\text{Sv/h}$	G $\mu\text{Sv/h}$	D $\mu\text{Sv/h}$	E $\mu\text{Sv/h}$	P $\mu\text{Sv/h}$
$H^*(BS)$	223	1461	745	165	42	35	43
$H^*(TEPC)$	142	898	511	90	35	27	32
$H^*(remc)$	332		1146	248	52	44	52
$H^*(SDD)$	220				38	38	40
$H^*(PDM)$	160	1525	705		45		45
H_{av}^*	237		829	169	44	36	42
$H_{p,slab}(PADC)_n$	84	559	400		22		37
$H_{p,slab}(10)$	94	600	402	50	20	17	31
H_E	47	321	194	36	10	8	12

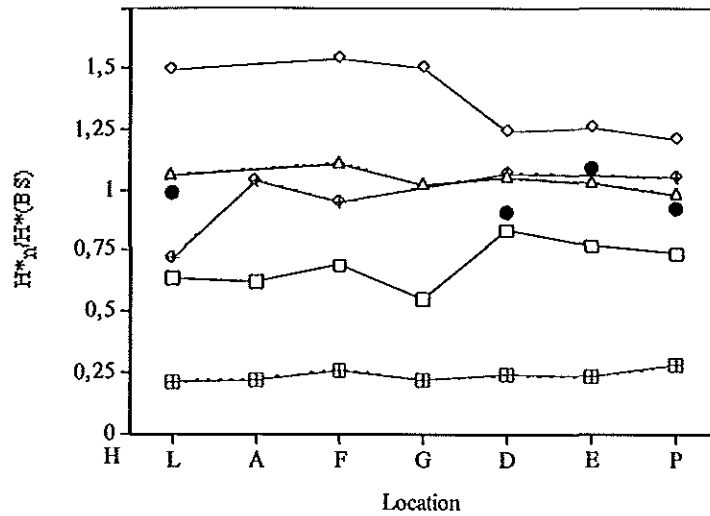


Figure 13: The neutron ambient dose equivalent rate as measured by different instrument categories normalised to the reference ambient dose equivalent rate determined with BS technique. Remmeter result is indicated with diamonds, TEPC result is indicated with squares, SDD result is indicated with filled circles and the average of the TEPC and remmeter result is indicated with triangles. Also shown is the ratio of the effective dose equivalent rate normalised to the reference results, squares with crosses. The ambient dose equivalent rate derived from the mean results of the PADC personal dosimeters is indicated by diamonds with crosses.

that the TEPC instruments read typically 0.7 of the reference ambient dose equivalent, while the remcounter overresponds by a factor of about 1.4. The average results of the two instruments are also shown in the table and in the figure and are, indeed, not significantly different from the reference results. This shows that the calibration fields used for the TEPC instruments as well as for this particular remmeter are not best choices. The $H^*(10)$ calculated from the mean personal dose equivalent as measured by PADC detectors, show quite a good agreement with the reference values. The difference is not significant. Also the area monitor based on a super heated drop detector (SDD) shows a very good agreement with the reference result.

To come to a conclusion about the best estimate of the ambient dose equivalent rate as well as its uncertainty at the various locations, the dose equivalent rate to be expected from TEPC detectors as well as from remmeters, were calculated from the reference results of the neutron

fluence measurements. Such calculations were possible for those detectors, which had a known energy response. The calculation demonstrate the influence of the neutron energy response of the detectors on the readings. It is important, that the measured results to which the calculated results are being compared, have first been critically examined. Otherwise conclusions will be hard to make.

For the TEPC instruments this discussion was described in section 4. Part of the results are also presented in Table 27. The calculations predict that the TEPC instruments used by AECL and KFA will measure 0.69 and 0.75 of the BS-results at Ringhals, and 0.85 and 0.76 at CLAB, respectively. These are 10% to 15% larger values than actually measured by the TEPC instruments. The prediction of the TEPC results within 15% starting with the BS fluence measurements implies that the BS dose equivalent rate is the better estimate of the true dose equivalent rate. Obviously the main differences in results between the two categories of instruments (TEPC and BS) are due to the energy response of the TEPC detectors.

Table 27: Comparison of measured and calculated neutron ambient dose equivalent rate values, $H^*(TEPC)$, normalised to the corresponding reference BS values, $H^*(BS)$. Mean values for Ringhals (RH) and CLAB are shown separately for the AECL and the KFA detectors.

$H^*(TEPC)$ $H^*(BS)$	AECL at RH	AECL at CLAB	KFA at RH	KFA at CLAB
Experimental results	0.59 ± 0.09	0.78 ± 0.06	0.67 ± 0.13	0.69 ± 0.03
Calculated results	0.69 ± 0.08	0.85 ± 0.02	0.75 ± 0.04	0.76 ± 0.05

Similar results for the remmeters are given in Table 28. The mean value for all locations are shown. The uncertainty corresponds to one relative standard deviation. The much larger uncertainty for the Ringhals-CLAB instrument reflects the fact, that this instrument was used in routine measurements by the staff at the power plants and were not reported as scientific results. For all three instruments of the Anderson & Braun type the disagreement with the

Table 28: The mean remmeter measured and calculated results, $H^*(remc)$, normalised to the mean reference BS results, $H^*(BS)$. The table gives the average ratio for all positions. Results are presented for the Anderson & Braun type of instruments (for instance the NM2 and Studsvik instruments) and the Leake instrument. The calculated results include adjustments for the different calibration sources used.

$\frac{H^*(remc)}{H^*(BS)}$	Anderson & Braun (IAR)	Anderson & Braun (GSF)	Studsvik (Ringhals - CLAB)	Leake (PTB)
Experimental result	0.94 $\pm 11\%$	1.35 $\pm 8\%$	1.00 $\pm 23\%$	1.38 $\pm 11\%$
Calculated result	1.14 $\pm 4\%$	1.60 $\pm 4\%$	1.59 $\pm 5\%$	1.48 $\pm 10\%$
Calibr. source	Mod. ^{252}Cf	$^{241}AmBe$	$^{241}AmBe$	Mod. ^{252}Cf

calculated results is larger than for the Leake-type instrument. For the former the difference is 15% to 20% , if the Ringhals-CLAB instrument is disregarded. For the Leake instrument the difference is 7%, which is hardly significant (the calculations lead to 7% larger values). For the Leake instrument the large difference between BS-results and the initial remmeter results is thus explained by its energy response. Again the BS reference results give the better estimate of the ambient dose equivalent rate than the remmeter. For the second type of remmeter the results are less conclusive.

A third independent area monitor used was the one based on a super heated drop detector (SDD). This particular instrument had been calibrated in monoenergetic neutron fields at PTB. At the four locations where a comparison between results obtained by the SDD detector and the BS is possible the mean ratio of the two instrument results become $0.98 \pm 8\%$, Table 26. This non-significant difference between two completely independent techniques is a remarkable result.

In summary, there is good evidence, that the selected reference results are good estimates of the true ambient dose equivalent rate. The uncertainty is estimated to be $\pm 15\%$ (1 relative standard deviation) as judged from the discussion above.

In Table 29 to Table 35 all the individual results accepted for calculation of mean values are presented for each location. In Table 29 to 35 similar results for the personal dosimeters are shown. The results are normalised to the readings per $H_p(10)$ for normal incidence of neutrons from a bare ^{252}Cf source. When more than one result in a particular instrument category is available a mean value (also for the BS) and a relative standard deviation have been calculated and is printed in fat. The remcounter results reported by the staff at Ringhals and CLAB have not been used for the calculations of the mean values, as they were usually the result of quick less precise measurements, however, sometimes repeated several times during the course of the exercise. The results are nevertheless of interest as it shows that the results of those field measurements, are in good agreement with results from comparable instruments used by other participants, see also Table 28. The relative standard deviation averaged for all positions becomes 12%, 19%, 21% and 27% for the BS, the remmeters, the TEPC and the PADC detectors (not including the ENEA dosimeter results). The best precision was obtained with the Bonner spheres. There is not any significant difference in precision between remmeters and TEPC instruments. The precision obtained with the PADC based personal dosimeters was slightly worse. An advantage with the TEPC instruments is their possibility to measure both neutrons and gammas. The precision in the total ambient dose equivalent rate is 12%, which is about half of the precision in the neutron dose equivalent rate.

A further observation from the tables is that the GM-tube based measurement results at Ringhals are 1.6 times larger than the photon dose equivalent rate values reported for the TEPC instruments. At CLAB the corresponding overestimate was 1.3. The reason for this was shown to be the very high energy photons created in (n,γ) -reactions. GM-tubes are known to overrespond to them. This degree of overestimate was possible to determine because of the good photon energy response, that the TEPC instruments have.

Table 29.A: The results of the measurements of $H^*(10)$ in the lock of reactor 4 at Ringhals. The reference value, $H_{n,ref}^*$, is calculated from the fluence measurements with Bonner spheres made by PTB.

Instrument category	H_n^* (mSv/h)	H_γ^* (mSv/h)	$H_{n+\gamma}^*$ (mSv/h)	$H_{n,ref}^*$ (mSv/h)	$H_n^* / H_{n,ref}^*$
<i>remcounters</i>					
<i>GM-tubes</i> Ringhals:					
Studsvik					
Dineutron	0.23	0.07	0.30	0.223	1.03
	0.17			0.223	0.76
IAR: And. Braun					
GSF: And. Braun	0.216	0.07	0.28	0.223	0.97
PTB: Leake	0.305			0.223	1.37
SSI	0.332			0.223	1.49
Mean value		0.07			
$\pm 1 s$	0.28	0.07		0.223	1.3
	$\pm 21\%$	$\pm 0\%$			$\pm 21\%$
<i>SDD</i>					
DCMN	0.220			0.223	0.99
<i>TEPC</i>					
AECL	0.138	0.047	0.186	0.223	0.62
KFA	0.121	0.046	0.168	0.223	0.54
CEA-Gren.	0.165			0.223	0.74
PTB		0.050			
SSI			0.151		
Mean value	0.14	0.048	0.17	0.223	0.63
$\pm 1 s$	$\pm 16\%$	$\pm 4\%$	$\pm 10\%$		$\pm 16\%$
<i>Bonner spheres</i>					
GSF	0.228			0.223	1.02
IAR	0.183			0.223	0.82
PTB	0.223			0.223	1.00
Mean value	0.221			0.223	0.95
$\pm 1 s$	$\pm 12\%$				$\pm 12\%$

Table 29.B: Results of measurements of the personal dose equivalent rate in the lock at reactor 4 at Ringhals. The quantity, $H_{p,n,slab}$, is the personal dose equivalent rate at 10 mm depth in a slab phantom, calculated from the Bonner spheres fluence measurements and directional data.

Type of detector	$H_{p,n}$ (mSv/h)	$H_{p,\gamma}$ (mSv/h)	$H_{p,n+\gamma}$ (mSv/h)	$H_{p,n,slab}$ (mSv/h)	$H_{p,n} / H_{p,n,slab}$
<i>TLD</i>					
Ringhals (LiB)	0.14			0.09	1.56
Ringhals (Albedo)	0.16	0.07	0.23	0.09	1.78
<i>PADC + TLD</i>					
ENEA	0.205			0.09	2.28
<i>PADC</i>					
AECL	0.110			0.09	1.22
NRPB	0.058			0.09	0.64
Mean value	0.084			0.09	0.93
$\pm 1 s$	$\pm 44\%$				$\pm 44\%$
<i>SDD</i>					
Ringhals: Apfel	0.23			0.09	2.56

Table 30.A: The results of the measurements of $H^*(10)$ at position A of reactor 4 at Ringhals. The reference value, $H_{n,ref}^*$, is calculated from the fluence measurements with Bonner spheres.

Instrument category	H_n^* (mSv/h)	H_γ^* (mSv/h)	$H_{n+\gamma}^*$ (mSv/h)	$H_{n,ref}^*$ (mSv/h)	$H_n^*/H_{n,ref}^*$
<i>remcounters</i>					
<i>GM-tubes</i>					
Ringhals:					
Studsvik	1.50	0.38	1.88	1.461	1.03
Dineutron	1.50			1.461	1.03
GSF: And. Braun	2.16			1.461	1.48
NPL: Harwell	2.68			1.461	1.83
SSI		0.49			
Mean value	2.42			1.461	1.66
$\pm 1 s$	$\pm 15\%$				$\pm 15\%$
<i>TEPC</i>					
AECL	0.94	0.30	1.24	1.461	0.64
KFA	0.97	0.28	1.24	1.461	0.66
CEA-Gren.	0.79			1.461	0.54
PTB		0.33			
SSI			0.99		
Mean value	0.90	0.30	1.16	1.461	0.62
$\pm 1 s$	$\pm 11\%$	$\pm 8\%$	$\pm 13\%$		$\pm 11\%$
<i>Bonner spheres</i>					
NPL	1.43			1.461	1.00
PTB	(1.46) ^a			1.461	(1.00)

a/ The NPL-result was used as input data

Table 30.B: Results of measurements of the personal dose equivalent rate at position A of reactor 4 at Ringhals. The quantity, $H_{p,n,slab}$, is the personal dose equivalent rate at 10 mm depth in a slab phantom, calculated from the Bonner spheres fluence measurements and directional data.

Type of detector	$H_{p,n}$ (mSv/h)	$H_{p,\gamma}$ (mSv/h)	$H_{p,n+\gamma}$ (mSv/h)	$H_{p,n,slab}$ (mSv/h)	$H_{p,n}/H_{p,n,slab}$
<i>TLD</i>					
Ringhals (LiB)	1.34			0.600	2.23
Ringhals (Albedo)	1.37	0.42	1.79	0.600	2.28
PTB (Albedo)	0.85	0.34	1.19	0.600	1.42
<i>PADC + TLD</i>					
ENEAC	0.58	0.28	0.86	0.600	
<i>PADC</i>					
AECL	0.76			0.600	1.27
NRPB	0.39	0.61	1.00	0.600	0.65
PTB	0.53			0.600	0.88
Mean value	0.56			0.600	0.93
$\pm 1 s$	$\pm 33\%$				$\pm 33\%$

Table 31.A: The results of the measurements of $H^*(10)$ at position F of reactor 2 at Ringhals. The reference value, $H_{n,ref}^*$, is calculated from the fluence measurements with Bonner spheres.

Instrument category	H_n^* (mSv/h)	H_γ^* (mSv/h)	$H_{n+\gamma}^*$ (mSv/h)	$H_{n,ref}^*$ (mSv/h)	$H_n^* / H_{n,ref}^*$
<i>remcounters</i>					
<i>GM-tubes</i>					
Ringhals:					
Studsvik	1.00	0.20	1.20	0.745	1.61
Dineutron	0.70			0.745	0.94
IAR: And. Braun	0.79	0.26	1.25	0.745	1.06
GSF: And. Braun	1.09			0.745	1.46
PTB: Leake	1.15			0.745	1.54
SSI		0.31			
Mean value	1.01	0.29		0.745	1.35
$\pm 1 s$	$\pm 19\%$	$\pm 12\%$			$\pm 19\%$
<i>TEPC</i>					
AECL	0.48	0.18	0.66	0.745	0.64
KFA	0.63	0.20	0.83	0.745	0.85
CEA-Gren.	0.43			0.745	0.58
PTB				0.745	
SSI			0.59		
Mean value	0.51	0.19	0.69	0.745	0.69
$\pm 1 s$	$\pm 20\%$	$\pm 6\%$	$\pm 17\%$		$\pm 20\%$
<i>Bonner spheres</i>					
GSF	0.91			0.745	1.22
IAR	0.69			0.745	0.93
PTB				0.745	
Mean value	0.80			0.745	1.07
$\pm 1 s$	$\pm 19\%$				$\pm 19\%$

Table 31.B: Results of measurements of the personal dose equivalent rate at position F of reactor 2 at Ringhals. The quantity, $H_{p,n,slab}$, is the personal dose equivalent rate at 10 mm depth in a slab phantom, calculated from the Bonner spheres fluence measurements and directional data.

Type of detector	$H_{p,n}$ (mSv/h)	$H_{p,\gamma}$ (mSv/h)	$H_{p,n+\gamma}$ (mSv/h)	$H_{p,n,slab}$ (mSv/h)	$H_{p,n} / H_{p,n,slab}$
<i>TLD</i>					
Ringhals (LiB)	0.64		1.06	0.40	1.60
Ringhals (Albedo)	0.70	0.35	1.09	0.40	1.75
PTB (Albedo)	0.54	0.25	0.79	0.40	1.35
<i>PADC</i>					
AECL	0.40			0.40	1.00
NRPB	0.37			0.40	0.93
PTB	0.41			0.40	1.03
Mean value	0.39			0.40	0.98
$\pm 1 s$	$\pm 5\%$				$\pm 5\%$

Table 32.A: The results of the measurements of $H^*(10)$ at position G of reactor 2 at Ringhals. The reference value, $H_{n,ref}^*$, is calculated from the fluence measurements with Bonner spheres.

Instrument category	H_n^* (mSv/h)	H_γ^* (mSv/h)	$H_{n+\gamma}^*$ (mSv/h)	$H_{n,ref}^*$ (mSv/h)	$H_n^* / H_{n,ref}^*$
<i>remcounters</i>					
<i>GM-tubes</i>					
Ringhals:					
Studsvik	0.10	0.10	0.20	0.165	0.61
Dineutron	0.20			0.165	1.21
IAR: And. Braun	0.12	0.10	0.22	0.165	0.73
GSF: And. Braun	0.23			0.165	1.39
PTB: Leake	0.25			0.165	1.51
SSI		0.12			
Mean value	0.20	0.11		0.165	1.21
$\pm 1 s$	$\pm 34\%$	$\pm 12\%$			$\pm 35\%$
<i>TEPC</i>					
AECL	0.074	0.068	0.142	0.165	0.45
KFA	0.106	0.063	0.169	0.165	0.64
PTB		0.072			
SSI					
Mean value	0.09	0.068	0.15		0.54
$\pm 1 s$	$\pm 25\%$	$\pm 7\%$	$\pm 11\%$		$\pm 25\%$
<i>Bonner spheres</i>					
GSF	0.142			0.165	0.86
IAR	0.120			0.165	0.73
PTB	0.165			0.165	1.00
Mean value	0.140			0.165	0.86
$\pm 1 s$	$\pm 16\%$				$\pm 16\%$

Table 32.B: Results of measurements of the personal dose equivalent rate at position G of reactor 4 at Ringhals. The quantity, $H_{p,n,slab}$, is the personal dose equivalent rate at 10 mm depth in a slab phantom, calculated from the Bonner spheres fluence measurements and directional data.

Type of detector	$H_{p,n}$ (mSv/h)	$H_{p,\gamma}$ (mSv/h)	$H_{p,n+\gamma}$ (mSv/h)	$H_{p,n,slab}$ (mSv/h)	$H_{p,n} / H_{p,n,slab}$
<i>TLD</i>					
Ringhals (LiB)	0.160	0.060 (LiF)	0.220	0.050	3.20

Table 33.A: The results of the measurements of $H^*(10)$ at position D at CLAB. The reference value, $H_{n,ref}^*$, is calculated from the fluence measurements with Bonner spheres.

Instrument category	H_n^* (mSv/h)	H_γ^* (mSv/h)	$H_{n+\gamma}^*$ (mSv/h)	$H_{n,ref}^*$ (mSv/h)	$H_n^*/H_{n,ref}^*$
<i>remcounters</i>					
<i>GM-tubes</i>					
CLAB:					
Studsvik	0.040			0.042	0.95
Dineutron	0.060			0.042	1.43
IAR: And. Braun	0.041	0.034	0.075	0.042	0.98
GSF: And. Braun	0.053			0.042	1.26
PTB: Leake	0.052			0.042	1.24
SSI		0.033			
Mean value	0.049	0.034		0.042	1.16
$\pm 1 s$	$\pm 14\%$	$\pm 2\%$			$\pm 13\%$
<i>SDD</i>					
DCMN	0.038			0.042	0.90
<i>TEPC</i>					
AECL	0.036	0.028	0.064	0.042	0.86
KFA	0.030	0.025	0.056	0.042	0.71
CEA-Gren.	0.039			0.042	0.93
PTB		0.025			
SSI			0.054		
Mean value	0.035	0.026	0.058	0.042	0.83
$\pm 1 s$	$\pm 13\%$	$\pm 7\%$	$\pm 9\%$		$\pm 13\%$
<i>Bonner spheres</i>					
GSF	0.044			0.042	1.05
IAR	0.036			0.042	0.86
PTB	0.042			0.042	1.00
Mean value	0.041			0.042	0.97
$\pm 1 s$	$\pm 10\%$				$\pm 10\%$

Table 33.B: Results of measurements of the personal dose equivalent rate at position D at CLAB. The quantity, $H_{p,n,slab}$, is the personal dose equivalent rate at 10 mm depth in a slab phantom, calculated from the Bonner spheres fluence measurements and directional data. The results reported by Ringhals were measured at Ringhals under similar conditions.

Type of detector	$H_{p,n}$ (mSv/h)	$H_{p,\gamma}$ (mSv/h)	$H_{p,n+\gamma}$ (mSv/h)	$H_{p,n,slab}$ (mSv/h)	$H_{p,n}/H_{p,n,slab}$
<i>TLD</i>					
Ringhals (LiB)	0.03	0.03 (LiF)	0.06	(0.020)	(1.50)
PTB (Albedo)	0.040	0.030	0.070	0.020	2.00
<i>PADC + TLD</i>					
BNEA	0.060			0.020	3.00
<i>PADC</i>					
PTB	0.022			0.020	1.10

Table 34.A: The results of the measurements of $H^*(10)$ at position E at CLAB. The reference value, $H_{n,ref}^*$, is calculated from the fluence measurements with Bonner spheres.

Instrument category	H_n^* (mSv/h)	H_γ^* (mSv/h)	$H_{n+\gamma}^*$ (mSv/h)	$H_{n,ref}^*$ (mSv/h)	$H_n^* / H_{n,ref}^*$
<i>remcounters</i>					
<i>GM-tubes</i>					
CLAB:					
Studsvik	0.030			0.035	0.86
Dineutron	0.040			0.035	1.14
IAR: And. Braun	0.033	0.026	0.059	0.035	0.94
GSF: And. Braun	0.044			0.035	1.26
PTB: Leake	0.044			0.035	1.26
SSI		0.022			
Mean value	0.040	0.024		0.035	1.15
$\pm 1 s$	$\pm 16\%$	$\pm 12\%$			$\pm 16\%$
<i>SDD</i>					
DCMN	0.038			0.035	1.09
<i>TEPC</i>					
ABCL	0.026	0.020	0.047	0.035	0.74
KFA	0.023	0.020	0.043	0.035	0.66
CEA-Gren.	0.031			0.035	0.89
PTB		0.020			
SSI			0.043		
Mean value	0.027	0.020	0.044	0.035	0.76
$\pm 1 s$	$\pm 15\%$	$\pm 2\%$	$\pm 5\%$		$\pm 15\%$
<i>Bonner spheres</i>					
GSF	0.036			0.035	1.03
IAR	0.032			0.035	0.91
PTB	0.035			0.035	1.00
Mean value	0.034			0.035	0.98
$\pm 1 s$	$\pm 6\%$				$\pm 6\%$

Table 34.B: Results of measurements of the personal dose equivalent rate at position E. This measurement was made at Ringhals on a similar transport cask with a similar load of fuel elements. The quantity, $H_{p,n,slab}$, is the personal dose equivalent rate at 10 mm depth in a slab phantom, calculated from the Bonner spheres fluence measurements and directional data made at CLAB.

Type of detector	$H_{p,n}$ (mSv/h)	$H_{p,\gamma}$ (mSv/h)	$H_{p,n+\gamma}$ (mSv/h)	$H_{p,n,slab}$ (mSv/h)	$H_{p,n} / H_{p,n,slab}$
<i>TLD</i>					
Ringhals (LiB)	0.04	0.04 (LiF)	0.07	(0.017)	(2.4)
Ringhals (Albedo)	0.03				

Table 35.A: The results of the measurements of $H^*(10)$ at position P at CLAB. The reference value, $H_{n,ref}^*$, is calculated from the fluence measurements with Bonner spheres.

Instrument category	H_n^* (mSv/h)	H_γ^* (mSv/h)	$H_{n+\gamma}^*$ (mSv/h)	$H_{n,ref}^*$ (mSv/h)	$H_n^* / H_{n,ref}^*$
<i>remcounters</i>					
<i>GM-tubes</i>					
CLAB:					
Studsvik	0.050			0.043	1.16
Dineutron	0.100			0.043	2.32
IAR: And. Braun	0.041	0.026		0.043	0.95
GSF: And. Braun	0.051			0.043	1.19
PTB: Leake	0.052			0.043	1.21
SSI		0.023			
Mean value	0.048	0.025		0.043	1.12
$\pm 1 s$	$\pm 13\%$	$\pm 9\%$			$\pm 13\%$
<i>SDD</i>					
DCMN	0.040			0.043	0.93
<i>TEPC</i>					
AECL	0.031	0.024	0.055	0.043	0.72
KFA	0.025	0.021	0.046	0.043	0.58
CEA-Gren.	0.040			0.043	0.93
PTB		0.012			
SSI			0.051		
Mean value	0.032	0.019	0.051	0.043	0.74
$\pm 1 s$	$\pm 24\%$	$\pm 33\%$	$\pm 9\%$		$\pm 24\%$
<i>Bonner spheres</i>					
GSF	0.047			0.043	1.09
IAR	0.037			0.043	0.86
PTB	0.043			0.043	1.00
Mean value	0.042			0.043	0.98
$\pm 1 s$	$\pm 12\%$				$\pm 12\%$

Table 35.B: Results of measurements of the personal dose equivalent rate at position P at CLAB. The quantity, $H_{p,n,slab}$, is the personal dose equivalent rate at 10 mm depth in a slab phantom, calculated from the Bonner spheres fluence measurements and directional data.

Type of detector	$H_{p,n}$ (mSv/h)	$H_{p,\gamma}$ (mSv/h)	$H_{p,n+\gamma}$ (mSv/h)	$H_{p,n,slab}$ (mSv/h)	$H_{p,n} / H_{p,n,slab}$
<i>TLD</i>					
PTB (Albedo)	0.030	0.020	0.070	0.031	1.29
<i>PADC + TLD</i>					
ENEA	0.040			0.031	1.29
<i>PADC</i>					
PTB	0.037			0.031	1.19

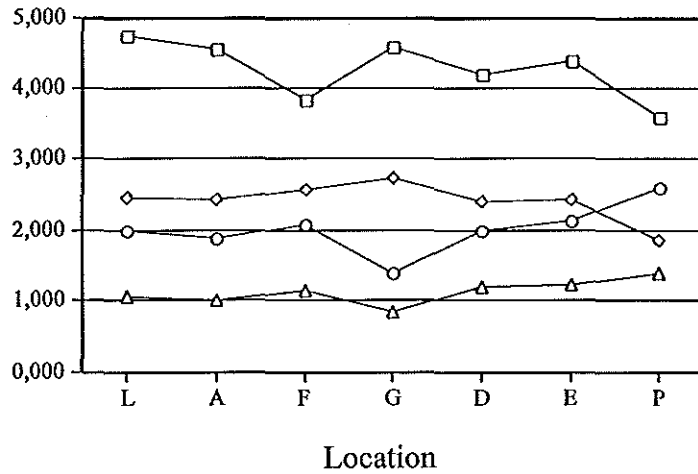


Figure 14: The neutron $H_n^*(10)/H_E$ (squared symbols) as well as $H_{p,slab}(10)/H_E$ (circles) according to ICRP 51 and ICRU 39. Also shown is the ratios of $H_n^*(10)/E$ (diamonds) and $H_{p,slab}(10)/E$ (triangles). See the text for details.

The operational dose equivalent quantities were defined to give an overestimate of the effective dose equivalent, H_E . This is illustrated in Figure 14, which shows the ratio between $H^*(10)_n/H_E$ as well as the ratio of $H_{p,n}(10)/H_E$. The overestimate is between 4,5 and about 2 for the two ratios, respectively. The ICRP has defined a new quantity in its Report 60 [4] to replace H_E called effective dose, E , in which radiation weighting factors, w_R , replace quality factors. In the report a new relation between quality factor, Q , and linear energy, L , is also defined for use with operational quantities. After the publication of Report 60, the ICRU has published its Report 49 [22], which gives revised stopping power data for protons and alpha particles. In Figure 14 the ratios between $H_n^*(10)$ and E as well as $H_{p,n}(10)/E$ are shown. The changes in stopping power presented as well as a new suggested relation between Q and neutron fluence (ICRP/ICRU draft report) have been considered in the calculations of the quantities. The overestimates now become smaller, about 2.5 for the ambient dose equivalent and just larger than 1.0 for the personal dose equivalent. All the numerical data are found in Table 36.

Table 36: The neutron ambient dose equivalent rate, for two different sets of quality factors suggested by ICRP, the effective dose equivalent defined by the ICRP in report 51 and the effective dose as now recommended by the ICRP in its report 60.

Quantity	L (mSv/h)	A (mSv/h)	F (mSv/h)	G (mSv/h)	D (mSv/h)	E (mSv/h)	P (mSv/h)
H^* old Q(L)	0.223	1.461	0.745	0.165	0.042	0.035	0.043
H^* Q(L) ICRP 60 ICRU 49	0.280	1.820	0.930	0.203	0.053	0.044	0.054
$H_{p,slab}$ old Q(L)	0.094	0.593	0.405	0.049	0.020	0.017	0.031
$H_{p,slab}$ ICRP 60 ICRU 49	0.122	0.756	0.516	0.061	0.026	0.022	0.041
H_E ICRP 51	0.046	0.321	0.197	0.036	0.010	0.008	0.012
E ICRP 60	0.114	0.751	0.458	0.074	0.022	0.018	0.029

6. Conclusions

The unique comparison exercise performed with various neutron spectrometers and neutron and photon dosimeters to specify the mixed radiation fields at workplaces in nuclear facilities was thoroughly evaluated. In the course of a very detailed analysis of the different spectrometric results various problems were recognized and later on resolved. Besides trivial mistakes, e.g. normalisation errors of Bonner sphere data (see p. 15 of Ref. [1]) and recoil proton spectra (see p. 76-78 of Ref. [1]), the incompatibility of the spectral fluence reported by one group with the other BSS data sets again showed that the BS response matrix must be carefully determined, e.g. by adjusting calculated response functions to experimental calibration data for each sphere diameter separately. The systematic discrepancy shown in Fig. 2 disappeared if the revised response matrix was used for unfolding of the IAR data set (see p. 35-38 of Ref. [1]). The scatter of the final results (Fig. 15) is now quite large for both the integral fluence and DE values but the overall agreement is much more satisfying although not perfect.

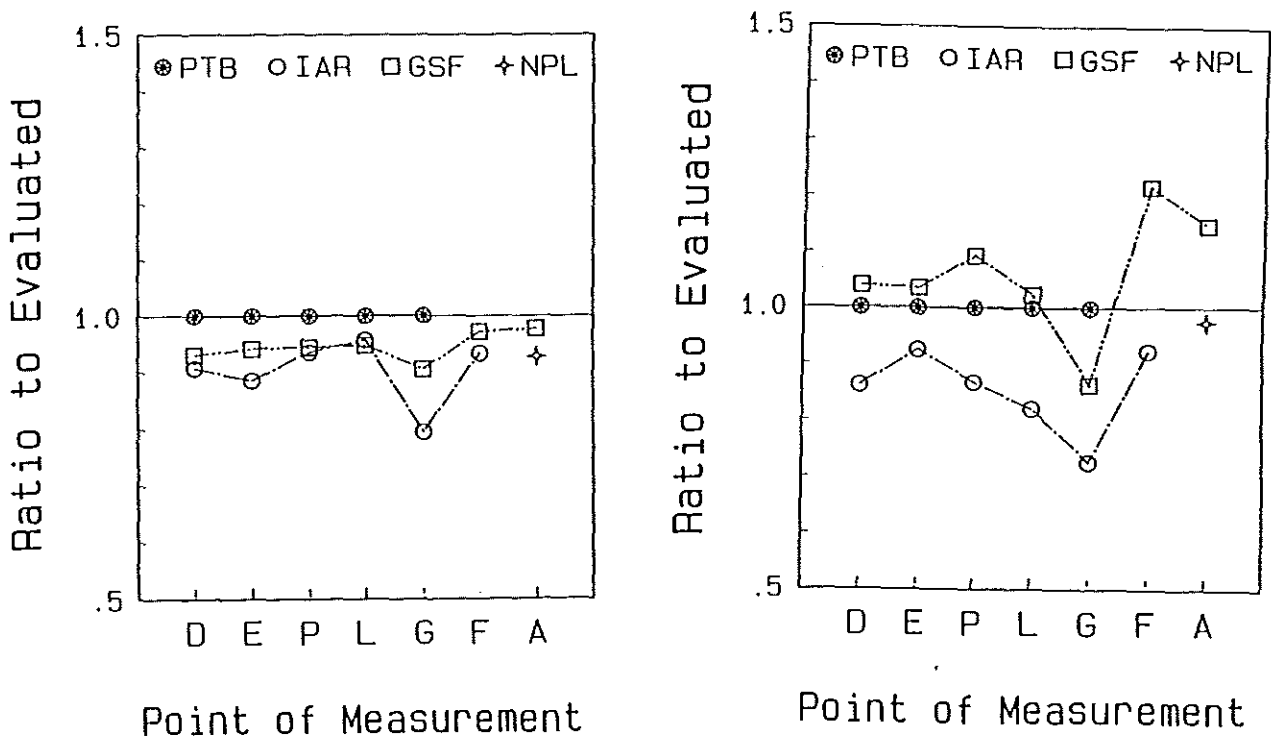


Fig. 15: Ratio of the total neutron fluence (left) and dose equivalent (right) as for Figure 2, but with the revised IAR data and the evaluated results for reference.

It might be concluded from this comparison that an evaluation of the final data sets may yield slightly lower integral values, but the revised data were submitted too late for a new analysis. The recommended spectral fluence (see Fig. 9 and Table 11) is therefore used for the interpretation of all dosimetric neutron data.

On the basis of the final evaluation, TEPCs give values for the total dose and gamma dose rates with a statistical uncertainty of less than 10%, dose equivalent rates, neutron dose equivalent rates and neutron quality factors with statistical uncertainties of less than 20%. However, the data delivered by the participants showed a spread of the neutron dose equivalent data of more than 40%. The evaluation of the dose equivalent data and the assessment of uncertainties is difficult, since each participant uses his own experience to set neutron gamma thresholds and to apply correction factors.

Traceability of results could be improved and uncertainties be minimised if a code of practice for TEPC dosimetry for radiation protection could be established. This code would have to include standard detector designs, calibration procedures and sources, evaluation procedures and recommendations with respect to basic nuclear data used in calibration and evaluation procedures such as stopping powers and W values.

In comparison to the Bonner sphere results, the dose equivalent readings of the TEPCs are lower by 30% on average, even though the readings of the latter had been corrected (see equation 4) on the basis of measurements with a neutron calibration source. Obviously, this correction was not sufficient for measurements in the fields encountered at the Ringhals reactors and at CLAB. A code of practice, as mentioned before, therefore, would have to include also recommendations for calibration sources and procedures, when TEPCs are used in different irradiation environments.

The TEPC measurements of gamma dose equivalents showed that Geiger Müller measurements of this radiation component were wrong probable due to the presence of a significant fraction of high energy photons in the incident fields.

The directional dependence of the neutron fluence could only be determined by means of sets of personal dosimeters simultaneously irradiated on phantoms. The evaluated spectral neutron

fluence could at least be separated in an isotropic and directional (chiefly A - P) part. Although a rough approach only, this analysis allowed to estimate limiting DE quantities showing that the ambient and personal DE values are always conservative estimates of the limiting quantities. The ambient DE values derived from these measurements are in reasonable agreement with the reference data (see Figs. 12 and 13).

In general, the neutron dosimeter results deviate from the reference values as expected in such soft neutron fields according to their response functions, e.g. moderator type remcounter overread up to 50% and TEPC systems underread in the same order of magnitude. Satisfying results were only obtained for a Studsvik-remcounter and a recently developed dosimeter based on superheated drop detectors. The latter system seems to be very promising for future use if some technical problems, e.g. the temperature dependence of the response, can be solved.

In summary it can be concluded, that neutron spectrometry is still required in order to establish dosimetric reference data. Bonner Sphere Spectrometers allow to determine ambient DE values to better than 15% for all neutron fields encountered at workplaces in nuclear facilities provided that the response matrix is properly determined. Recoil proton spectrometers may additionally be employed to improve the energy resolution in the neutron energy region beyond 10 keV.

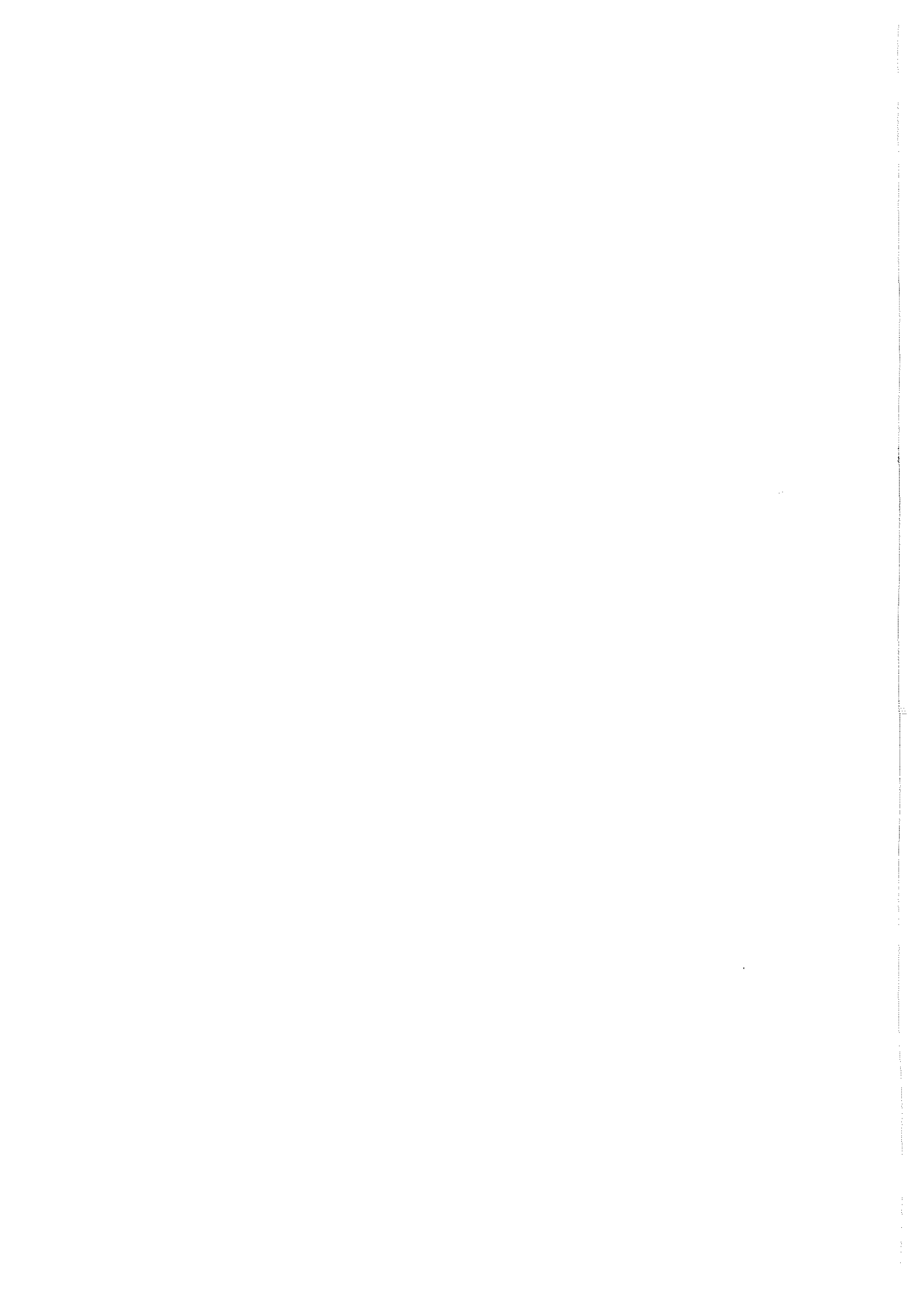
Commonly used area dosimeters must be calibrated at the workplace or in similar fields prepared in the laboratory if DE readings to better than 20% are required. Sets of personal dosimeters with rough spectrometric properties, irradiated on phantoms, can be reliable tools to determine personal, ambient and limiting DE quantities if the directional and energy dependent response is known.

Unexpected discrepancies were observed for the readings of different photon dosimeters. The about 50% higher reading of GM counter based on dosimeters than the TEPC systems may be caused by the high energy photons present. Additional investigations are needed to explain the different readings.

7. References

- [1] Klein, H., Lindborg, L. (Eds.) (1995a) *Determination of Neutron and Photon Dose Equivalent at Workplaces in Nuclear Facilities of Sweden - An SSI-EURADOS Comparison Exercise*. Part I: Measurements and Data Analysis. SSI-Report 95-15, Stockholm, 1995.
- [2] International Commission on Radiological Protection. *Data for Protection Against Ionising Radiation from External Sources: Supplement to ICRP Publication 15*. Pergamon Press, Oxford, 1971, Publication 21.
- [3a] International Commission on Radiation Units and Measurements, *Determination of Dose Equivalent Resulting from External Radiation Sources*. ICRU Report 39, Bethesda, 1985.
- [3b] Wagner, S., Großwendt, B., Harvey, I.R., Mill, A.J., Selbach, H.J., Siebert, B.R.L. *Unified Conversion Function for the New ICRU Operational Radiation Protection Quantities*. Radiat. Prot. Dosim **12**, 231-235 (1985).
- [4a] International Commission on Radiological Protection. *Recommendations of the ICRP*, ICRP Publication 60, Pergamon Press, Oxford, 1991
- [4b] Leuthold, G., Mares, V., Schraube, H. *Calculation of the Neutron Ambient Dose Equivalent on the Basis of the ICRP Revised Quality Factors*. Radiat. Prot. Dosim. **40**, 77-84, (1992).
- [5] Alevra, A.V., program TRESPE, privat communication, 1993
- [6] Berg, S., McElroy, W.N. *A Computer-Automated Iterative Method for Neutron Flux Spectra Determination by Foil Activation (SAND II)*, AFWL-TR 67-41, Kirtland, 1967
- [7] International Commission on Radiation Units and Measurements. ICRU Report 36, Microdosimetry. Bethesda, MD, 1983
- [8] Varma, M.N. *Calibration of Proportional Counters in Microdosimetry*. In: Proceedings of the 8th Symposium on Microdosimetry, EUR 8395, Harwood Academic, pp. 1051-1059 1983.
- [9] Dietze, G., Edwards, A.A., Guldbakke, S., Kluge, H., Leroux, J.B., Lindborg, L., Menzel, H.G., Nguyen, V.D., Schmitz Th., Schuhmacher, H. *Investigation of Radiation Protection Instruments Based on Tissue Equivalent Proportional Counters - Results of a EURADOS Intercomparison*. CEC-Report, EUR 11867, 1988.
- [10] Dietze, G., Booz, J., Edwards, A.A., Guldbakke, S., Kluge H., Leroux, J.B., Lindborg, L., Menzel, H.G., Nguyen, V.D., Schmitz, Th., Schumacher, H. *Intercomparison of Dose Equivalent Meters Based on Microdosimetric Techniques*. Radiat. Prot. Dosim. **23**, 227-234, (1988).
- [11] Lindborg, L., Grindborg, J.E., Gullberg, O., Samuelson, G., Uotila, P. (1995b) *TEPC Measurements with the Covariance Method on Board Aircraft*. Rad. Prot. Dosim.. (in press).
- [12] Pihet, P., Gerdung, S., Grillmaier, R.E., Kunz, A., Menzel, H.G. (1992). *Critical Assessment of Calibration Techniques for Low Pressure Proportional Counters Used in Radiation Dosimetry*. Rad. Prot. Dosim. **44**, No. 1-3 pp.115-120.
- [13] Schmitz, Th., Kramer, H.M., Booz, J. (1989) *Assessment of the Photon Response of a TEPC; Implementation of Operational Quantities into Radiation Protection*. Radiat. Prot. Dosim. Vol. **29**, No. 1-2 pp. 69-73.
- [14] Alberts, W.G., Dietz, E., Guldbakke, S., Kluge, H., Schuhmacher, H. (1988). *Radiation Protection Instruments Based on Tissue Equivalent Proportional Counters: Part II of an International Intercomparison*. PTB-Report PTB-FMRB-117

- [15] Schmitz, Th., Nilsson, U., Marchetto, H., Nguyen, V.D., Schuhmacher, H., Waker, A.J. (1995) *TEPC Measurements* In: Klein, H.; Lindborg, L (Eds.) (1995) *Determination of Neutron and Photon Dose Equivalent at Workplaces in Nuclear Facilities of Sweden - An SSI-EURADOS Comparison Exercise. Part I: Measurements and Data Analysis*. SSI-Report 95-15, Stockholm, 1995 .
- [17] Menzel, H.G., Lindborg, L., Schmitz, Th. Schuhmacher, H . and Waker, A.J (1989) *Intercomparison of Dose Equivalent Meters Based on Microdosimetric Techniques: Detailed Analysis and Conclusions*. Radiat. Prot. Dosim. 29, 55-68.
- [18] International Commission on Radiological Protection. *Data for Use in Protection Against External Radiation..* ICRP Publication 51. Pergamon Press, Oxford, 1987.
- [19] Hollnagel, R.A. *Dose Equivalent in the ICRU-slab*. Physikalisch Technische Bundesanstalt, Braunschweig, Germany. 1995. Personal communication.
- [20] International Commission on Radiation Units and Measurements. *Measurements of Dose Equivalents from External Photon and Electron Radiations*. ICRU Publication 47, Bethesda, 1992.
- [21] Siebert, B.R.L. and Schuhmacher, H. *Quality Factors, Ambient and Personal Dose Equivalent for Neutrons Based on the New ICRU Stopping Power Data for Protons and Alpha Particles*. Radiation Protection Dosimetry 58 (3)177-183 (1995).
- [22] International Commission on Radiation Units and Measurements, Bethesda, USA. 1985. Publication 49.
- [23] The response of some photon dosimeters to slow neutrons. W.G. Alberts and colleagues, Physikalisch Technische Bundesanstalt, Braunschweig, Germany. 1984. 6:th International IRPA Congress, Compacts Volume III, pp 1161-1164. Published by Fachverband für Strahlenschutz e. V., Germany.





SSI-rapporter 1999

SSI reports 1999

99:01 Publikationer 1998

Statens strålskyddsinstitut

99:09 Säkerhets- och strålskyddsläget vid de svenska kärnkraftverken 1998

Statens strålskyddsinstitut

99:02 SSI:s projekt avseende avveckling av kärntekniska anläggningar – en förstudie
Avdelningen för avfall och miljö, Avdelningen för personal- och patientstrålskydd, Administrativa staben.
Henrik Efraimsson, Hans Ehdwall, Thommy Godås, Peter Hofvander, John-Christer Lindhé, Juha Lumpus, Ingemar Lund, Lars Malmqvist, Erik Welleman 50 SEK

99:10 SSI's International Development Cooperation (SIUS)

Annual report 1998
Gábor Szendrő, Sten Grapengiesser, Gunnar Johansson 50 kr

99:03 Föreskrifter om skydd av människors hälsa och miljön vid slutligt omhändertagande av använt kärnbränsle och kärnavfall - bakgrund och kommentarer
Avdelningen för avfall och miljö

99:11 SSI:s granskning av SKBs FUD program 1998

Avdelningen för avfall och miljö.
Mikael Jensen 80 kr

99:04 Calibration in Medical Diagnostic Beams at the Swedish Secondary Standard Dosimetry Laboratory
Avdelningen för miljöövervakning och mätning.
Jan-Erik Kyllönen and Jan-Erik Grindborg 30 SEK

99:12 SKI:s och SSI:s granskning av SKBs systemredovisning i FUD-program 98

Avdelningen för avfall och miljö 50 kr

99:05 Long-term funding and faithfulness to the original goal
Department of Waste and Environmental Protection
Gabriella Sjögren

99:13 Determination of the Neutron and Photon Dose Equivalent at Work Places in Nuclear Facilities of Sweden. An SSI – EURADOS comparison exercise. Part 2: Evaluation.

Avdelningen för miljöövervakning och mätning.
D. Bartlett, P. Drake, L. Lindborg, H. Klein, Th. Schmitz and M. Tichy 100 kr

99:06 Personalstrålskydd inom kärnkraftindustrin
Avdelningen för personal- och patientstrålskydd
Ann-Christin Hägg, Thommy Godås, Lars Malmqvist, Peter Hofvander, Ingemar Lund och Erik Welleman 50 SEK

99:07 Erfarenheter från 1998 års avfalls- och miljöinspektioner och viss annan tillsyn vid de svenska kärntekniska anläggningarna
Avdelningen för avfall och miljö 40 SEK

99:08 Avveckling av kärnkraftverk i USA – en reserapport.
Avdelningen för avfall och miljö, Avdelningen för personal- och patientstrålskydd.
Henrik Efraimsson, John-Christer Lindhé, Lars Malmqvist, Ingemar Lund och Erik Welleman. 60 SEK



STATENS STRÅLSKYDDSinSTITUT, SSI, är en central tillsynsmyndighet med uppgift att skydda människor, djur och miljö mot skadlig verkan av strålning. SSI arbetar för en god avvägning mellan risk och nytta med strålning, och för att öka kunskaperna om strålning, så att individens risk begränsas.

SSI sätter gränser för stråldoser till allmänheten och till dem som arbetar med strålning, utfärdar föreskrifter och kontrollerar att de efterlevs, bland annat genom inspektioner. Myndigheten informerar, utbildar och ger råd för att öka kunskaperna om strålning. SSI bedriver också egen forskning och stöder forskning vid universitet och högskolor.

Myndigheten medverkar i det internationella strålskyddssamarbetet. Därigenom bidrar SSI till förbättringar av strålskyddet i främst Baltikum och Ryssland. SSI håller beredskap dygnet runt mot olyckor med strålning. En tidig varning om olyckor fås genom svenska och utländska mätstationer och genom internationella varnings- och informationssystem.

SSI har idag ca 120 anställda och är beläget i Stockholm.

THE SWEDISH RADIATION PROTECTION INSTITUTE (SSI) is a government authority with the task of protecting mankind and the living environment from the harmful effects of radiation. SSI ensures that the risks and benefits inherent to radiation and its use are compared and evaluated, and that knowledge regarding radiation continues to develop, so that the risk to individuals is minimised.

SSI decides the dose limits for the public and for workers exposed to radiation, and issues regulations that, through inspections, it ensures are being followed. SSI provides information, education, and advice, carries out research and administers external research projects.

SSI participates on a national and international level in the field of radiation protection. As a part of that participation, SSI contributes towards improvements in radiation protection standards in the former Soviet states.

SSI is responsible for co-ordinating activities in Sweden should an accident involving radiation occur. Its resources can be called upon at any time of the day or night. If an accident occurs, a special emergency preparedness organisation is activated. Early notification of emergencies is obtained from automatic alarm monitoring stations in Sweden and abroad, and through international and bilateral agreements on early warning and information.

SSI has 120 employees and is situated in Stockholm.



Statens strålskyddsinstitut
Swedish Radiation Protection Institute

Adress: Statens strålskyddsinstitut; S-171 16 Stockholm;

Besöksadress: Karolinska sjukhusets område, Hus Z 5.

Telefon: 08-729 71 00, Fax: 08-729 71 08

Address: Swedish Radiation Protection Institute;

SE-171 16 Stockholm; Sweden

Telephone: + 46 8-729 71 00, Fax: + 46 8-729 71 08

www.ssi.se